4-2002

Electrical Resistivity Tomography and Induced Polarization Techniques with Paired Vertical Resistivity Probes

Adrian Ezeagu

ELECTRICAL RESISTIVITY TOMOGRAPHY AND INDUCED POLARIZATION TECHNIQUES WITH PAIRED VERTICAL RESISTIVITY PROBES

by

Adrian Ezeagu

A Thesis
Submitted to the
Faculty of The Graduate College
in partial fulfillment of the
requirements for the
Degree of Master of Science
Department of Geosciences

Western Michigan University
Kalamazoo, Michigan
April 2002

ACKNOWLEDGEMENTS

My profound appreciation goes to God for his mercies and spiritual guidance and my parents and siblings for their love and support.

I would like to acknowledge the help and advice of my main thesis advisor, Dr. William Sauck, and other members of my committee, Dr. Estella Atekwana and Dr. Daniel Cassidy.

I would also like to thank the Graduate College of Western Michigan University and the Geological Society of America for providing me with some financial aid.

Finally, I would like to thank the following people: Leslie Lance for helping with editing and formatting of the text; Jeff Spruit and Hans Johannes of MDEQ and Malcorm Pirnie respectively for providing me with background information about the site; Gamal Zidan for helping me with initial site preparation and data acquisition; Shannon Wong and Gerald Unterreiner for tour of the soil laboratory.

Adrian Ezeagu

ELECTRICAL RESISTIVITY TOMOGRAPHY AND INDUCED POLARIZATION TECHNIQUES WITH PAIRED VERTICAL RESISTIVITY PROBES

Adrian Ezeagu, M.S.

Western Michigan University, 2002

The aim of this research is to use electrical resistivity and induced polarization (IP) techniques to image in detail the vertical and lateral distribution of resistivity and chargeability in the subsurface region between two or more boreholes. The method involves installing electrodes mounted on PVC pipes in the boreholes. The distribution of resistivity and chargeability around the boreholes is then calculated. The large number of measurements taken is then inverted to produce tomographs or images showing subsurface distribution of resistivity and chargeability. Four cross-hole measurement arrays (pole-pole, dipole-pole dipole-dipole and pole-dipole) were employed in acquiring tomographic data. The tomographs produced show resistive and conductive zones which may were related to the lithology and moisture content in the subsurface, as well as an image of the extent of invasion by the backfill material used to fill the annular space round the pipes (probes). The induced polarization measurements were not very useful due to the problem of contact potentials. Electrical resistivity tomography can therefore provide a means for high-resolution discrete sampling of a subsurface plane and more adequately define zones in petroleum contaminated aquifers which may relate to geochemical zonation.

TABLE OF CONTENTS

Table of Contents—continued

CHAPTER

LIST OF TABLES

LIST OF FIGURES

List of Figures...Continued

CHAPTER 1

INTRODUCTION

Problem

According to the Michigan DEQ 1999 Report, two hundred and forty seven hazardous waste treatment, storage or disposal sites in Michigan are subject to corrective action requirements.The predominant hazardous substances stored in underground tanks are petroleum products. Leaking underground storage tanks can contaminate both the surrounding soil and the underlying ground water. The study will focus on the use of electrical resistivity tomography, which is a geophysical method to map resistivity variations in a heterogeneous geological medium between two boreholes.

The method is particularly important in remediation of contaminated groundwater and soil. Unlike earlier work done in the study area (Groncki, 1999 whose results show only vertical resistivity profiles), this method will provide a two dimensional image of the subsurface. This may allow for a more detailed interpretation of part of a contaminant plume as well as their temporal variations,and thus supplement the information currently provided by water quality data from the monitoring wells. Maesurements will be accomplished through vertical resistivity probes. Once the probes have been installed, data acquisition rate is fast and can be

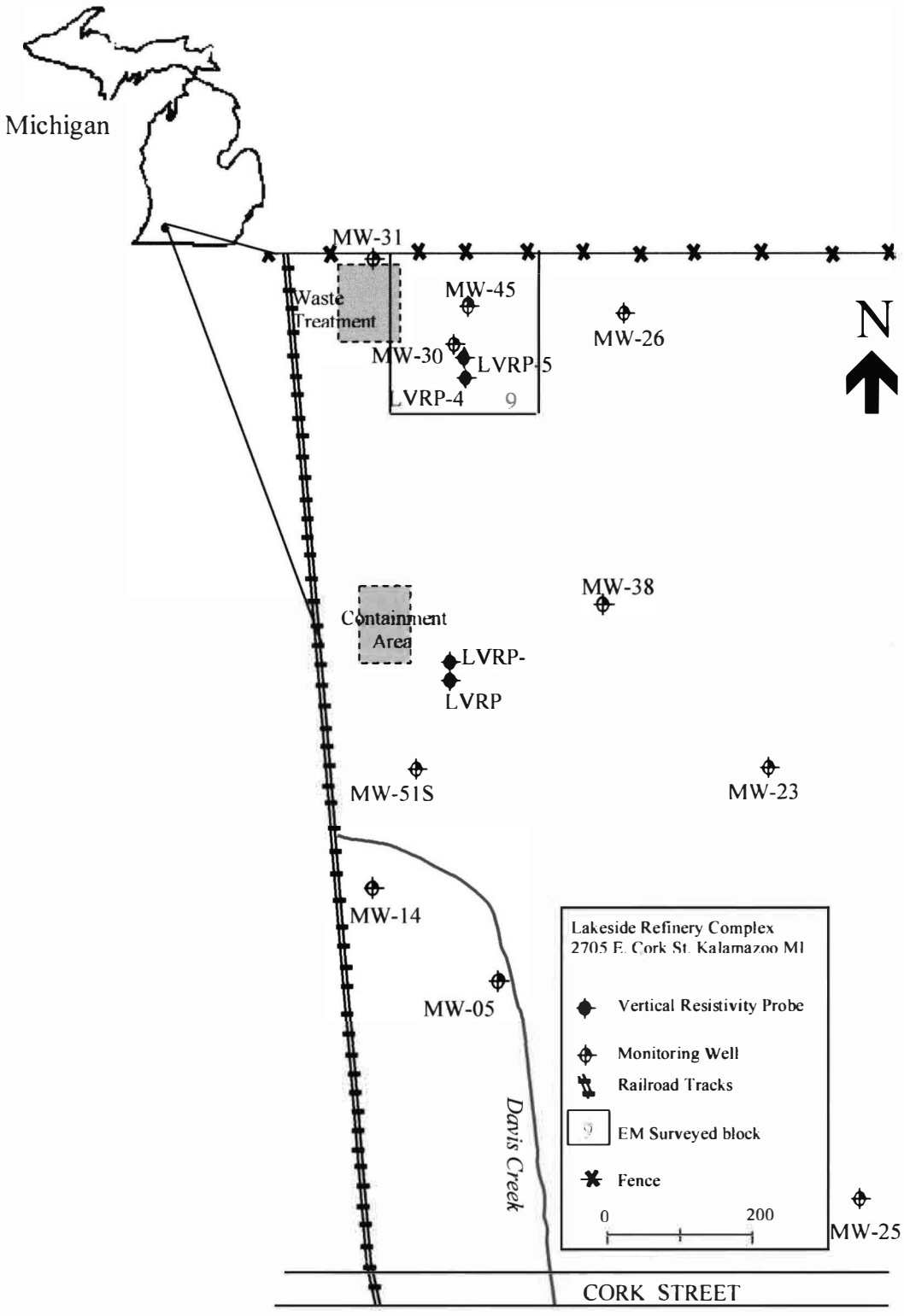

Figure 1. Site Map Showing Location of Vertical Resistivity Probes.

conducted by one person. In addition, the technology is quite simple and minimally intrusive.

However, to achieve this, a set of objectives must be met. These include: (1) finding a suitable location to install the probes, (2) construction of the probes in such a way that they will not leak formation fluids and still allow them to retain their structural integrity, (3) install the probes in such a manner that the electrodes make contact with the formation, (4) characterize the lithology from core samples recovered during drilling, (5) take vertical resistivity and chargeability measurements over a period of time to ensure measurements are repeatable, (6) take cross-hole measurements, and (7) find a suitable 2-D resistivity/IP inversion algorithm for generation of tomographs.

The study area is part of a former refinery located in Kalamazoo Township, Kalamazoo County, Michigan (Figure 1). After the closure of the facility, the site served primarily as a storage depot for fuel and petrochemical products. During the lifetime of the refinery, several petroleum spills were documented and reported. The impact of these accidents were confirmed when Dell Engineering, Inc. in 1992 and 1993 carried out some site investigations and were able to map two areas of subsurface contamination (Weston, 1997).

In 1996 and 1997, the USEPA (Region 5) removed all the superficial tanks and pipelines, leaving the Michigan DEQ responsible for remediation of soil and ground water contamination. Over the past decade, several environmental companies were contracted by the MDEQ to conduct hydrogeologic and hydrogeochemical

studies. Thus, a large number of monitor wells were installed on the site. Cross-borehole measurements were not taken, and therefore interpretations could only be limited to simple layered geologic structures inferred from irregularly spaced boreholes.

Site Geology and Hydrogeology

According to Deutsch et al. (1960), the three major physiographic units in the Kalamazoo area are the dissected outwash plains, the morainal highlands and the glaciated channels. These are unconsolidated deposits and range in thickness from 50ft-600ft. Aquifer units are composed mainly of sands with varying amount of gravel. The aquifers in the region are generally classified as semi-confined with perched aquifers sometimes found in the clays. Groundwater discharge is to Davis creek, which flows Northwesterly. Average annual recharge in the area is about nine inches. Annual water table fluctuation in the area is about 2-3 ft, typical for Michigan. Depth to water table is between 17-20 ft in the upland areas and decreasing to only a couple feet at the base of the bluffs.

Literature Review

Electrical resistivity tomography is a geophysical method that provides a high resolution spatial image of the subsurface resistivity in a plane between two or more boreholes. The method is analogous to X-ray imaging as applied in the medical field where the technology was first proposed by Henderson and Webster, (1978).

LaBreque and Ward, (1988) studied the inversion of borehole to borehole resistivity data. Their work was however limited to prismatic anomalies in a homogeneously resistive medium. Park and Van, (1991) used 3-D resistivity modeling for the interpretation of electrical data from an experiment designed to detect leaks from ponds. Daily et al. (1992) used cross-hole electrical resistivity tomography to image the resistivity distribution before and during two infiltration experiments. One conclusion they reached from their results is that water moved through the unsaturated sediments more rapidly than previous studies have estimated. The electrical resistivity tomographs generated from their study also yielded images of the infiltration plume that could be useful for delineating hydrology of the site. Based on this, Ramirez et al. (1993) used electrical resistivity tomography techniques to map subsurface liquids as flow occurs during natural processes (such as surface water infiltrating the vadose zone) and cleanup processes (such as underground steam injection). Daily et al. (1995) reported on the potential of resistivity imaging as a tool to monitor liquid contaminant leaks in controlled experiments carried out at the Oregon Graduate Institute. Most recently, Maillol et al. (1999) reported that electrical resistivity tomography can be used to image water-filled voids and thus provide an adequate technique in addressing environmental and geotechnical problems in former underground mining areas.

Interpretation of data from resistivity tomography surveys requires both a forward modeling routine and an inverse solution program. Geophysics over the last 20 years has witnessed substantial progress in the research for techniques of solving

geophysical forward and inverse problems. This is indeed also as a result of improved computer capabilities. Techniques for solving the forward problem include the finite element method (Cairlet, 1991); the finite difference method (Thomee, 1989); and the boundary-element methods (Wendland, 1987). Techniques for solving the inverse problem include the least square method applied to 2-D problems (Shima, 1992). Most recently, due to improved computer capabilities, inversion algorithms that combine both the forward and inverse solutions using different schemes exist. These include full and approximate 3-D inversion algorithms that combine the finite element and iterative least squares methods (Sasaki, 1994); rapid 2-D resistivity and IP inversion using the least squares method, including a forward modelling subroutine used to calculate the theoretical resistivity values (Loke, 1996).

CHAPTER II

THEORY

Electrical Resistivity

The electrical prospecting method involves the detection of sub-surface effects produced due to electric current flow in the ground.

The methods used to measure the properties of geologic material can be divided into two; methods using applied current (electrical resistivity, induced polarization, and electromagnetic); and methods using natural current flow (telluric, magnetelluric and self-potential). This study will be restricted to applied current using electrical resistivity and induced polarization techniques.

Electrical Properties of Earth Material

Electrical currents can be propagated through earth material through electronic, electrolytic (ionic), and dielectric conduction.

In water-bearing rocks, conduction is electrolytic and the conducting medium is aqueous and contains salts. The resistivity (ρ) of a rectangular or cylindrical solid material, having resistance (R), cross-sectional area (A), and length (L) is given by:

$$\rho = RA/L \qquad (1)$$

Such a resistance R depends on the applied voltage V across the ends of the sample and the resultant current I flowing through the area A where:

$$R=V/I \tag{2}$$

Conductivity $\sigma = 1/\rho$ is related to Ohm's law by;

$$\sigma = 1/\rho = L/RA = (I/A)/V/L = \mathbf{JE} \text{ (Telford et al. 1990)} \tag{3}$$

Where **J**= current density (Am^{-2}), and **E** is the electric field intensity (Vm^{-1})
For water bearing geologic material, the resistivity depends on the amount of water present, salinity of such water and the geometrical distribution of such water in pores and fissures.

Factors Affecting Resistivity of Earth Material

Porosity is defined as the space between rock grains that can allow fluids to move through the rock. The relationship between porosity and resistivity is provided by Archie's law (Archie, 1942), for unconsolidated granular sediments, which states that bulk resistivity ρ_o is inversely proportional to fractional porosity ϕ raised to a power (m) and directly proportional to the saturation index (S) raised to power (n) times water resistivity ρ_w. This is mathematically stated as follows:

$$\rho_o = a\phi^{-m}S^n\rho_w \tag{4}$$

Where tortuosity (a) is the length of the path of a fluid passing through a unit length of rock. The tortuosity depends on grain size and sorting and has values that lie between 0.5 and 2.5. Cementation factor (m) lies between 1.2 and 2.5 and is nominally 1.3 for unconsolidated sands. The saturation exponent (n) usually has a value of 2.

One other factor affecting resistivity is temperature. Extremes of temperature affect rock resistivity markedly. Very high temperature may drive water away as steam. On the other hand, very low temperature may freeze water contained in pores and cause a very large increase in resistivity. For moderate temperatures, conductivity increases with temperature since viscosity is decreased, implying increased mobility of ions. The relationship between resistivity and temperature change in an electrolytic solution is given by :

$$\rho_T = \rho_{20°} e^{-0.022(T-20)} \tag{5}$$

Where ρ_T is the resistivity at a temperature, T; and ρ_{20} is the resistivity at 20° C, (Keller, 1966).

Resistivity Theory

The basis for the method is that when a current is passed into the ground through an electrode, subsurface variation in conductivity alters the current flow. This in turn alters the distribution of electric potential which when measured between

two points on the surface gives us the resistivity of the geologic material from which the type of geologic material can be inferred.

The potential about a single current electrode is developed from two basic concepts. Consider a current density **J** flowing in an isotropic, homogeneous medium. If density is in amperes per meter squared, then the electric field **E** is related to resistivity ρ through Ohm's law as follows:

$$\mathbf{E} = \rho \mathbf{J} \tag{6}$$

Electric field **E** =gradient of a scalar potential U ($\mathbf{E} = -\nabla U$), thus

$$\mathbf{J} = -\sigma \nabla U \qquad (\sigma = 1/\rho) \tag{7}$$

In regions of finite conductivity, charge is conserved according to Gauss' law and therefore, the divergence of current density is equal to zero ($\nabla \cdot \mathbf{J} = 0$)

Combining $\mathbf{E} = \rho \mathbf{J}$ and $\nabla \cdot \mathbf{J} = 0$, we have

$$\nabla \cdot \mathbf{J} = 1/\rho \, \nabla \mathbf{E} = 1/\rho \, \nabla^2 U = 0 \tag{8}$$

Where U is the electric potential function defined by

$$\mathbf{E} = -\nabla U . \tag{9}$$

For a current I introduced in an infinite homogeneous medium at any point, the potential at any given distance (r) from the source is only a function of (r) such that $U = f(r)$, hence Laplace equation reduces to:

$\partial^2 U / \partial r^2 = \frac{2}{r} \partial U / \partial r = 0$ Since $\nabla^2 U = 0$, with general solution given as

$A - B/r = U$ Where A and B are arbitrary constants. (10)

Boundary Conditions

The potential U as (r) approaches infinity is zero $(r \to \infty)$, therefore A=0. But **J** at any point (r) is given by:

$$\mathbf{J} = -1/\rho \frac{\partial U}{\partial r} = \frac{B}{\rho r^2} \tag{11}$$

From Gauss' law, total current flowing out of a spherical surface of radius (r) is given by:

$$I = \int \mathbf{J} \cdot dA = \int \mathbf{J} \cdot 4\pi r^2 dr \tag{12}$$

Therefore $I = 4\pi r^2 \frac{B}{\rho r^2}$ and $B = \frac{\rho I}{4\pi}$ (13)

For a given semi-infinite homogeneous earth, total current is half of the above thus

$$U = \frac{B}{r} = \frac{\rho I}{2\pi r}$$

This is the equation of potential distribution around an isolated point electrode on the surface of a homogeneous half-space earth.

In practice, there is a bipolar arrangement where current goes in at one point and comes out at another point (Figure 2). The potential at a point due to such an arrangement is given by:

$$U = I\rho/2\pi(1/r_1 - 1/r_2) \tag{15}$$

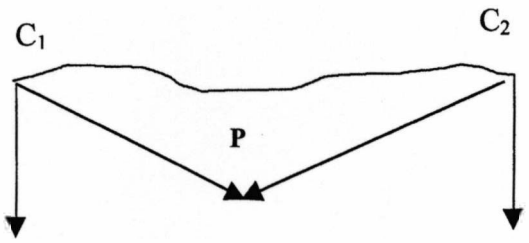

Figure 2. Two Current Electrodes at Surface.

However, due to the problem of contact resistance between the electrode and the earth that would result from such an arrangement (where the current electrodes are also used to measure the potential difference), four electrodes are actually used (two current electrodes and two potential electrodes, (Figure 3). Thus, the potential difference ΔU developed at the surface due to current flow from both current electrodes becomes:

$$\Delta U = \frac{I\rho}{2\pi}\left[\left(\frac{1}{AN} - \frac{1}{BN}\right) - \left(\frac{1}{AM} - \frac{1}{BM}\right)\right] = I\rho\left(\frac{K}{2\pi}\right), \tag{16}$$

where the 2π and the term in the bracket is the geometric factor. The resistivity calculated in this case is called apparent resistivity because we are no longer dealing with a homogeneous geologic medium. Neither will it be an average of a particular point nor an average of a particular volume of geologic material. The resistivity calculated will vary with respect to position and direction of the electrode arrays. Each apparent resistivity measurement in this context is however calculated through an equivalent homogeneous half space.

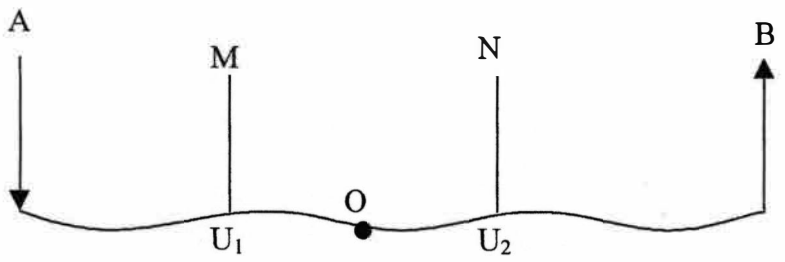

Figure 3. Current and Potential Electrode Pair on the Surface of the Earth.

Current Flow Across Horizontal Stratigraphic Boundaries

Over horizontal layers in a heterogeneous earth media, current flow lines tend to bend in such a way that current preferentially flows towards the lower resistivity portion of the media. For the case of a high resistivity layer over a lower resistivity layer, current flow lines will be bent toward the normal to the interface and as the electrodes are spaced farther and farther apart, more of the current flows to a deeper

and deeper depth. Conversely, for the case of a low resistivity layer overlying a high resistivity layer, the opposite occurs (Telford et. al. 1990).

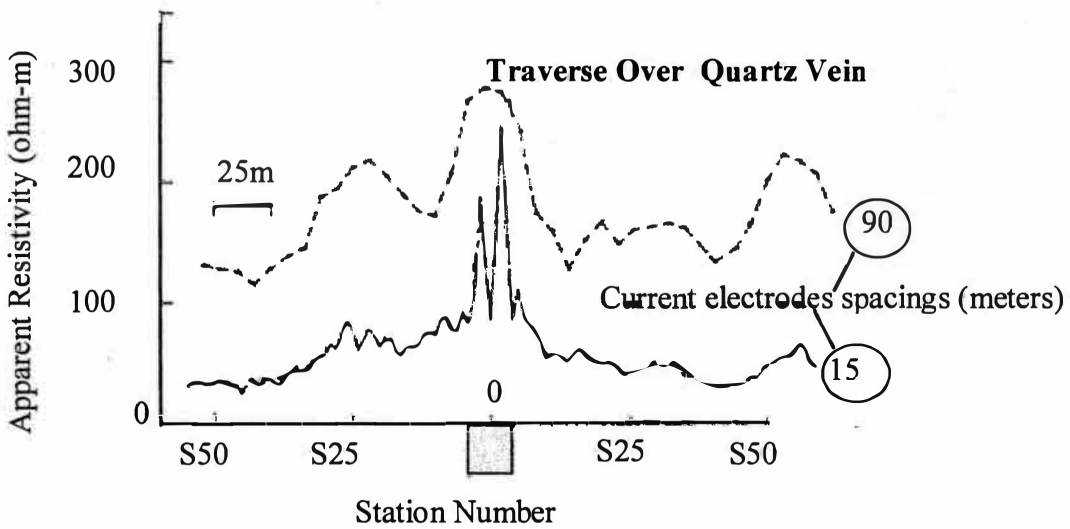

Figure 4. Field Resistivity Profile Over Resistive Quartz Veins, Adapted from Kumar, 1973.

Current Flow Across Vertical Stratigraphic Boundaries

This is the situation that will be simulated with the vertical resistivity probes in the study area. A number of workers like Kumar, (1973). conducted theoretical resistivity profiles across conductive/resistive sheet-like or vertical dykes using parameters such as electrode spacing, vein-width and resistivity contrast. He reported that for a conventional Wenner profile over a conducting/resistive vein, the signature of the anomaly can be of a variety of shapes; but it is important to collect the data at very close intervals in order to observe minor highs and lows. This may be indicative of the thickness of the veins, (Figure 4). In the figure above, traverse over the

resistive quartz vein (current electrode spacing of 90m and 15m), the smaller spacing produced a central minimum flanked by two maxima while the larger spacing produced a clear maximum.

Brass et al. (1981) compared field results and theoretical curves obtained from different resistivity arrays over a graphite deposit. He suggested the use of medium spacing, arguing that minimas and maximas seen over geologic bodies with small electrode spacing are due to inhomogeneities of the overburden, and target resolution decreases with increasing electrode spacing.

Induced Polarization

The effect known as induced polarization was first detected by Schlumberger, (1920). The method over the years was applied in prospecting for disseminated sulfide and base metals. Most recently, induced polarization has been applied to detection of contaminants and in the environmental industry (Vanhala et. al., 1992; Olhoeft, 1992; Ward et al., 1995).

Induced polarization is similar to and is an extension of the resistivity method. The arrangement for taking measurement is the same as resistivity. The method involves measurement of the slow decay of voltage in the ground after current has been turned off.

It has been established that two main phenomena, electrode polarization and membrane polarization, cause induced polarization effects.

Electrode Polarization

Metallic minerals disseminated in the earth cause electrode polarization. Movement of ions in electrolytes usually carries the current in the ground. At the mineral-electrolyte interface, the ions accumulate because of the delay required for conversion of the mode of conduction from ionic to electronic (oxidation and reduction reactions). On current termination, the built up charges return to equilibrium by redistributing themselves back into the electrolyte. The polarization effect causes the equivalent resistance of the mineral to increase with time, (Figure 5).

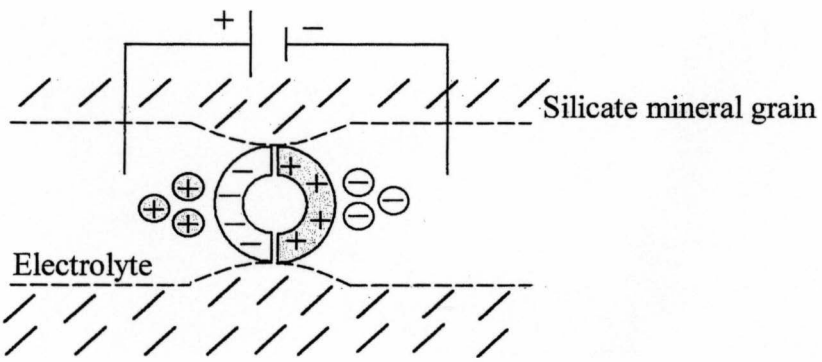

Figure 5. When Pore Space is Blocked by Metallic Particles, Electrode Polarization Occurs and Charges Accumulate on Application of an Electric Field.

Membrane Polarization

Membrane polarization is usually associated with clays. The surface of clay minerals is normally negatively charged. When in contact with electrolyte, the positive charges

in the electrolyte accumulate next to the negative charges of the clay. This build up of charges can be up to two or three layers so that they now repel any other positive charge. On cessation of the excitation current, the ions return to their equilibrium state and this redistribution of charges constitute the voltage to be measured, Figure 6.

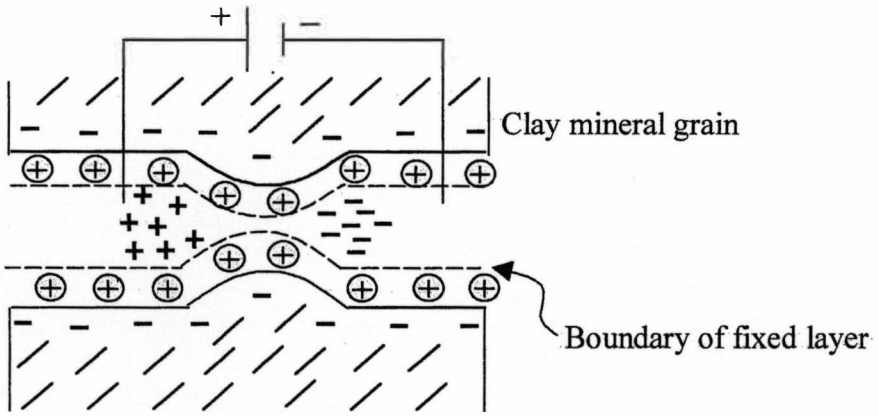

Figure 6. Charge Build up When an Electric Field is Applied to a Porous Layer with Pores Several Sizes Smaller than the Boundary Thickness, Resulting in a Net Charge Dipole.

Induced Polarization Measurements

There are three main modes of induced polarization measurements, time domain, frequency domain, and phase domain.

Time Domain

In the time domain mode, current is normally passed into the ground for a specific duration of time (500 ms, 1000 ms or 2000 ms etc.). The current injected is a

square wave (Figure 7), which in the presence of a chargeable (chargeability is the physical property measured) ground, on current termination drops to a small polarizable voltage Vs (Figure 8), and then declines asymptotically to zero. A similar phenomenom occurs when current is switched on. In order to avoid problems of charge build-up, the current pulse is alternately switched to positive and negative polarities.

In practice, non-polarizable electrodes are generally used for the potential electrodes. This is because metallic electrodes in contact with groundwater or any electrolyte in the subsurface generate large contact potentials. Non-polarizable electrodes consist of a metal electrode, for example copper, in contact with a saturated solution of one of its salts, in this case copper sulfate. This is all enclosed in a non-conductive pipe with a porous base.

There are two time domain induced polarization measures or effects that can be measured. The first is a single sample of decay voltage, normalized by peak charging voltage, expressed in millivolts per volt (mV/V). Interest is in the ratio of the decay voltage Vs at a particular time after current cut off to the normal voltage Vp. The delay is to avoid electromagnetic transients, which dominate in the first tenth of a second.

The second, chargeability, is the most common and widely used time domain induced polarization measure. It is defined as the integrated area under an induced polarization curve between times t_1 and t_2, normalized by the primary voltage Vp (Sheriff, 1991).

$M = (1/Vp)\int V_t dt.$, sometimes simplified to milliseconds. (17)

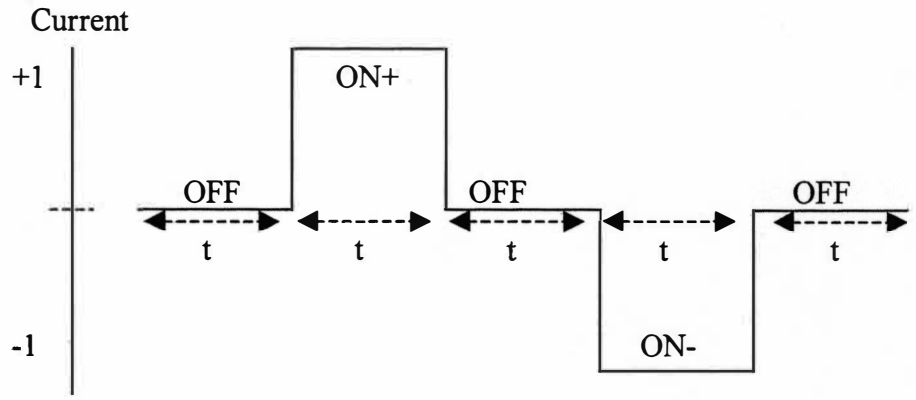

Figure 7. Time Domain Symmetrical Current Waveform with Equal Injection Times.

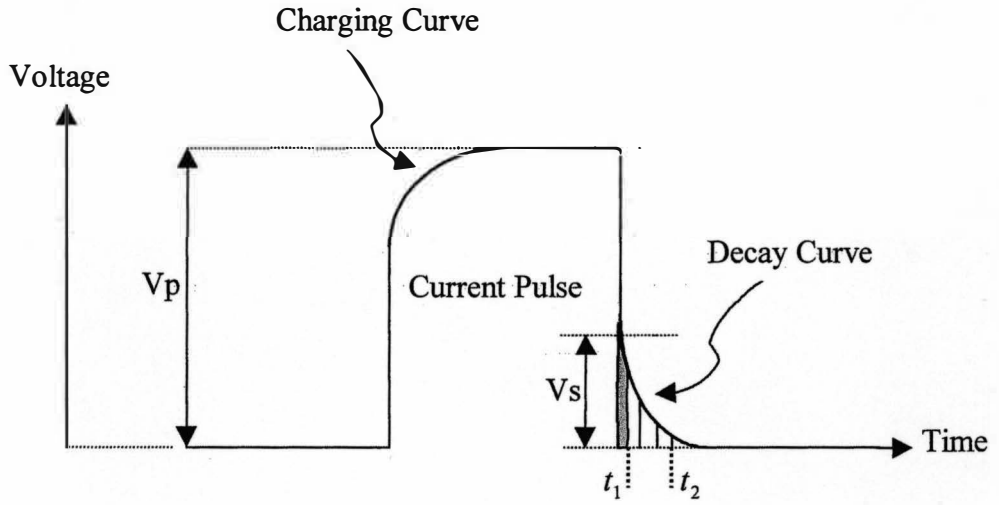

Figure 8. Voltage Charging and Decay Curve Due to a Square Wave Signal. The Shaded area Represents the Time Delay Before Induced Polarization Effects can be Measured and the area Between t_1 and t_2 Represents the Window for Measuring the Voltage Decay.

In the second type of induced polarization measure, current is passed into the ground at two or more different frequencies in other to determine the variation of apparent resistivity with frequency.

The third type of induced polarization is the direct measure of phase lag between the transmitter current and reciever voltage at one or more frequencies.

Measurements in the study area was restricted to time domain so frequency and phase domain effects are not shown here. Time-domain results can be converted to frequency and phase and vice versa by way of Fourier transform theory (Sheriff, 1991).

CHAPTER III

SITE CHARACTERIZATION

Electromagnetic Survey

The main purpose of doing this initial survey was to determine where to install the vertical resistivity probes to be used in the study

The Geonics EM-31-MK2 (Serial number 9522001) Ground Conductivity Meter with its integrated data logging system is an electromagnetic instrument that works on the principles of electromagnetic induction. The transmitter coil of the instrument produces a time varying primary field, which on coupling with the ground induces some current to flow in conducting bodies in the subsurface. The receiver coil of the instrument measures the secondary magnetic field generated by the subsurface circulating currents. Therefore the instrument receiver measures that part of the transmitter signal that is 90 degrees out of phase with the transmitter. The instrument is also capable of measuring the in-phase component of the transmitter signal. The EM31-MK2 instrument has a dipole transmitter and receiver with coils 3.66 meters apart. Quantities measured by the EM-31 are apparent conductivity of the ground in milliSiemens per meter (mS/m) with conductivity ranges of 10 to 1000mS/m, hence it is sometimes called the ground conductivity meter; and an in-phase component measured in parts per thousand and a range of ± 20 parts per

thousand (ppt). The data logger has a capacity of about 8,000 records when reading both components. The instrument can operate in horizontal or vertical dipole modes and can acquire data at a maximum rate of 0.4 seconds for either of the components. A set of functional checks is always performed before using the instrument; (this is as specified by the manufacturers). These checks include adjusting the in-phase reading to zero with a tolerance ± 0.1 ppt; adjusting the conductivity reading to a tolerance of ± of 0.2; and to ensure the sensitivity of the instrument, the conductivity reading should change between 22-26 mS/m when the mode switch is set to compensation position.

The EM31 data were acquired using a line spacing of 10ft along East-West profiles on the 200ft. x 200ft. block (Block 9 in Figure 1); . Data were collected at the rate of 0.4 sec/reading in the vertical dipole mode with fiducial marks at every 20-ft along each of the profile

The ideal location to install the probes should be near an existing well where the stratigraphy is known and where the fluid level as well as the thickness of the light non-aqueous phase liquid (LNAPL) is known. Based on this initial survey, the area near the vicinity of MW-30 was chosen. This monitoring well is known to have free product or LNAPL (0.3 meters thick) and is close to the boundary of contaminated and uncontaminated area, (inferred from EM-31). However, this location has the disadvantage that stratigraphic information is very poor. The drillers log only mentioned odor and gave the depth at which the well was screened (8 ft to 28 ft). Therefore, we can only infer that the free product and any water conductivity

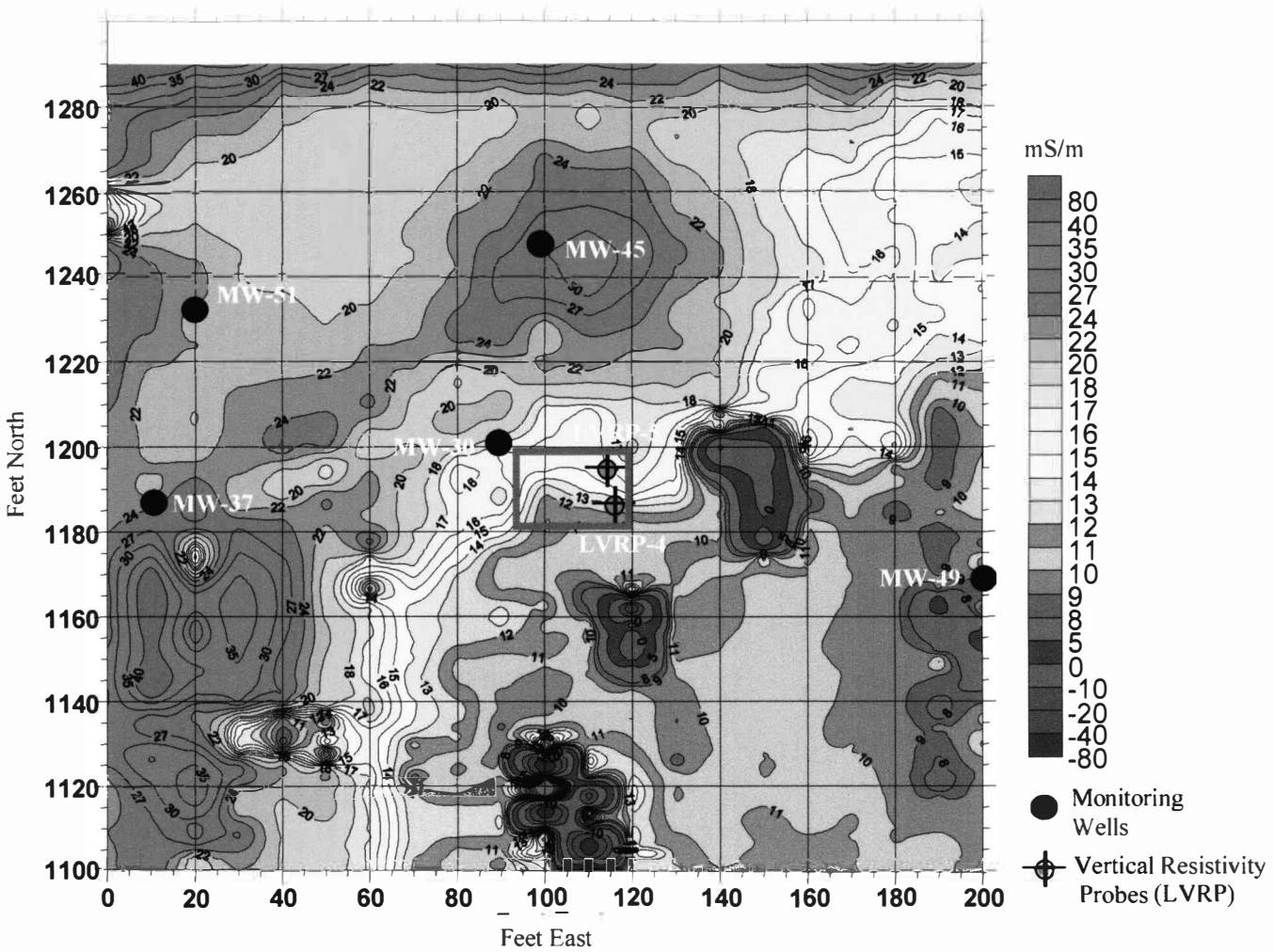

Figure 9. Lakeside, Block 9; EM-31 Conductivity (S-N Lines, Oct. 2000). Box Shows Area for Figure 11.

data is coming from anywhere within this depth range. In order to accurately define the boundary between the contaminated and clean sediments, a 20-ft x 25-ft block east of MW-30 was therefore further surveyed with EM31-MK2 using a line spacing of 5 feet and the result shown in Figure 11. To make the vertical resistivity probes cross this boundary, single lines were run slowly and carefully in the North-South and East-West directions. The vertical resistivity probes were eventually installed at either side of this boundary along a nearly North-South orientation and 5 ft apart, (Figure 12).

Data Treatment

The field data were downloaded to a PC via a DOS-based program, Geonics MK2. Then the file was accessed and edited with a Geonics M2K Windows-based program, DAT31W. The program creates an ascii data file, from the original binary file which is exported to SURFER. A contour map is generated after re-sampling to a uniform grid.

During editing the field geometry was corrected for marker positions (20 ft; 10 ft and 4 ft intervals, respectively) that resulted from variations in walking speed of the operators. The next correction involved setting the line limits as defined during field data acquisition (left = 200 ft, right = 400 ft). The data levels of the in-phase component were shifted accordingly in order to start from zero in the graphical displays. The quadrature data levels are usually more stable and therefore left unchanged. The gridding type used was Kriging. Grid parameters used included grid

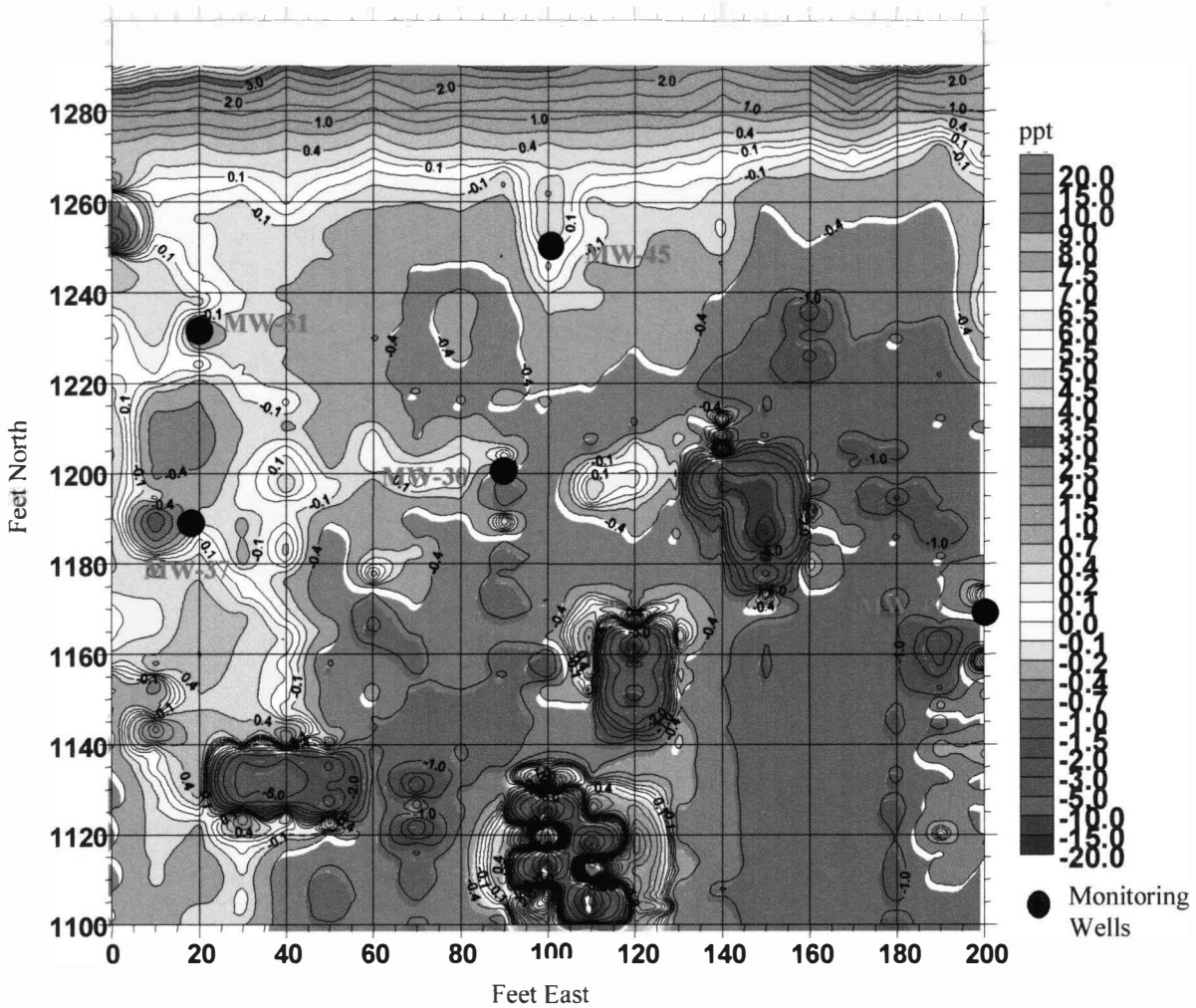

Figure 10. Lakeside, Block 9; EM-31 In-Phase (S-N Lines, Oct. 2, 2000).

intervals of 2.5 ft; 1.25 ft; and 0.5 ft, respectively, and search radii of 30 ft; 15 ft; and 6 ft, respectively.

Results and Discussion

A map of terrain conductivity, in milliSiemens per meter, (Figure 9) and a map of in-phase (metal detection, in parts per thousand, Figure 10) anomalies were produced for the 200ft x 200ft block. In general, the terrain conductivity map shows the northeast and western part of the block to be more conductive (14 mS/m to > 80 mS/m). The western part is where the capture and monitoring wells installed by Malcolm-Pirnie (Company contracted by the MDEQ to clean up the site) as part of their remediation system are located. It is also lower in elevation and therefore some of the high conductivities could be contribution from a shallow water table. The high conductivities observed in the northeastern part of the block could be due to the presence of clays and the effect of contamination. The drillers log from MW-45 describes the samples recovered during drilling as brown-black-gray petroluem soaked silty sand clay. This is between 1.2 meters to 2.7 meters depth. The Southeastern part of the map with conductivities of 10 mS/m or less is mainly wooded and served primarily as a dump site for scrap metals, concrete, fence wires, pipes, fuel hoses, etc. During the preparation of this site, most of these surface metals were collected and dumped at the southern part of the map (location:100 East, 1120 North). This is because this part of the area already has partially buried fence-wires and pipes that could not be removed. The in-phase (metal detection) map, being more

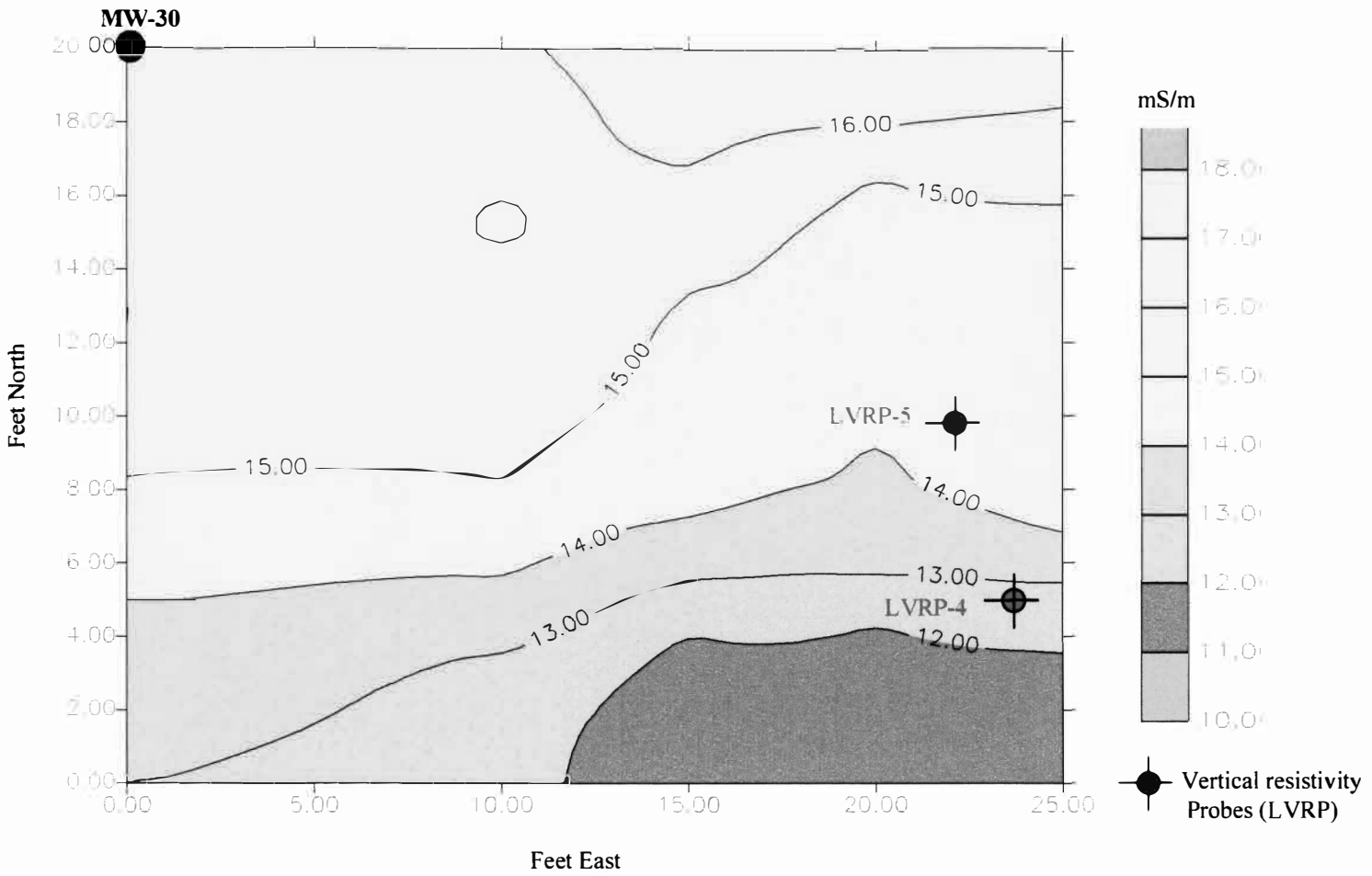

Figure 11. Lakeside, EM-31 Conductivity S-W of MW-30, Block 9, (S-N Lines, Nov. 2000).

sensitive to shallow metals, was able to discriminate against the dumped pile of metals and some monitoring well covers. The other anomalies shown on this map are from scattered surface metals.

Laboratory Measurement of Resistivity

This was done in order to measure directly the true resistivity of the samples. The importance of these laboratory measurements is that they will serve as an independent check against the resistivity distribution with depth recorded by the vertical resistivity probes to be installed in both boreholes.

Sample Preparation

Two-foot split spoon samples from the two boreholes drilled were collected and stored in glass jars. Distilled water was later added to the samples to ensure total saturation and facilitate current transmission. This is to accommodate for moisture loss that occurred before measurements could be taken. The samples were left in this condition overnight in a 100% humidity environment. This was done to minimize fluctuation in electrical resistance reading between measurements.

Equipment

An Iris Syscal R-2 resistivity meter, a 6 volt power source, a gallon of distilled water, filter papers, four steel wire meshes cut to match the cross-section of the

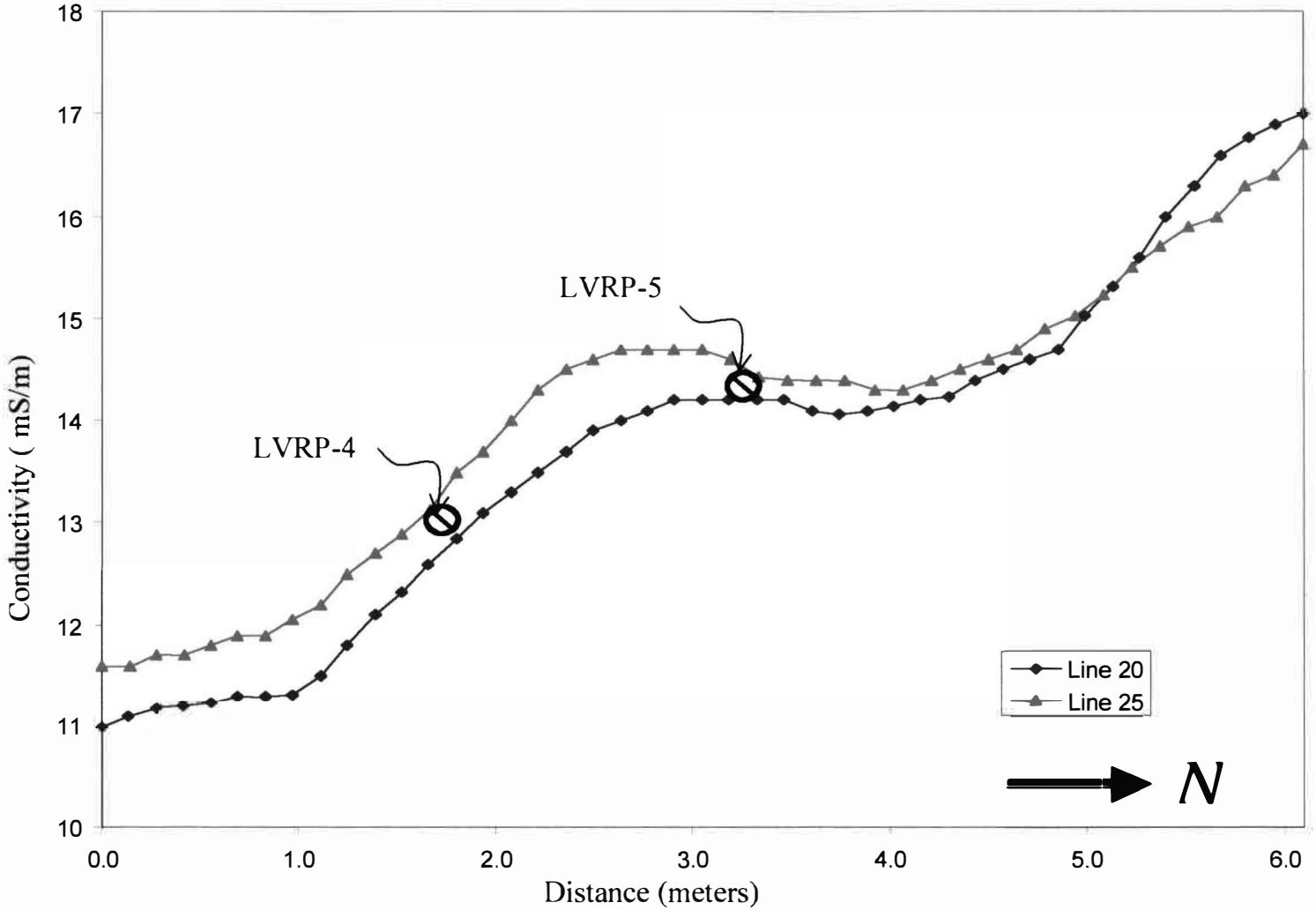

Figure 12. Conductivity Profiles Along Lines 20-East and 25-East of Figure 11.

samples, copper wires, and a pair of 75 k-Ohm resistors attached to the current input wires were the equipment used

Method

A 75 k-Ohm resistor was soldered in series in the current wires, which were then attached to two of the steel wire meshes. The remaining copper wires were similarly attached to the other two steel wire meshes and served as the potential electrodes (Figure 13). A pair comprising one current and one potential electrode separated by filter paper was then set at the bottom of the glass beaker. A split-spoon sample from one of the glass jars was then dropped into the 250 ml glass beaker, crushed and compressed to fit the mould of the beaker. This is done to shape the sample into regular cylindrical form and ensure good electrical contact between sample and electrodes. Similarly, the second pair of electrodes separated by a filter paper was placed on the cylindrical sample and an insulated weight put on top to provide good contact. The length and cross-sectional area of the sample in the beaker were then measured.

This assembly was then enclosed in a plastic bucket into which additional water was added to maintain 100% humidity. The experimental assembly was then left to sit for 10 minutes after which the setup was attached to the resistivity meter to take the first set of readings. Thereafter, readings were taken at 10-minute interval until there was less than 10% change between successive readings. This procedure was repeated for all the samples.

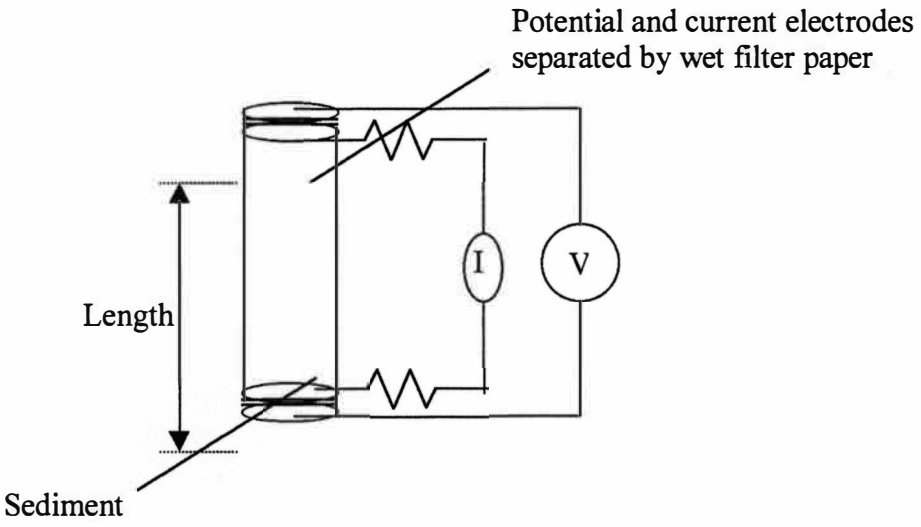

Figure 13. Laboratory Measurement of Resistivity of Sediment.

Results

The measurement from the resistivity meter gave voltage (V)/current (I), which is resistance. To measure resistivity, the length (L) and cross-section (A) of each sample was included to give:

$$\text{Resistivity } (\rho) = VA/IL \tag{18}$$

The result is presented in Tables 1 and 2.

Since the samples are from continuous cores from grade to total depth, a semilog plot of depth versus resistivity is shown on Figure 14. It must be stressed that this experiment was designed to give only the bulk resistivity of the sections

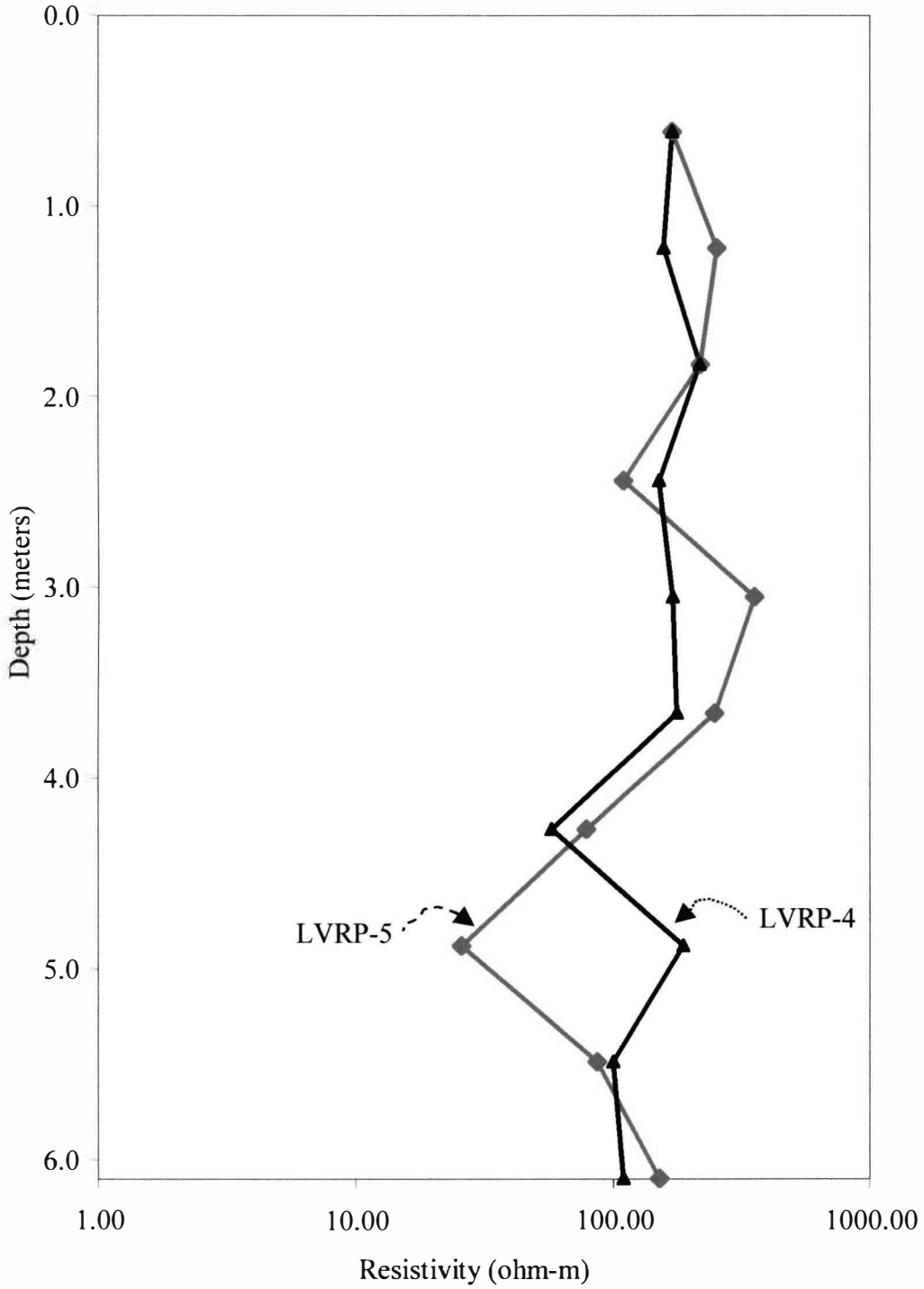

Figure 14. True Resistivity Vs Depth for Core Samples From LVRP-5 and LVRP-4.

Table 1

Laboratory Resistivity Measurements for LVRP-4

Depth (meters)	V/I (ohms)					Average (V/I)	Lithology	Length (m)	Radius (m)	Area (m2)	ρ =VA/IL
0-0.6						na	clay		3.00E-02	2.83E-03	na
0.6-1.2	1086	1193	1099	1098	1097	1114.6	clay	2.00E-02	3.00E-02	2.83E-03	157.59
1.2-1.8						na	clay		3.00E-02	2.83E-03	na
1.8-2.4	1583	1583	1621	1634	1609	1606	sand+gravel	3.00E-02	3.00E-02	2.83E-03	151.38
2.4-3.0	2125	2104	2113	2122	2092	2111.2	sand+gravel	3.50E-02	3.00E-02	2.83E-03	170.57
3.0-3.6	2317	2244	2226	2283	2221	2258.2	sand+gravel	3.60E-02	3.00E-02	2.83E-03	177.38
3.6-4.2	715	718	717	713	703	713.2	sand	3.50E-02	3.00E-02	2.83E-03	57.62
4.2-4.8	2535	2672	2661	2678	2688	2646.8	sand	4.00E-02	3.00E-02	2.83E-03	187.12
4.8-5.4	1258	1286	1281	1262	1301	1277.6	sand	3.60E-02	3.00E-02	2.83E-03	100.36
5.4-6.0	1556	1726	1692	1673	1724	1674.2	sand+gravel	4.30E-02	3.00E-02	2.83E-03	110.10

Table 2

Laboratory Resistivity Measurements for LVRP-5

Depth (meters)	V/I (ohms)					Average(V/I)	Lithology	Length(m)	Radius(m)	Area	$\rho = VA/IL$
0-0.6	2231	2224	2232	2226	2209	2224.4	clay	3.70E-02	3.00E-02	2.83E-03	170.00
0.6-1.2	2576	2698	2762	2734	2669	2687.8	clay	3.00E-02	3.00E-02	2.83E-03	253.35
1.2-1.8	1835	2340	2378	2298	2363	2242.8	clay	2.90E-02	3.00E-02	2.83E-03	218.70
1.8-2.4	1103	1196	1176	1169	1180	1164.8	sand+gravel	3.00E-02	3.00E-02	2.83E-03	109.79
2.4-3.0	4404	3813	3897	3664	3786	3912.8	sand+gravel	3.10E-02	3.00E-02	2.83E-03	356.92
3.0-3.6	3063	3083	3125	3075	3047	3078.6	sand+gravel	3.50E-02	3.00E-02	2.83E-03	248.73
3.6-4.2	1027	1022	1023	1016	1054	1028.4	sand	3.70E-02	3.00E-02	2.83E-03	78.60
4.2-4.8	820	814	815	816	815	816	sand	9.00E-02	3.00E-02	2.83E-03	25.64
4.8-5.4	1691	1688	1677	1687	1683	1685.2	sand	5.50E-02	3.00E-02	2.83E-03	86.64
5.4-6.0	2054	2046	2045	2038	2040	2044.6	sand+silt	3.80E-02	3.00E-02	2.83E-03	152.15

measured. Therefore the interpretation of the results from this experiment will only be in terms of the conductivity or resistivity of the sections.

Both plots in general show a similar trend; higher resistivity associated with the vadose zone down to a depth of about 1.8 meters. At a depth of 2.4 meters, both curves show a slight decrease in resistivity to about 100 Ohm-meters. Thereafter the resistivity increased up to a maximum of 328 Ohm-meters for LVRP-5 and 218 Ohm-meters for LVRP-4. This increase occurred between 2.4 to 3.7 meters for LVRP-4 and 2.4 to 3.0 meters for LVRP-5. From the field description of samples (appendix A), these are the depths at which odor from the hydrocarbon contamination was first detected. Below these depths, low conductivity zones are encountered. LVRP-5 shows a minimum resistivity of 25 Ohm-meters which coincides with the water table as measured during drilling (water table was at 4.85 meters). Note, the length of the sample recovered between 4.2 and 4.8 meters (LVRP-5) is unusually longer than the other samples. The sample was a compact unit and not loose as some of the other recovered samples. The profile from LVRP-4 shows a minimum of 57 Ohm-meter at a depth of about 4.2 meters. This did not coincide with the water table (water table was at 4.57 meters). This may, of course, be as a result of poor sample recovery during drilling. Another contaminated section occurs between 5.5 to 6.1 meters, which was described in the field drilling log sheet (Appendix A).

Grain Size Analysis

The purpose of the grain size analysis was to classify the core samples according to whether they are gravels, sands or fines (clays and silts). Statistical analysis was carried out to determine their degree of sorting and ultimately have an idea of derived textural properties, such as porosity, which affect the flow of current and consequently apparent resistivities values from the vertical resistivity probes.

Method

Continuous core samples at two feet intervals were collected from grade to total depth (20 feet) for each of the boreholes drilled. The samples were first dried in an oven set at a temperature of 75 degrees Celsius for a period of 72 hours. Subsequently each of the samples was crushed and weighed. To obtain information on the grain-size distribution, each of the crushed samples was passed through a set of sieves selected to achieve the desired lithological classification. The sieve numbers selected according the U.S. standard sieve classification were #230, #100, #60, #35, #18, #10 and all sizes less than the #230 sieve size were classified as fines. The sieves were stacked in such a way that the coarsest sizes are retained at the top and the finest sizes retained in the bottom sieve. According to the Wentworth scale, developed in 1922, particle sizes retained in the #10 sieve are classified as gravels; particles retained between #10 and #230 sieves are sands ranging from coarse to very fine and particle sizes passing through the #230 sieve were classified as fines.

This classification is achieved by shaking the stacked set of sieves in a vibratory machine for 10 minutes. The particle sizes retained in each of the sieves are carefully weighed and the weight recorded as a percentage of the whole sample. This procedure was repeated for each of the core samples.

The graphic measures used in the statistical analysis of the data were those defined by Folk and Ward (1957) where the graphic mean is given by:

$$(\phi_{16} + \phi_{50} + \phi_{84})/3 \tag{19}$$

And the standard deviation is given by:

$$(\phi_{84} - \phi_{16})/4 + (\phi_{90} - \phi_{5})/6.6 \tag{20}$$

The graphic mean describes the lithology according to the Wentworth scale (Table 3.), while the graphic standard deviation describes the degree of sorting.

The descriptive terms used by Folk and Ward (1957) for standard deviation based on phi units is given below:

<0.35ϕ	Very well sorted
0.35ϕ to 0.50ϕ	Well sorted
0.50ϕ to 0.71ϕ	Moderately well sorted
0.71ϕ to 1.00ϕ	Moderately sorted
1.00ϕ to 2.00ϕ	Poorly sorted
2.00ϕ to 4.00ϕ	Very poorly sorted
>4.00ϕ	Extremely poorly sorted

Table 3

Grain-size Classification (modified from Boggs, 1995)

U.S Standard Sieve Mesh	Millimeters	Phi (ϕ) Units	Wentworth Size Class
	4096	-12	
10	2.00	-1	Gravel
18	1.00	0	Very coarse sand
35	0.50	1	Coarse sand
60	0.25	2	Medium sand
120	0.125	3	Fine sand
230	0.0625	4	Very fine sand
	0.0039	8	Silts
	0.00006	14	Clays

The phi (ϕ) unit is based on a logarithmic phi scale proposed by Krumbien, 1934:

$$\phi = - \log_2 S \qquad (21)$$

Where ϕ is phi size and S is grain-size in millimeters. This scale allows graphical plotting and statistical calculations of grain size data.

Result

The result of this analysis is presented in Figure 15. The result shows that the lithology ranges from very fine sand to coarse gravel in both boreholes. An important observation from the analysis is the absence of clay in any significant quantities to warrant its classification, however the first 1.8 meters from the surface has significant amount of fines (which are composed of silts and clays). This is important because clay minerals in the presence of moisture affect current flow and ultimately resistivity/conductivity measurements. This observation will be taken into account in the interpretation of resistivity inversion results from the boreholes.

Another important observation is variation in lithology between both boreholes. This is despite the fact that they are only 1.5 meters apart. This variation is also supported from the split-spoon blow counts recovered during drilling (Appendix B). The blowcounts are indicative of how loose or compact the material being penetrated is. Any sudden increase or decrease in the number of blows can be associated with a change in lithology. The blow counts from both boreholes

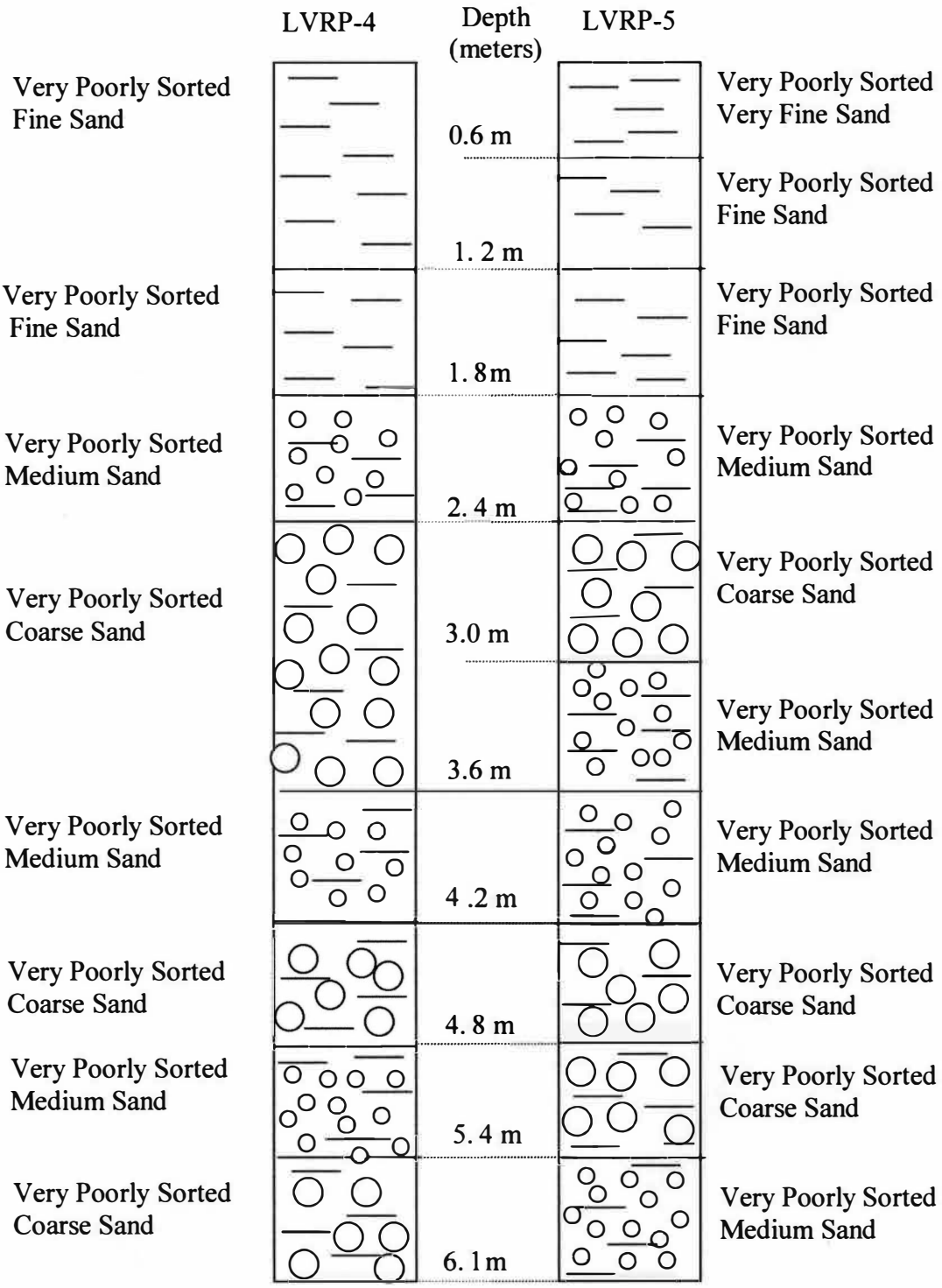

Figure 15. Lithology Based on Grain-Size Analysis.

(Appendix B) exhibits these increases and decreases but at different depth intervals thereby supporting the observed lateral variation in lithology as calculated from the grain size analysis.

CHAPTER IV

METHODS

Vertical Resistivity Probes Design

Vertical resistivity probes are stainless steel screws mounted on the outside of a polyvinylchloride (PVC) pipe. The screws (electrodes) are aligned at two-inch intervals, which allows for dense sampling if needed. Current can be injected through these electrodes and the potential measured using any source and receiver combination

Previous studies (e.g. Schneider and Greenhouse, 1992; Sauck, 1998; and Atekwana et al, 2000) reported on experiments with VRPs for the purpose of detecting light non-aqueous phase liquids contaminations.

The design used in this study is modeled after Groncki, 1999, whose design improves on earlier ones with removable four-contact inner probes built by Sauck (of Western Michigan University). This inner sliding probe is used to establish contact with four electrodes at a time inside the PVC.

The PVC pipes used in this study have an outer diameter of two inches and come in 10 foot-threaded sections. Holes were first drilled at the same time into the PVC pipes, and 1/8 inch thick by 1/4 inch wide plastic strips. All electrical wirings were done on these plastic strips.

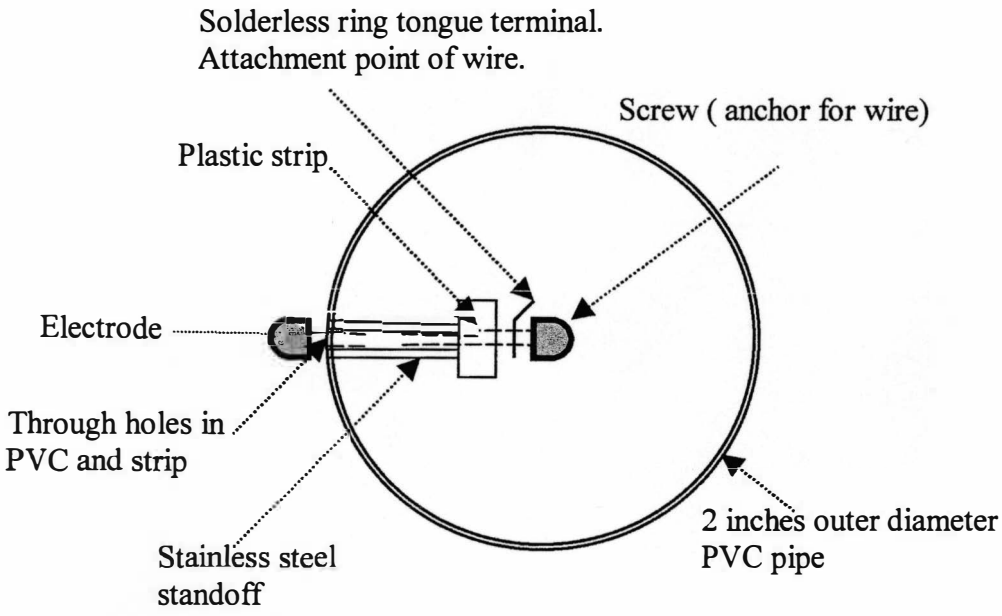

Each wire is first crimped into a solderless ring tongue terminal. The electrodes are then screwed through this terminal and the plastic strip into a threaded

Figure 16. Plan View of VRP Installed in Study Area. Drawings are Schematic and do not Represent Actual Thicknesses or Dimensions.

stainless steel standoff (Figure 16). The standoff ensures electrical continuity between the inner screws and the outer screws (electrodes) which makes contact with the formation. It also functions as an alternative to cutting slots on one side of the PVCs to do the electrical wirings. These slots compromise the structural integrity of the PVC pipes and are prone to leakage after installation in the subsurface thereby contaminating the data eventually sought from the probes. A special kind of water resistance sealant that is not affected by gasoline or oil was used to seal around the holes and threaded joints before coupling the PVC sections.

The wire attached to each of the screws is color coded for easy numbering. The numbered and color-coded wires are hard-wired into a 50-pin communication plug. A matching bundle of the same color-coded wires and plugs completes the connection between the electrode and the surface switch box and measurement instrument.

Borehole Effects

The way in which a test hole or well is drilled, completed and tested has a significant effect on geophysical logs made in that well (Hodges and Teasdale, 1991). VRPs are like galvanic logging tools in that the measuring device is hoisted downhole, or in the case of VRPs, at least in this study, permanently installed in the subsurface.

Drilling processes disturb the formation and fluids adjacent to the drill hole. According to Keys, (1997), borehole effects on geophysical logs can be categorized as those produced by drilling fluid, mudcake, borehole diameter changes and well construction materials. This creates distinct measurement volumes known as zones. In the study area, these zones may include the flushed, invaded and undisturbed zones (Figure 17), which may have resulted from the bentonite-sand mixture used to backfill the hole after installation of the probes.

Every resistivity measurement will therefore be the sum of contributions from each of these zones. The contributions will depend on the geometry of the system being used according to the following equation from Hallenburg, (1998):

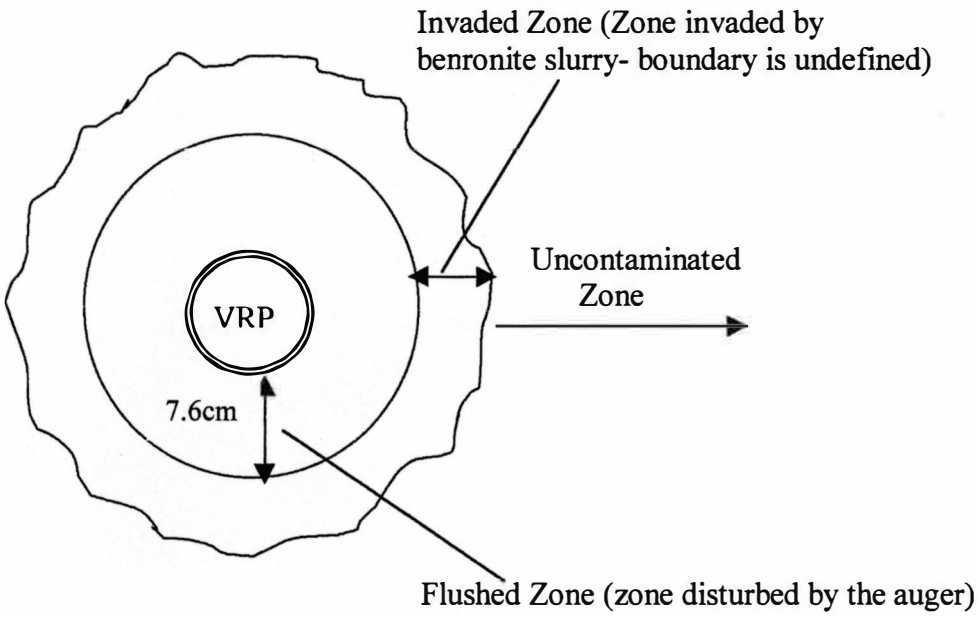

Figure 17. One Dimensional Invasion Geometry.

$$R_a = G_f R_f + G_i R_i + G_u R_u \quad (22)$$

Where R_a = the apparent resistivity

G = the geometric factor

Subscript f, i, and u stand for flushed, invaded, and undisturbed zones.

In the study area, longer spacings of 0.3 meter between the current and potential electrodes were employed to investigate further out into the formation, thereby minimizing the conductivity contribution from the backfill material.

Resistivity and Induced Polarization Measurements

The instrument used in acquiring data in the study area is the Iris Syscal R-2 resistivity and induced polarization system. The instrument measures lateral and vertical distribution of resistivity within geologic bodies, (It has three modes of operation: Transmitter-Receiver Time Domain for resistivity and induced polarization, Transmitter-Receiver Frequency Domain, and Transmitter-Only Domain). Various electrode arrays are available: Schlumberger, Wenner, gradient and Dipole arrays. The internal memory can store up to 1022 readings with full information including current, voltage, chargeability, geometric parameters and station number. The instrument has the ability to continuously stack readings to minimize noise.

In the study area, data were acquired in the Transmitter-Receiver Time Domain mode in order to simultaneously record resistivity and induced polarization parameters (chargeability) with an equal time on, time off injection and relaxation time. The pulse duration used in all the measurements is 2000 milliseconds which, according to the manufacturers, gives the best quality of measurement. The instrument automatically determines the time from which samples will be taken, the delay time for the induced polarization curve, and the delays before the induced polarization sampling points, all in units of milliseconds (Figure 18).

The chargeability (M) calculated by the system is a weighted average of the average partial apparent chargeabilities (M1, M2, M3, and M4) of four IP windows. This is expressed as follows:

$$M = \frac{120 \cdot M1 + 220 \cdot M2 + 420 \cdot M3 + 820 \cdot M4}{120 + 220 + 420 + 820} \tag{23}$$

Where the M-values are expressed in mV/V.

The chargeability values can be downloaded from the Syscal as raw values or values normalized with respect to a standard decay curve. The numbers appearing in the numerator and denominator represent the width of the IP windows shown in the figure above, expressed in milliseconds (ms).

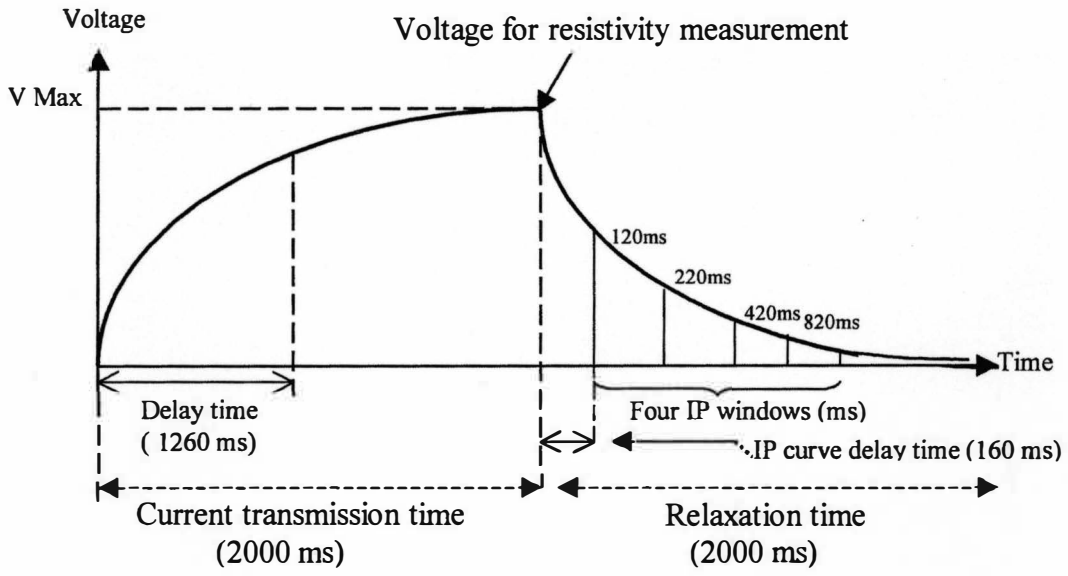

Figure 18. Schematic of Induced Polarization Curve showing Transmission and Relaxation Time Parameters used in Study Area.

The power source used to drive the current electrodes was from a 6-volt direct current supply. Each data point was stacked four times to reduce noise and stored on

the system. The option for the type of electrode array selected from the system measures only the raw value of V/I (resistance in Ohms). This is necessary because a majority of the measurement to be done involve cross-hole measurements with arrays of different configurations. All the arrays and configurations of electrodes are, however, variants of the four electrode scheme introduced earlier. The apparent resistivities to be calculated will therefore be the product of the resistance and a geometric factor in a full space.

Single Hole Resistivity and IP Measurement Arrays

Pole-Dipole

For this array, one of the current electrodes is placed at infinity on the surface. The effect from this remote electrode is assumed to be negligible. The spacing between the potential electrode is represented as "a" and "na" represents integer multiples of the potential electrodes spacing. Current is injected through electrodes A and B (at infinity, not shown) and the potential measured between M and N electrodes.

Measurement was acquired by profiling from surface to total depth of 6.1 meters using "a" and "na" spacing of 5, and 10 centimeters (that is, n = 2). Data were collected over a period of 4 months. During this period, readings from electrodes with poor signal to noise ratio were deleted and not used in presenting the results. The formula for calculating the apparent resistivity (ρ_a) of this common array is based on the configuration given below (Figure 19) is:

$$\rho_a = 4\pi an(n+1)\frac{V}{I} \qquad (24)$$

Units are in Ohm-m and the data is plotted as apparent resistivity versus depth.

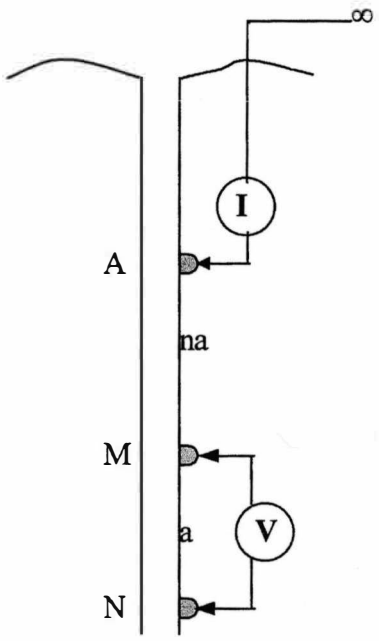

Figure 19. Configuration for Pole-Dipole.

Wenner

This is one of the more widely used "standard arrays" with equal spacing between all the electrodes. Spacing used in acquiring data in the study area are 5 and 10 centimeters. The measurement was repeated over a period of 3-4 months until the measurements were repeatable. During this period, readings from electrodes that

made bad electrical contact with the formation were identified and deleted during data processing.

The formula for calculating the apparent resistivity (ρ_a) of this array is based on the configuration given below (Figure 20):

$$\rho_a = 4\pi a \frac{V}{I} \tag{25}$$

Result are presented as apparent resistivity against depth on a log-linear plot

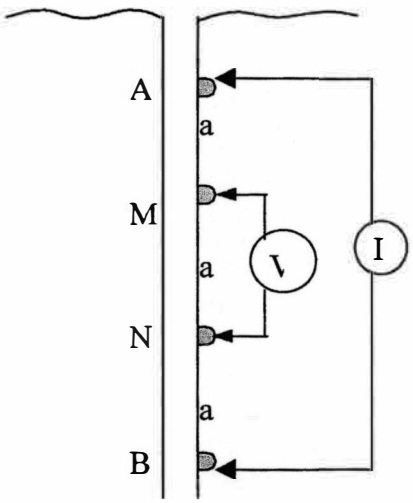

Figure 20. Configuration for Wenner Array.

The use of 4π in the above formulas is for simplicity. In reality, when the array is near the surface, a value of 2π should be used. When the depth exceeds several "a" spacings, this value progressively increases to 4π.

Cross-hole Resistivity and IP Measurement Arrays

Cross-hole Pole-Pole

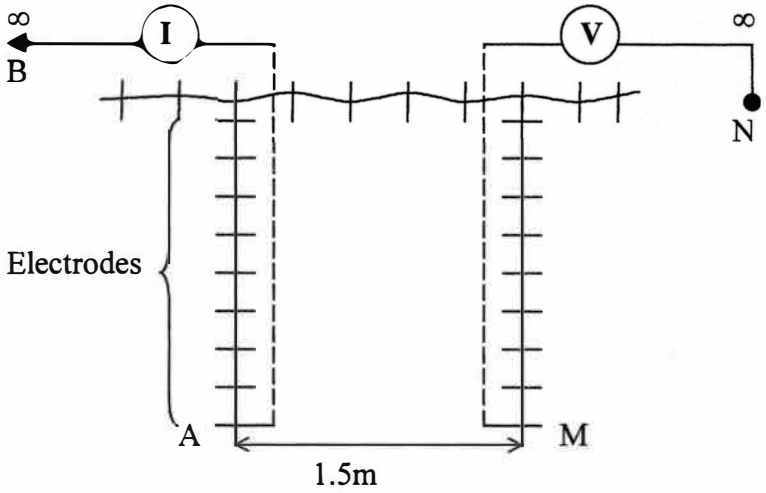

Figure 21. Cross-hole Pole-Pole Array.

In this configuration, one of the current electrodes and one of the potential electrodes are placed at infinity on the surface. In the diagram above, surface electrodes are included because the inversion software used for this study requires surface electrodes in order to successfully carry out the inversion routine. The cross-hole pole-pole data were acquired by taking each of the electrodes as a current source and all other electrodes as receivers. A total of 800 data points were recorded from the near surface to total depth of 6.1 meter. Data points were at every 0.3-meter. The formula for calculating the apparent resistivity (ρ_a) is:

$$\rho_a = 4\pi a \frac{V}{I} \tag{26}$$

Where a=0.3 meter

Cross-hole Dipole-Dipole

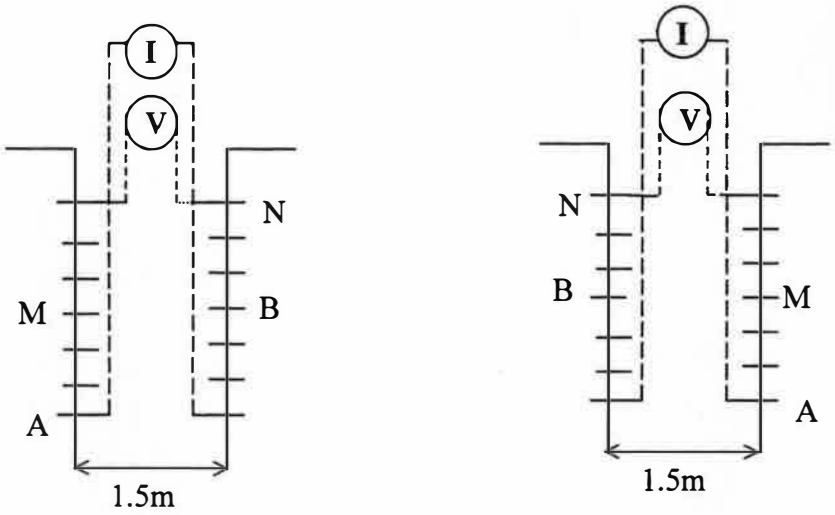

Figure 22. Two Independent Symmetrical Configurations for Cross-Hole Dipole-Dipole. A and B Represent Current Electrodes, While M and N Represent Potential Electrodes. Adapted from Bing and Greenhalgh, 2000.

The separation between AM and BN electrodes is 0.3 meter (Figure 22). For each A-M position, B-N is moved from bottom to top in the second borehole. A-M is then moved up the next level and the measurement repeated. The electrode arrangement is switched in the second borehole and the whole measurement repeated. In this way, all active electrodes serve as sources and receivers. The measurements were also presented as a log-linear plot of apparent resistivity versus depth.

To calculate the apparent resistivity with such configuration, the geometric factor representing the electrode spacing must first be calculated. From the above diagram, potential developed at M is due to current flow from A to B:

$$Vm_{A-B} = \frac{I\rho}{4\pi}\left[\frac{1}{AM} - \frac{1}{\sqrt{(AM)^2 + (AB)^2}}\right] \tag{27}$$

Where V = voltage (volts)

I = current (amperes)

ρ_a = apparent resistivity (Ohm-m)

Potential developed at N is due to current flow from A to B:

$$Vn_{A-B} = \frac{I\rho}{4\pi}\left[\frac{1}{\sqrt{(AB)^2 + (BN)^2}} - \frac{1}{BN}\right] \tag{28}$$

Potential difference between M and N:

$$\Delta V = Vm - Vn = \frac{I\rho}{4\pi}\left[\frac{1}{AM} - \frac{1}{\sqrt{(AB)^2 + (AM)^2}} - \frac{1}{\sqrt{(AB)^2 + (BN)^2}} + \frac{1}{BN}\right]$$

$$\Delta V = Vm - Vn = \frac{I\rho}{4\pi}\left[\frac{1}{0.3} - \frac{1}{\sqrt{(1.5)^2 + (0.3)^2}} - \frac{1}{\sqrt{(1.5)^2 + (0.3)^2}} + \frac{1}{0.3}\right]$$

$$\Delta V = Vm - Vn = \frac{I\rho}{4\pi}[3.33 - 0.64 - 0.64 + 3.33] \tag{29}$$

$$\Delta V = Vm - Vn = \frac{I\rho}{4\pi}[6.66 - 1.29] \tag{30}$$

$$\Delta V = Vm - Vn = \frac{I\rho}{4\pi}[5.37] \tag{31}$$

$$\rho_a = \frac{4\pi}{5.37}\left(\frac{\Delta V}{I}\right) \tag{32}$$

Measurements were also made using AM, BN spacing of 0.058 meters, but the inversion software (RES2DINV) however could not handle the number of electrodes involved in each borehole (122 electrodes), the software can only handle up to a maximum of 64 electrodes in each borehole.

Cross-hole Pole-Dipole

In a Cross-hole Pole-Dipole Array (Figure 23), one of the current electrodes is placed at infinity. The distance between A and M is 0.3 meters. For each A-M position, N is moved from top to bottom at 0.3-meter intervals. The electrodes are then switched and the measurement repeated. A total of 720 data points were recorded from a depth of 0.6 meter to 6.1 meters. The geometric factor used in calculating the apparent resistivity is calculated as above but each data point requires a different geometric factor as electrode N moves from top to bottom.

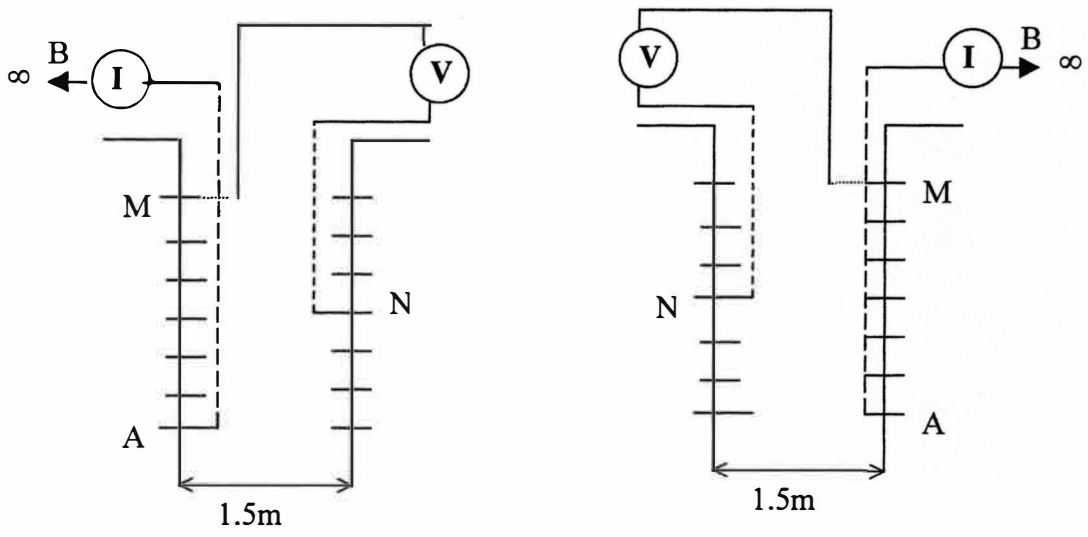

Figure 23. Cross-Hole Pole-Dipole Array.

Cross-hole Dipole-Pole

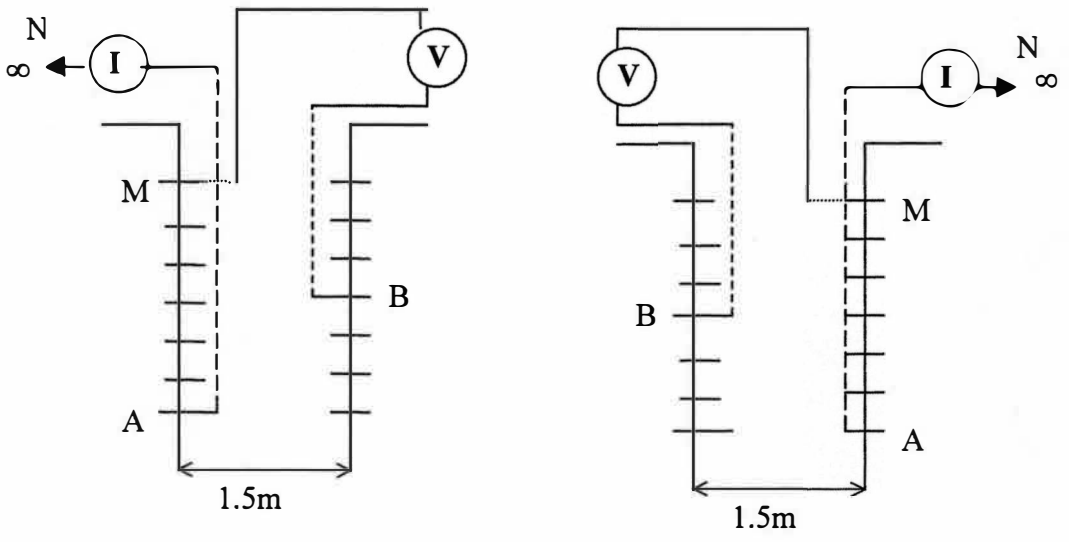

Figure 24. Cross-Hole Dipole-Pole Array.

Here, one of the potential electrodes is placed at infinity. The distance between A and M is 0.3 meters. For each A-M position, B is moved from top to bottom at 0.3-meter intervals. The electrodes are then switched and the measurement repeated. A total of 720 data points were recorded from a depth of 0.6 meter to 6.1 meters. The geometric factor for this array is calculated in a similar way as that of the pole-dipole configurations.

CHAPTER V

RESULTS AND DISCUSSION

Vertical Resistivity Measurements

Pole-Dipole and Wenner Arrays

Results from vertical pole-dipole array collected at various times using 5cm and 10cm potential electrode spacing are presented in Figures 25-28, Figures 25 and 26 show the results from both probes using two different arrays while Figures 27 and 28 compare the use of two different electrode spacing. Figure 25 represents the profiles from LVRP-4. This is located in the less contaminated (from EM-31 terrain conductivity map (Figure 11 and 12) and drilling log (Appendix A)) area of the two probes. Figure 26 shows the apparent resistivity versus depth obtained from LVRP-5. This profile shows lower resistivity values between 1.2m-2m than results from the previous probe. The maximum resistivity reached within this section is about 80 Ohm-m compared to about 260 Ohm-m for LVRP-4. The residual to free product color gradation ranges from dark brown to gray to black. At the residual product to water table (3.1-4.8m) interval, the resistivity profile from this probe also show values higher by 10-20 Ohm-m.

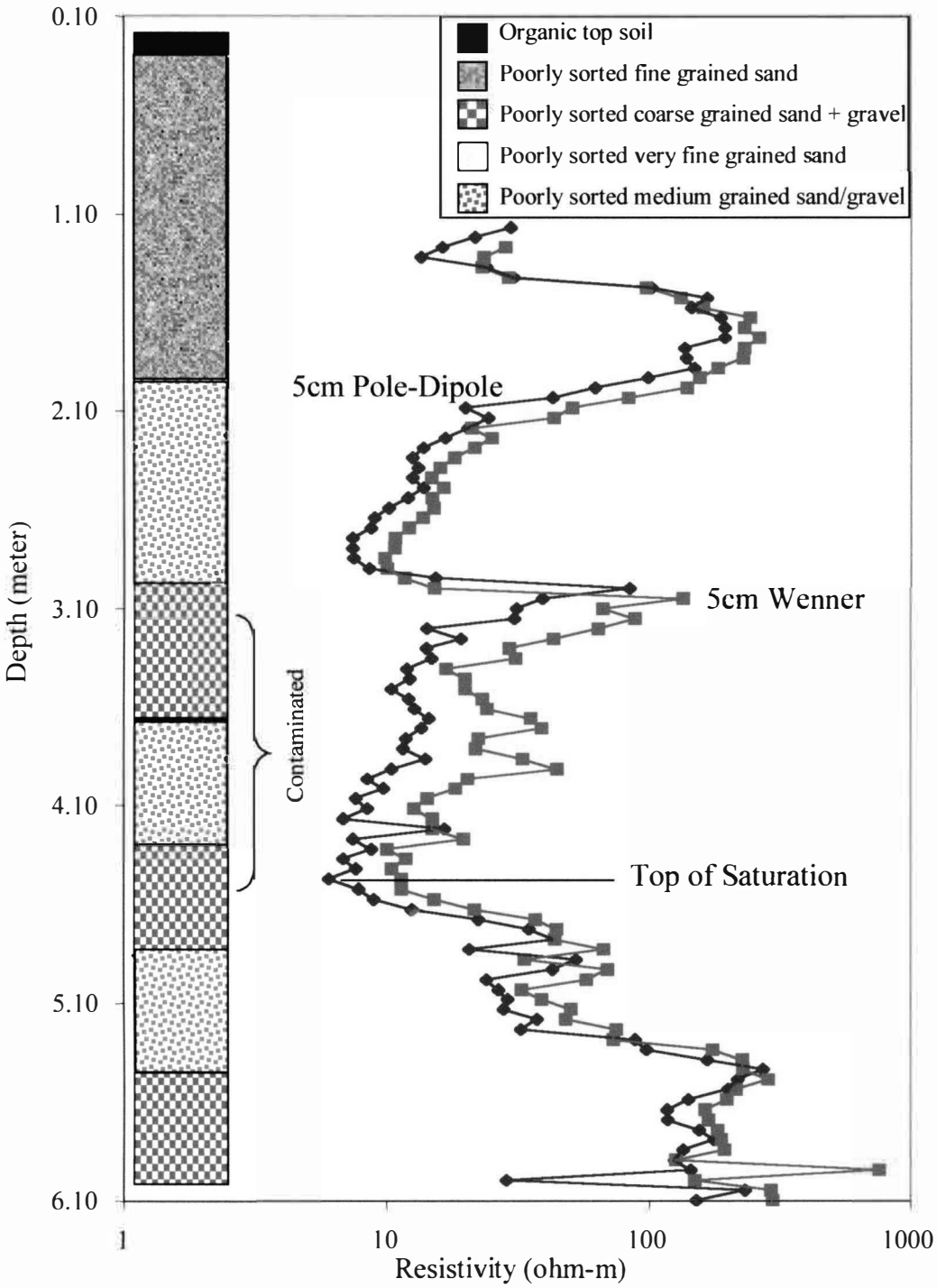

Figure 25. Vertical Resistivity Profile for Wenner and Pole-Dipole Array Using 5cm Spacings, LVRP-4.

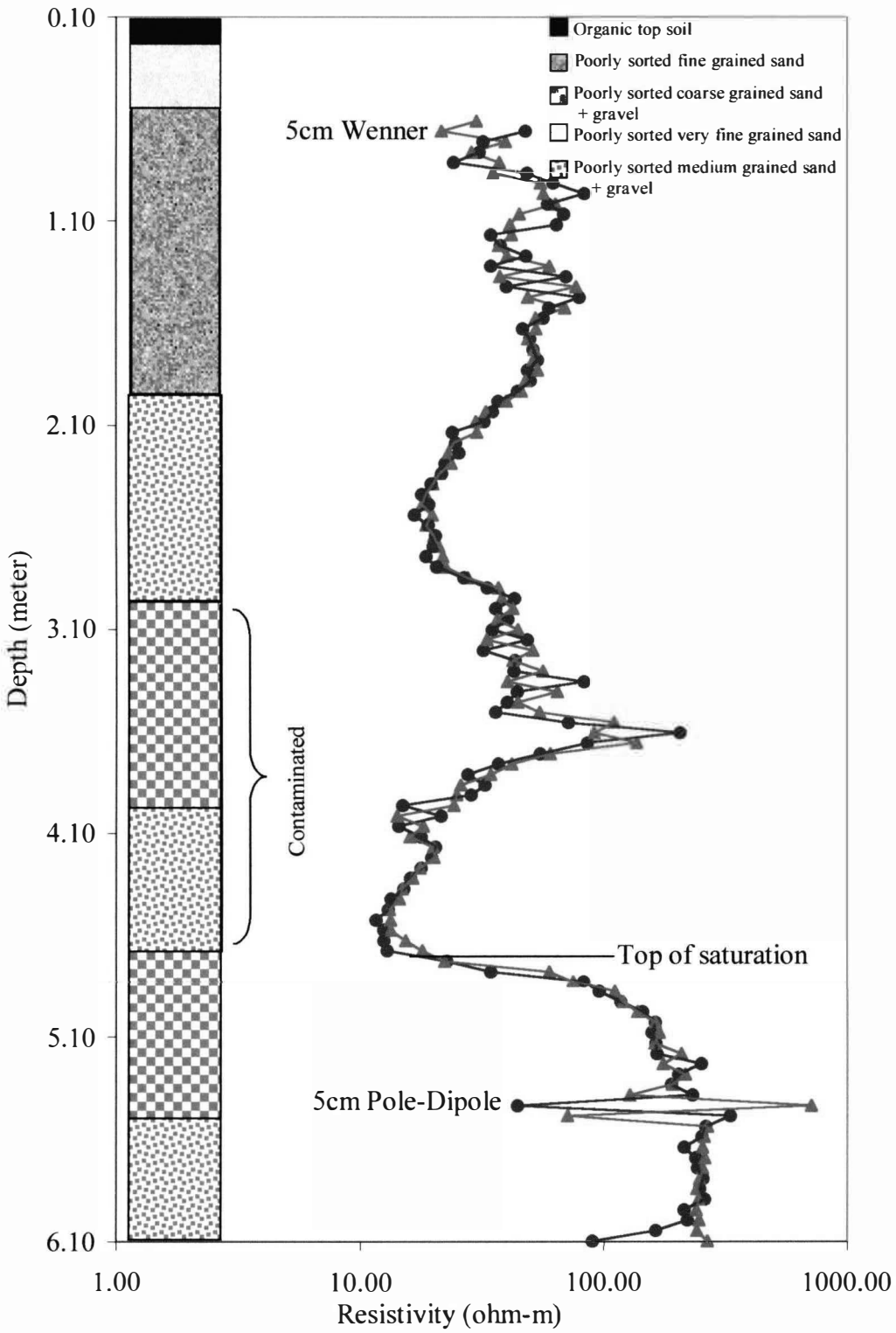

Figure 26. Vertical Resistivity Profile for Pole-Dipole and Wenner Arrays Using 5cm Spacing, LVRP-5.

The apparent resistivity profile for LVRP-4 (Figure 25) shows a resistive (50-260 Ohm-m) section from 1.2m to 2m. This may be as a result of low moisture content in the soil at the time measurements were taken because other arrays like cross-hole dipole-dipole and pole-dipole array did not result in the same profile between this interval. A progressively conductive section (10-45 Ohm-m) was observed from 2-2.8m. This progression occurs as we go from the fine/ coarse-grained sands and gravels to medium sands. The lower resistivities observed in the medium sands is as a result of it's higher water retaining capacity than gravels. This pattern is generally repeated in the profiles down to the top of the saturated zone. The lower resistivities occurring between 2m and the top of the saturated zone is primarily due to the fact that during the drilling process, bentonite loss into the surrounding formation was very high. This required more bentonite this time mixed with fine sands to be pumped to backfill the annular space around the probes. This improved electrical contact between the formations and the electrodes. Bentonite has high ionic concentration of mobile sodium, sulfate, bicarbonate, chloride, and potassium. The effect of this is low resistivity around the annulus of the VRP. With time, these ions are leached out into the formation resulting in increasing resistivity around the annulus of the VRP. Previous investigators (e.g. Keller et al, 1991, have documented this. The depth at which hydrocarbon was first detected (~3.25m) during drilling show a resistivity drop of about 60 Ohm-m. The hydrocarbon-contaminated section (3.25m-4.7m) is divided into two sections, 3.25m-4.2m is dark brown in color while 4.2m-4.7m is gray in color. The spike to the right recorded at 4.2m denotes the

difference in resistivity between these sections. The small peaks and troughs recorded within this section are due to inhomogeneities in the geology (sands and gravels) and the different wetting phases of gasoline and water. Others (Sauck, 2000 and Atekwana et al., 2000), have looked at the geoelectrical signatures in LNAPL spill sites and their model can be applied to this site. The progressive decrease in resistivity down to the top of the saturated may be explained as resulting from total dissolved solid (TDS) leachate which is periodically flushed down from an intimately mixed hydrocarbon, water, oxygen, and soil near the base of the vadose zone. The leachate itself being a product of conductive organic and carbon acids produced by microbial degradation. These acids lead to a reduction in pH causing the leaching of soluble salts from surrounding formations. This TDS enriched zone ultimately results in higher conductivity values in the hydrocarbon plume.

The same scenario is obtained in LVRP-5 (Figure 26), however, within the saturated zone, the spike recorded at 5.5m is purely lithologic. This is supported from grainsize analysis (figure 15) and the split-spoon blowcount results (Appendix B)

The higher resistivities recorded from both probes in the saturated zone may not be unconnected with the fact that during the drilling process, this section of the hole collapsed and was not invaded by the bentonite slurry used to backfill the annular space around the probes. This explains the high resistivity contrast of about 1:70 in the vertical profiles from the probes when compared with a contrast of about 1:10 from the laboratory resistivity measurements (figure 14). The profiles from both are similar though the resistance readings from the Wenner array produced higher

values (Appendix C). The Wenner array is a nested array, when arrays are nested and given the same current and current electrode separation, the voltage received at the potential electrodes which is a larger faction of the current electrode gives larger values. The implication is that the signal to noise ratio is higher making the profile produced by the Wenner array to more realistically represent the resistivity distribution observed from the probes.

Figures 27 and 28 show the effect of using larger electrode spacing. Overall the larger spacing produced smoother profiles. Using larger electrode spacings allows a larger volume of formation to be sampled thereby minimizing the effect of the bentonite slurry annulus.

Induced Polarization

Figures 29 – 32 show the induced polarization profiles from both probes using 5cm pole-dipole and Wenner arrays. Both arrays show an increase in chargeability values (0-25 mV/V) at about 1.4m to about 1.8m, in LVRP-4 (Figures 29 and 31) while only the Wenner array show this increase in LVRP-5 (Figures 32). This increase can be interpreted qualitatively to be the result of induced polarization response in a clay-rich zone. In contrast, the resistivity profile along the same depth interval indicates a resistive geoelectric section. The high resistivity within this zone could be attributed to low moisture content in the formation due to evaporation and plant transpiration.

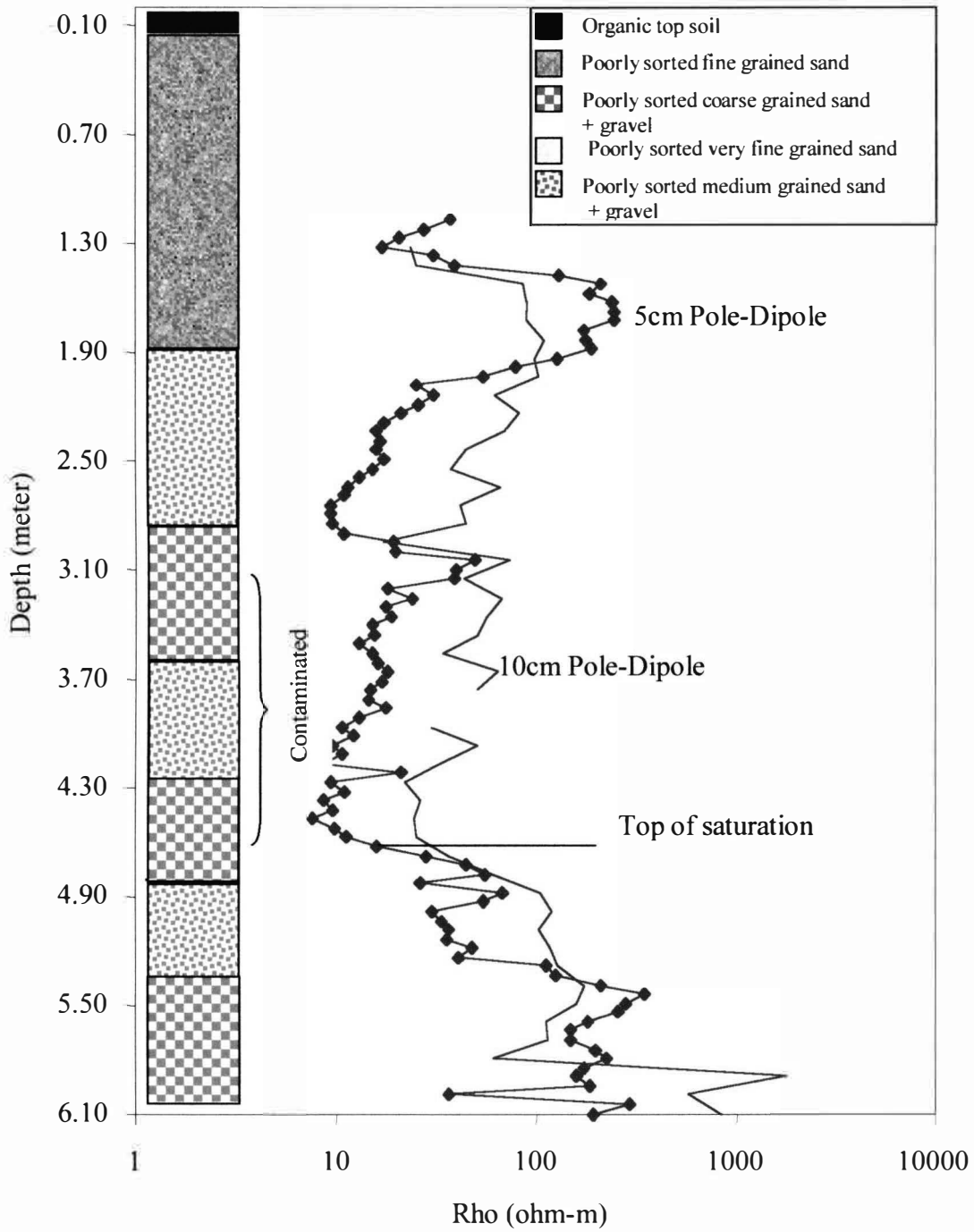

Figure 27. Vertical Resistivity Profile for Pole-Dipole Array Using 5 cm and10 cm Spacings, LVRP-4.

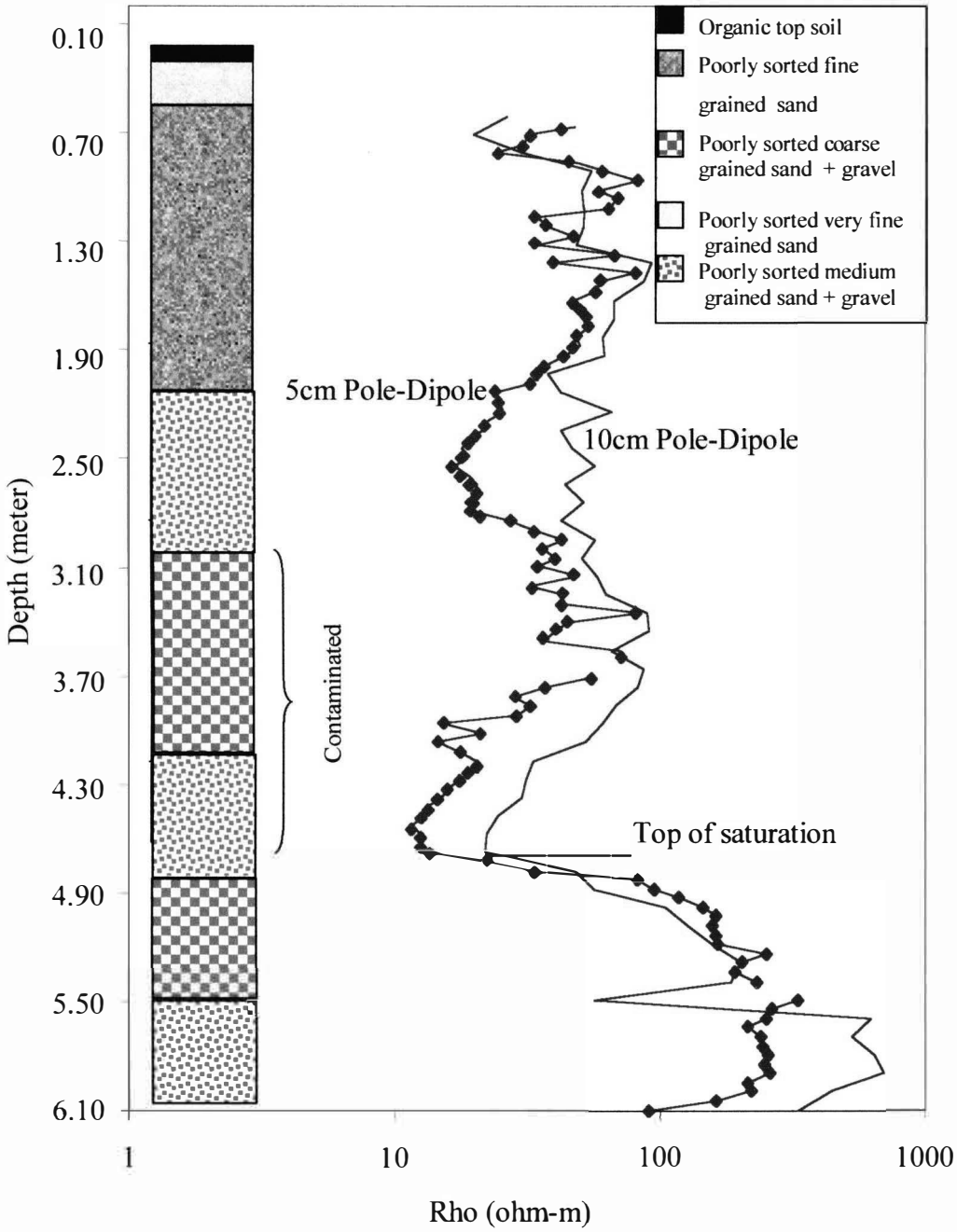

Figure 28. Vertical Resistivity Profile for Pole-Dipole Array Using 5 cm and 10 cm Spacings, LVRP-5.

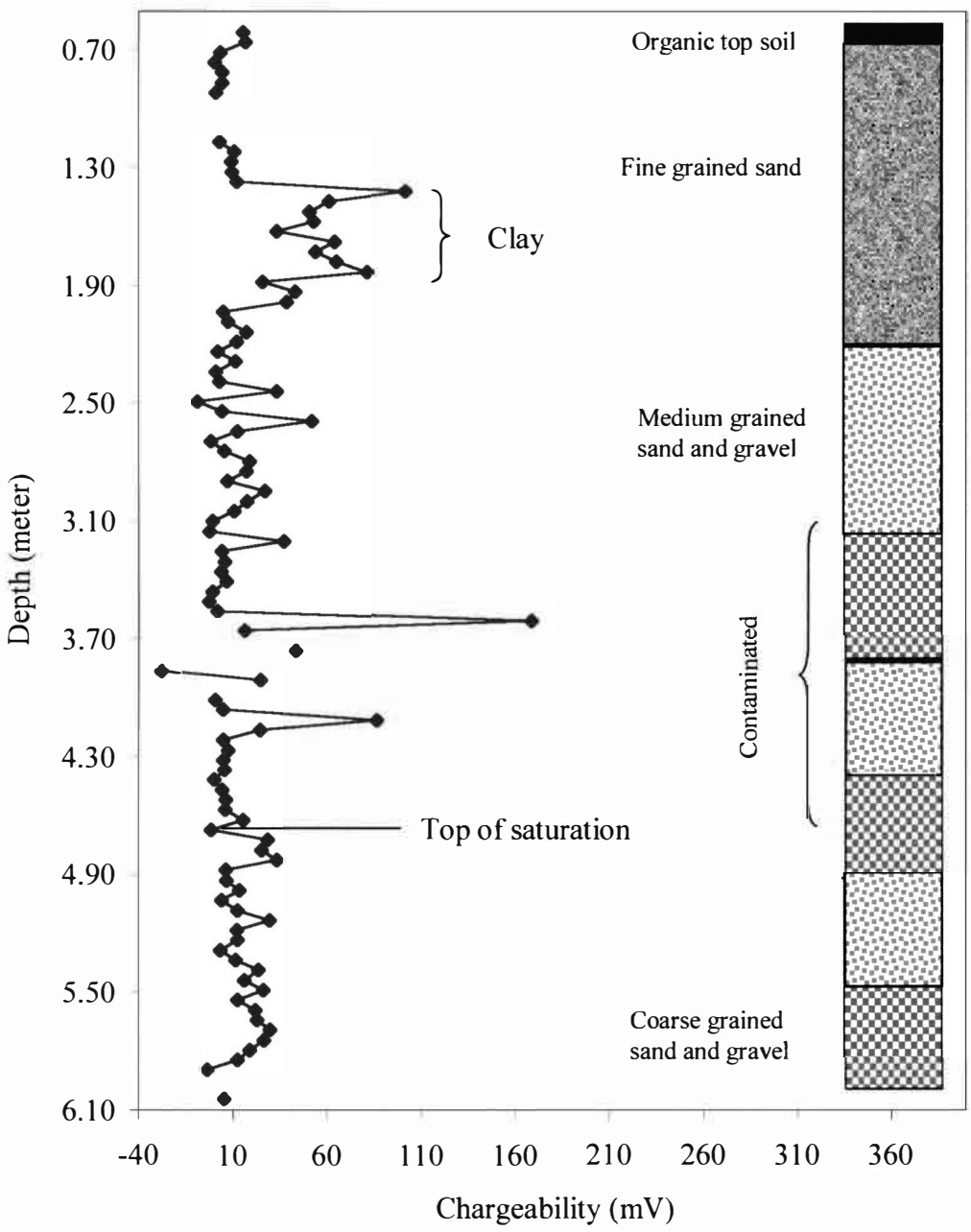

Figure 29. Induced Polarization Profile Using Vertical Pole-Dipole Array (5cm Spacing), LVRP-4.

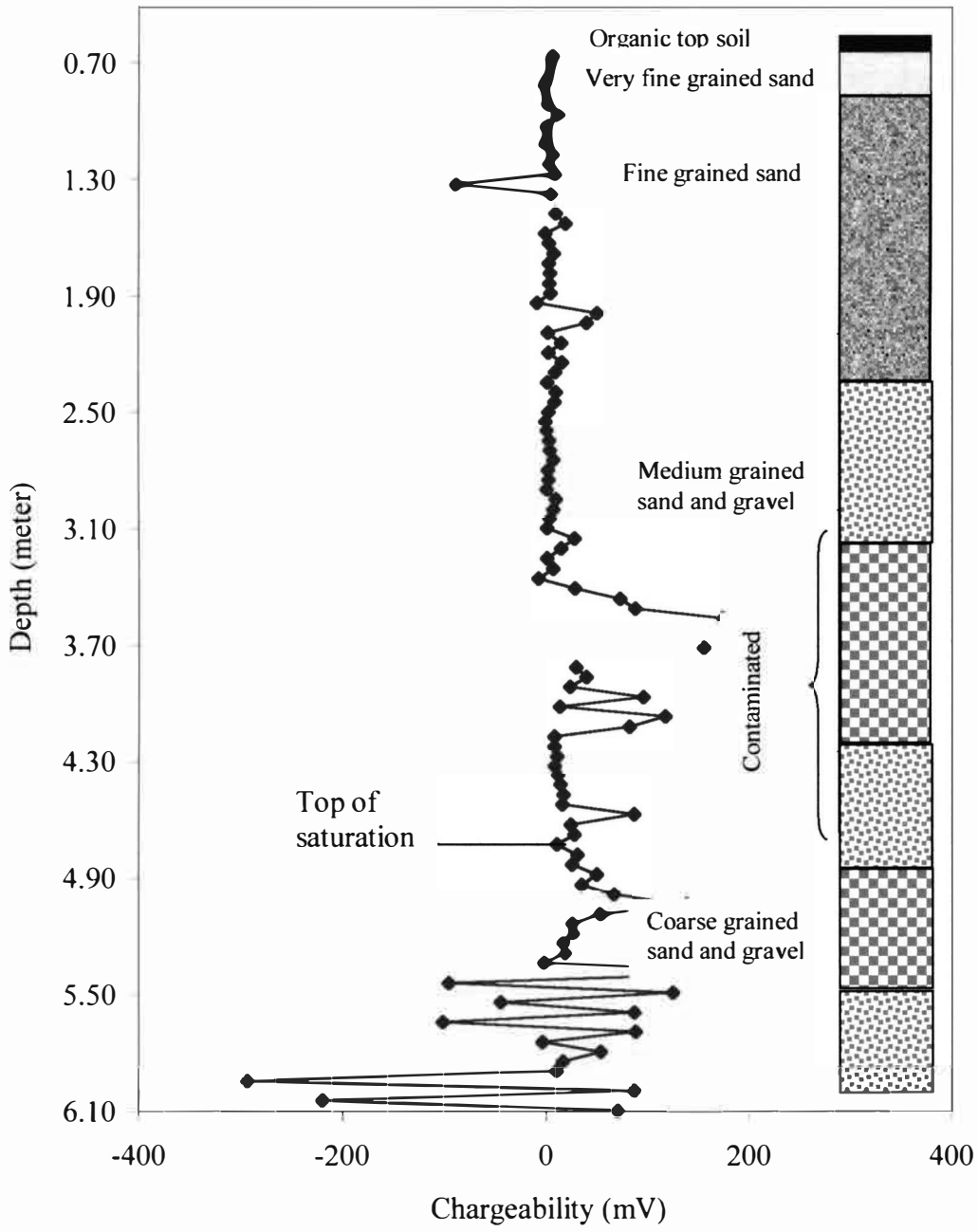

Figure 30. Induced Polarization Profile Using Vertical Pole-Dipole Array (5cm Spacing), LVRP-5.

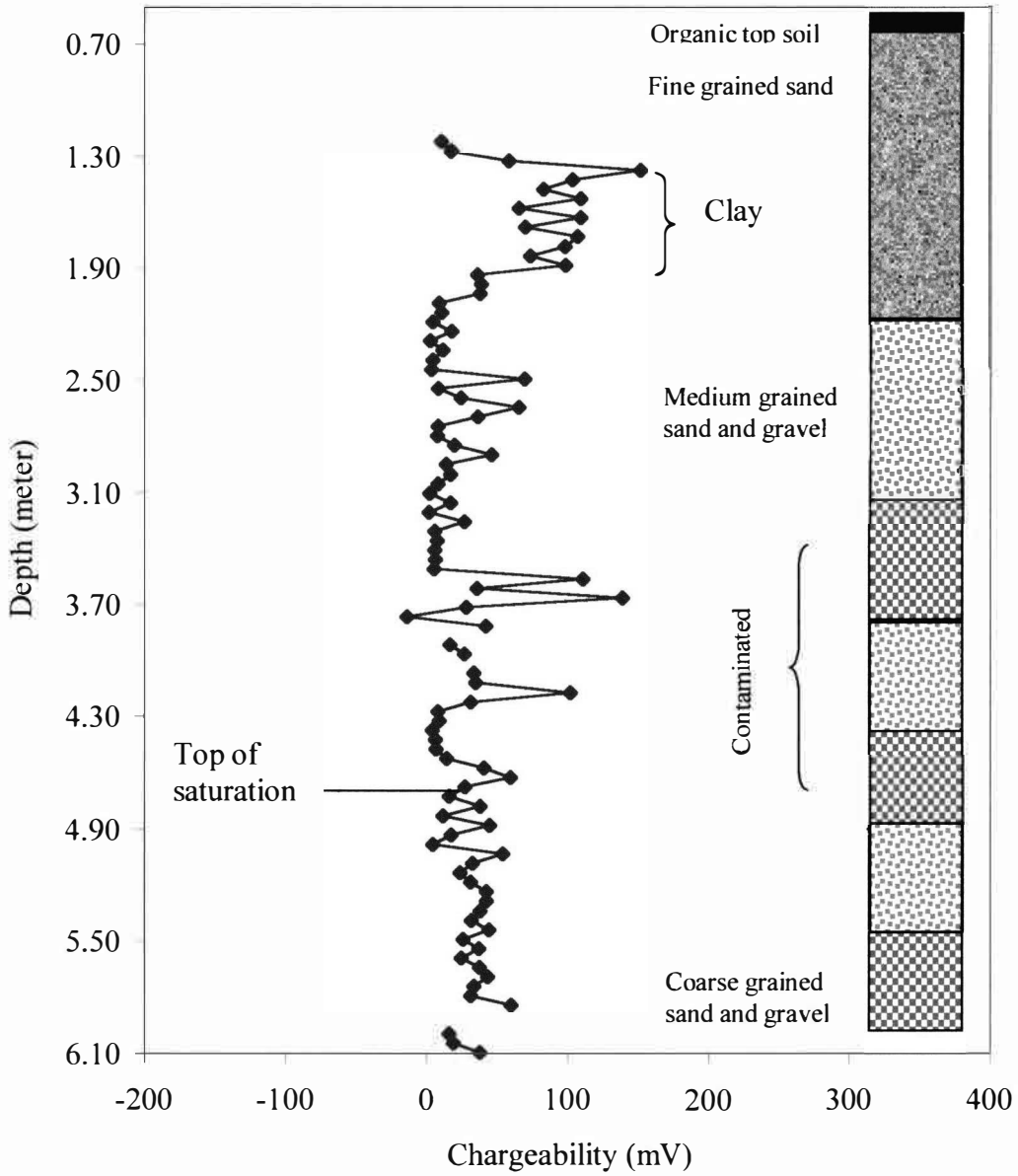

Figure 31. Induced Polarization Profile Using Vertical Wenner Array (5 m Spacing), LVRP-4.

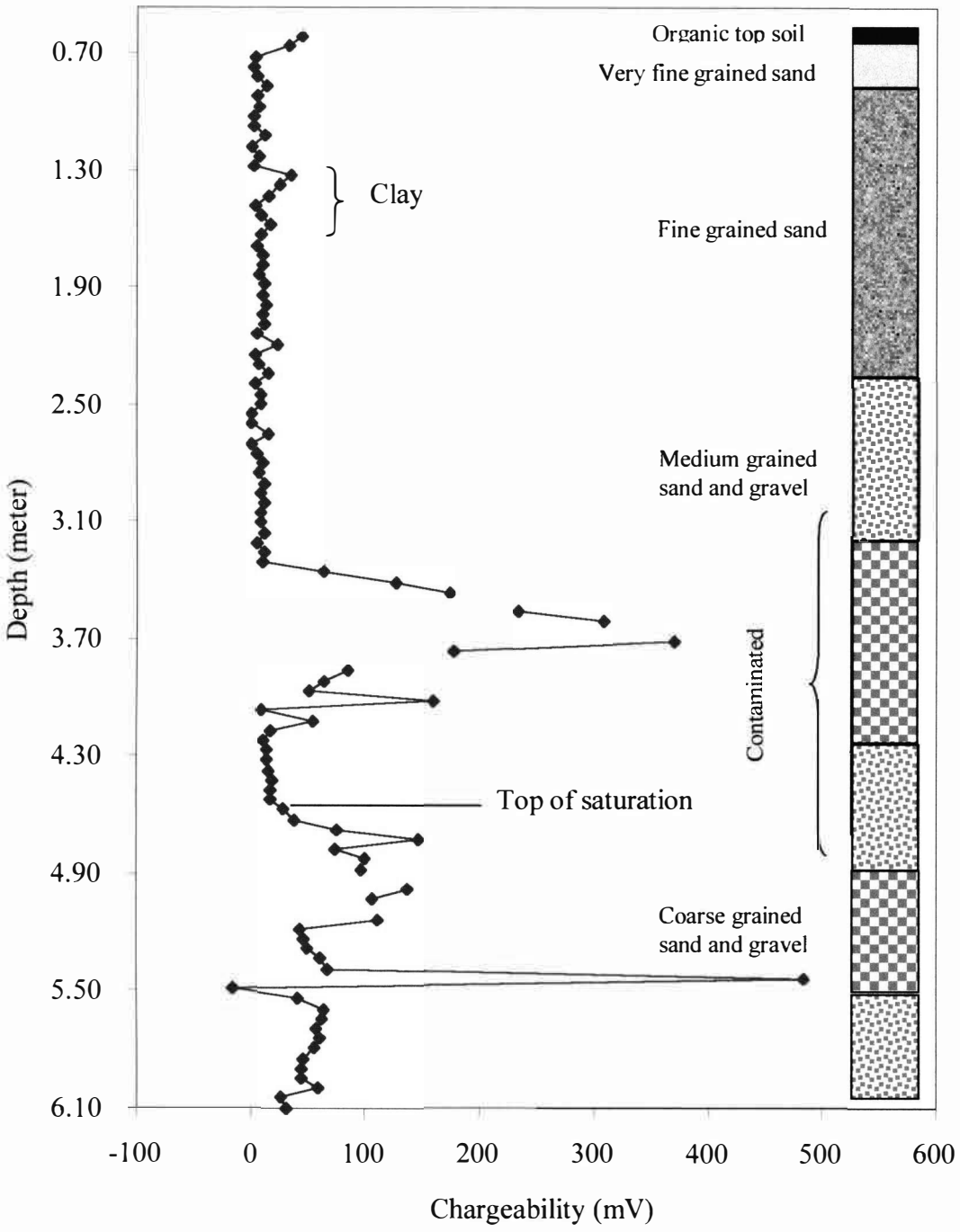

Figure 32. Induced Polarization Profile Using Vertical Wenner Array (5cm Spacing), LVRP-5.

Within the contaminated depth interval, 3.1m – 4.5m, only the results from the pole-dipole array in LVRP-5 (Figure 30) show a definite shift to higher chargeability values and thereafter become noisy. One consistency in all the profiles is a zero chargeability value at the water table. Negative chargeability values can arise from instrument error, electromagnetic coupling, polarizable layered earth of type K or Q or may be due to 2-D and 3-D bodies, (Nabighian and Elliot, 1976; Sumner, 1976).

In LVRP-5 (Figure 30) we have a negative at 1.3m. This suggests instrument error as this negative was not shown on the other profiles. Below the top of the saturated zone, chargeability values from LVRP-5 (Figure 30 and 32) are very erratic and the negatives and high positivesmay not be unusual due to the bipolar nature and depolarization process associated with induced polarization (Sumner, 1976).

Results of Cross-hole Measurements

Inversion of Cross-hole Measurements

In order to generate a model (image) of the subsurface distribution of resistivity and induced polarization, a rapid 2-D geophysical inversion software (RES2DINV), developed by Loke and Barker, (1996) was used. Their inversion algorithm is based on the smoothness-constrained, non-linear least-square optimization technique (deGroot-Hendlin and Constable, 1990, Sasaki, 1992). The algorithm also includes a forward modeling subroutine used to calculate the apparent resistivity values.

The inversion process starts with the estimation of an initial homogeneous earth model (first iteration only) by the program. This is based on initial and minimum damping factors set by the user. This is done to stabilize the inversion process. Usually, the minimum damping factor is set to 20 percent of the initial damping factor. After several trial runs, the model that best matches the observed data were produced with initial and minimum damping factors of 0.16 and 0.03. This is based from a range of (0.25 and 0.1) for noisy datasets and (0.05 and 0.01) for less noisy datasets. Since the anomalies in the study area are expected to be horizontal (deduced from drilling), a weighting value of 0.5 was selected for the vertical / horizontal filters, this optimizes the inversion process and produces smoother models elongated in a horizontal sense. A value of 1 or 2 is used if the expected anomalies are elongated in a vertical sense. Other convergence criteria applied include a minimum root-mean-square error change of 5 percent, below which the inversion process stops.

Since apparent resistivity data in general exhibits log-normal distribution, the option to use logarithm of the resistivity values was chosen from the program. This had the added advantage of allowing the program to filter out unusually high or low values.

The conventional Gauss-Newton method was selected to implement the least square technique. This is because the measured data exhibited a resistivity contrast of greater than 10:1. This generally gave better models consistent with geology of the location of where the vertical resistivity probes were installed.

The 2-D model used for cross-borehole data by the inversion program consists of quadrilateral blocks whose dimensions are equal to the spacings between electrodes. An alternative model with finer blocks can also be used and in some cases produced better results. The electrodes are divided into three sets; surface electrodes, electrodes in borehole 1 (LVRP-4) and electrodes in borehole 2 (LVRP-5). This arrangement determines the dimensions of the model blocks as earlier stated. The x, y, and z location of these electrodes is also required in the data format in order for the program to successfully carry out the inversion, however, where they do not exist, dummy electrodes are inserted in the appropriate missing locations.

After each run of a dataset, if the model generated is judged to be unsatisfactory due to very high root mean square error values, the erroneous data points were deleted or trimmed in a submenu titled "RMS error statistics" and the dataset re-run. The model results are displayed as contoured sections of apparent resistivity (Ohm-m) and chargeability (mV/V) against depth. They are presented below.

Cross-hole Pole-Pole

Figure 33 shows the final reconstructed resistivity model from the cross-hole pole-pole array. The model shows a conductive zone (5-169 Ohm-m) located from 1.28 m to about 2.0 m. This coincides with the very fine sand-clay interval recovered from both boreholes. Below this is a high resistive zone (408-2359 Ohm-m) located from about 2 m-3.8 m whose boundaries are not well defined in a horizontal sense. A

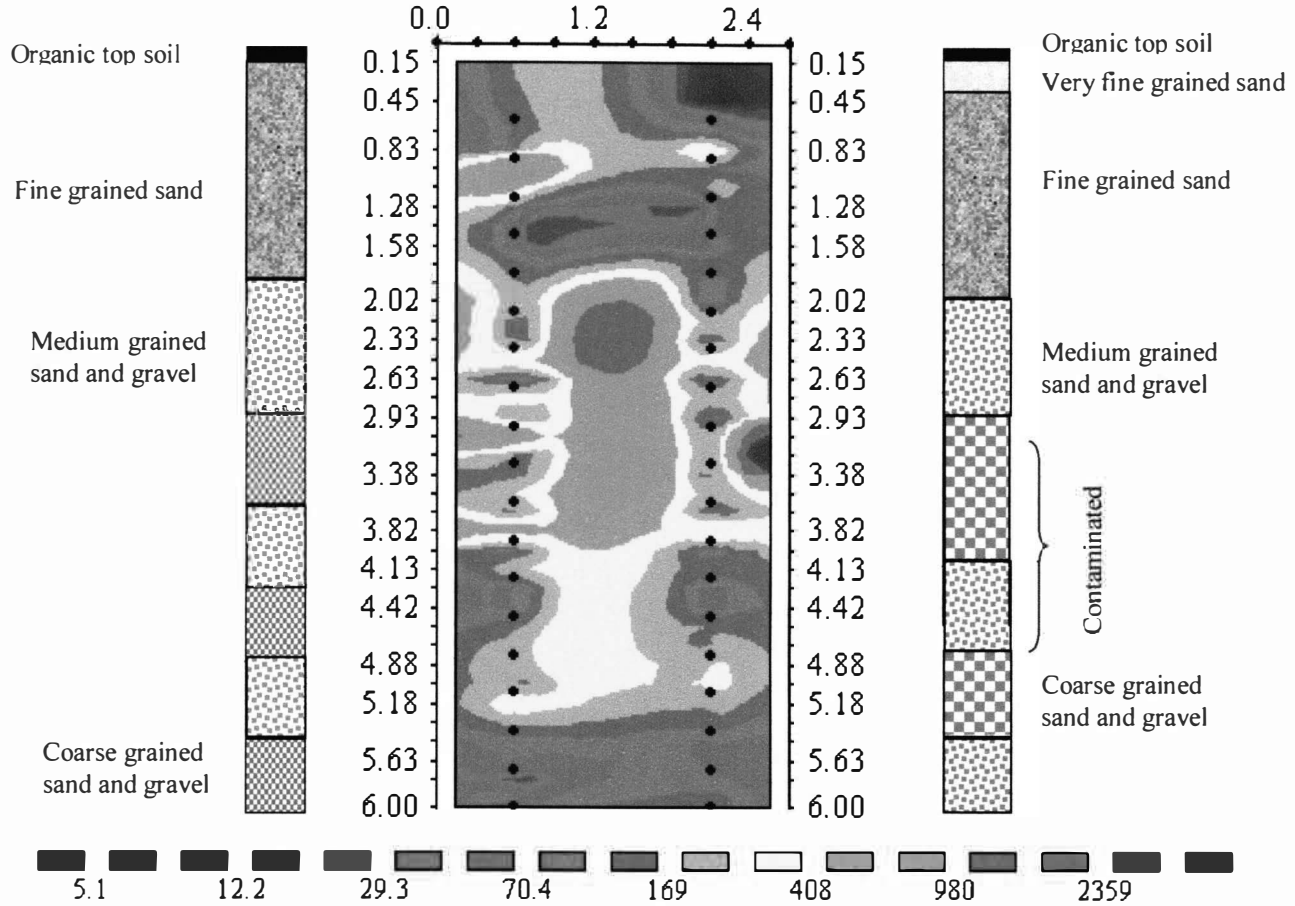

Figure 33. Resistivity Image in Ohm-m, Using Electrode Spacing 0.3m, Iteration 6 RMS Error = 8.6%, Obtained from Cross-hole Pole-Pole Array. The Dots Represents Electrodes, Left (LVRP-4), Right (LVRP-5). Lithology Shown on Sides.

zone of intermediate resistivity (169-408 Ohm-m) located between 3.82m-5.18m depth may be associated with the contaminated section of the subsurface. The top of the saturated zone is at about 4.42 m, water table elevation from nearby monitoring well (MW-30) put the water table at about 4.9 m. The resistivity change observed at about 5.5 m corresponds with the change observed in the vertical profiles and is therefore associated with change in lithology. In terms of depth resolution with regards to the saturated zone, the inversion model may be a little bit off. It is however interesting to note that the reconstructed resistive structure occurs in the coarse sands and gravels which provided a preferential pathway for hydrocarbon migration and ultimately the bentonite slurry that invaded the formation during the backfilling process. Therefore, though the model did not show the geoelectrical zonation associated with the contaminated section, it provides us with a glimpse of the effect and extent of the bentonite invasion which ultimately affected the calculated and predicted models.

Cross-hole Pole-Dipole

Figure 34 shows the final reconstructed resistivity model from the pole-dipole array. The resistivity inversion result shows one high conductive zone (16-104 Ohm-m) located between 1.0m-1.7m, two resistive zones (165-412 Ohm-m) that extend from 2.0m to 3.8m and 4.42m-5.18m. The resistive structure in the contaminated section of the subsurface is consistent with that of the previous model except that it is more pronounced. The same conductive zone (66-104 Ohm-m) as the previous

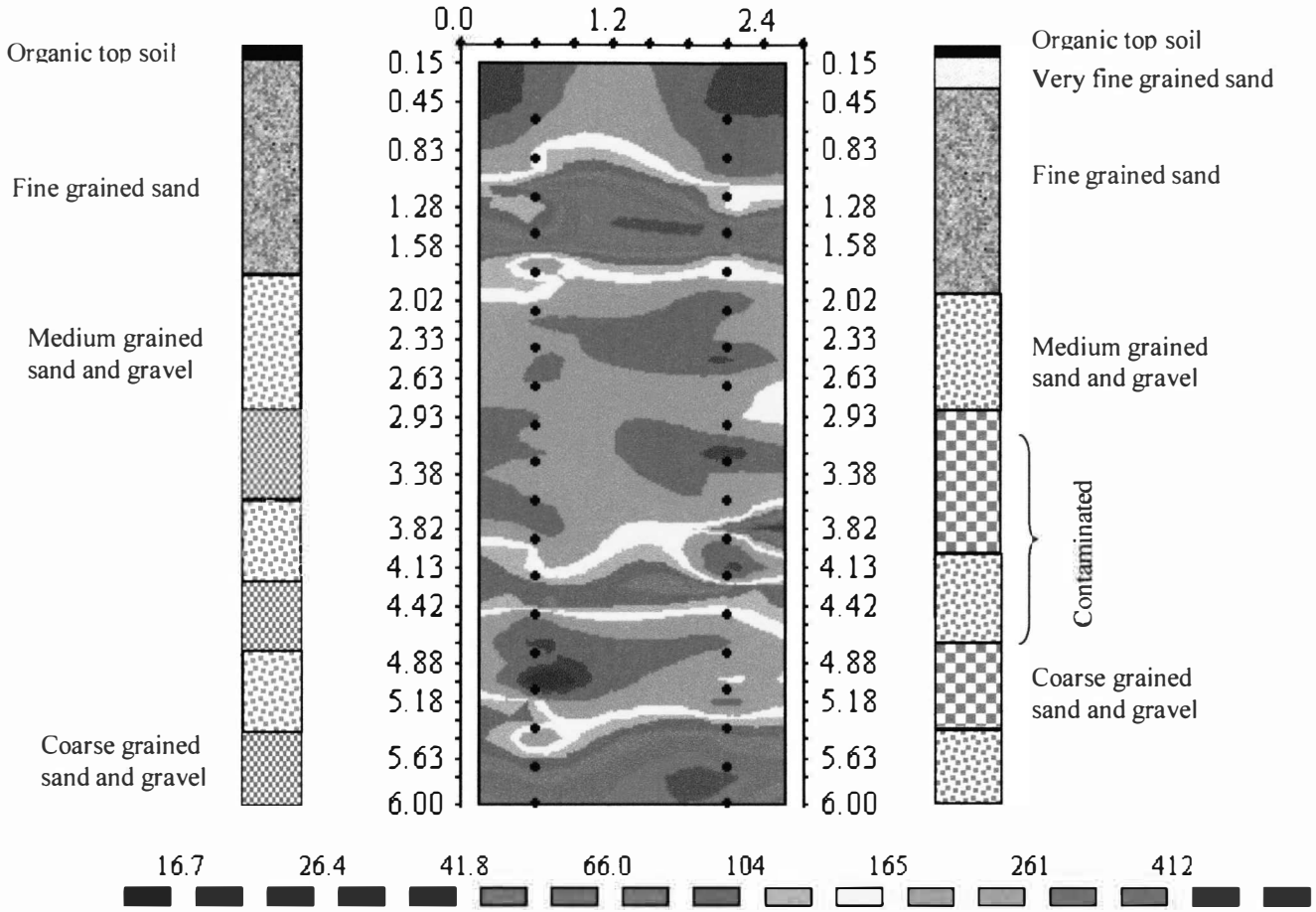

Figure 34. Resistivity Image in Ohm-m, Using Electrode Spacing 0.3m, Iteration 5 RMS Errors of 1.2%, Obtained from Cross-hole Pole-Dipole Array. The Dots Represents Electrodes Left (LVRP-4), Right (LVRP-5) . Lithology Shown on Sides.

model is also present at 4.42 m as well as the change in resistivity observed at 5.5 m. The conductive structure below this depth as well as in the previous model may be due edge effect and are therefore interpreted as an artifact from the reconstruction algorithm.

Cross-hole Dipole-Pole

Figure 35 shows the final reconstructed resistivity inversion from cross-hole dipole-pole array. The result shows one conductive and two resistive zones. The conductive zone (43.8-149 Ohm-m) is approximately at depths of 0.83m – 2.0m, a high resistivity zone (235-373 Ohm-m) from 2m to about 3.82m and an intermediate resistive zone (149-275 Ohm-m) located between 3.82m to 5.18m. The reconstructed resistivity structures between 4.42 m-5.5 m is similar to the previous two model but less defined horizontally. However, the structure recovered at the top (0-0.83) as well as below 5.5 m are artifacts from the reconstruction algorithm.

Cross-hole Dipole-Dipole

Figure 36 shows the final reconstructed resistivity inversion result from cross-hole dipole-dipole array. The model shows two conductive zones (31.7 to 105 Ohm-m) located at 1.0m to 1.85m and 4.0m to 4.85m; and a high resistivity zone (634-2102 Ohm-m) from 4.72m –6.0m. The first conductive zone corresponds to the depth location of the fine sands obtained from the borehole logs while the second is probably the top of the saturated zone which may have been elevated due to

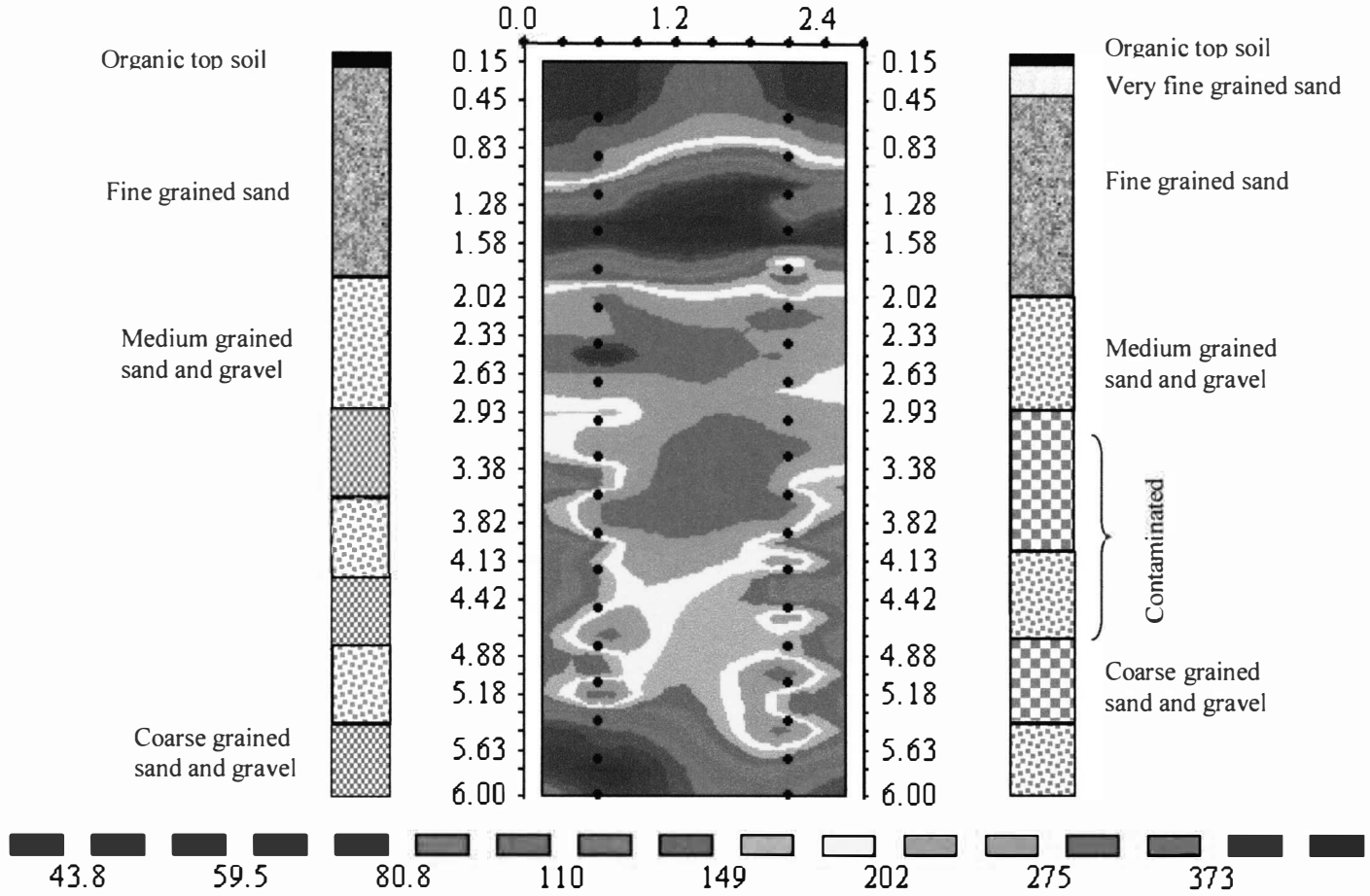

Figure 35. Resistivity Image in Ohm-m, Using Electrode Spacing 0.3m, Iteration 4 RMS error =0.7%, Obtained from Cross-hole Dipole-Pole Array. The Dots Represent Electrodes, Left (LVRP-4), Right (LVRP-5). Lithology Shown on Sides.

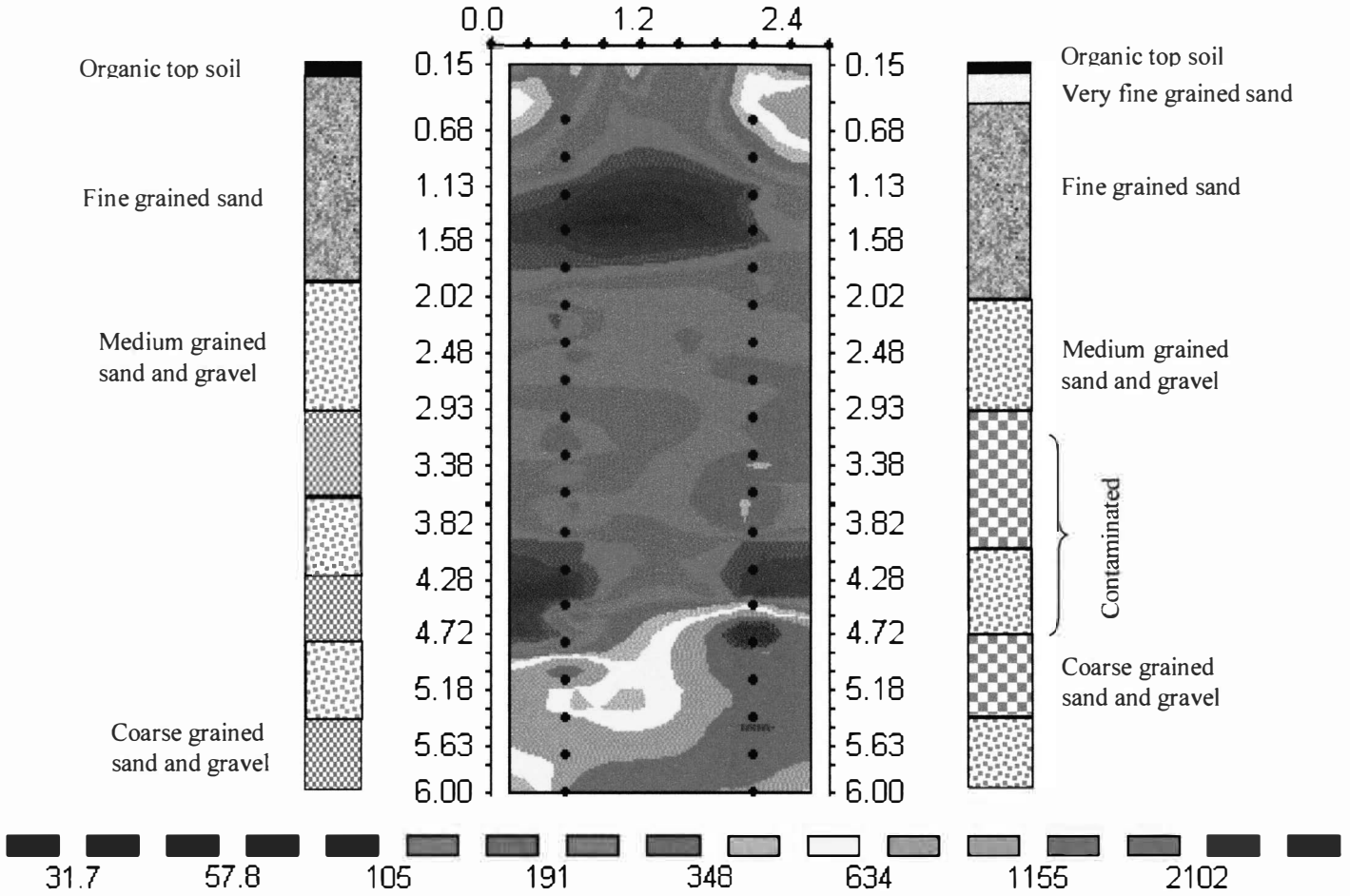

Figure 36. Resistivity Image in Ohm-m, Using Electrode Spacing 0.3m, Iteration 4 RMS error =5.3% , Obtained from Cross-hole Dipole-Dipole Array. The Dots Represent Electrodes, Left (LVRP-4), Right (LVRP-5). Lithology Shown on Sides.

bentonite slurry which may have retarded the downward percolation of water or formation fluid leakage into one or two of the probes.

Figure 37 shows the results of vertical resistivity plotted from cross-borehole dipole-dipole measurements taken over a period of five months. The average daily precipitation record of six days prior to and on the day of measurement is shown for comparison. At the top of the saturation zone (4.8m), there is a progressive decrease in resistivity that does not follow the precipitation pattern. These decreases in resistivity may be as a result of increase in the total dissolved solids released from the microbial degradation in the contaminated section (3m-3.6m). In the saturated zone, no meaningful explanation could explain the variation in resistivity at the specified depths. The increases and decreases could not be correlated to the precipitation pattern either. Therefore no attempt is made to explain the cause of the resistivity variations within this zone.

Results from LVRP-2 and LVRP-3

The probes are located in the southern part of the study area. The probes are installed to depths of 10.1m and 10.4m respectively. Both probes are installed in a contaminated region. Lithological data is not available and the water table elevation from nearby monitoring wells resides between 5.1 to 6.1 meters.

The resistivity model (figure 38) shows a high conductivity zone (23.2 - 106 Ohm-m) from 6.85m to total depth in LVRP-3. No free product has been

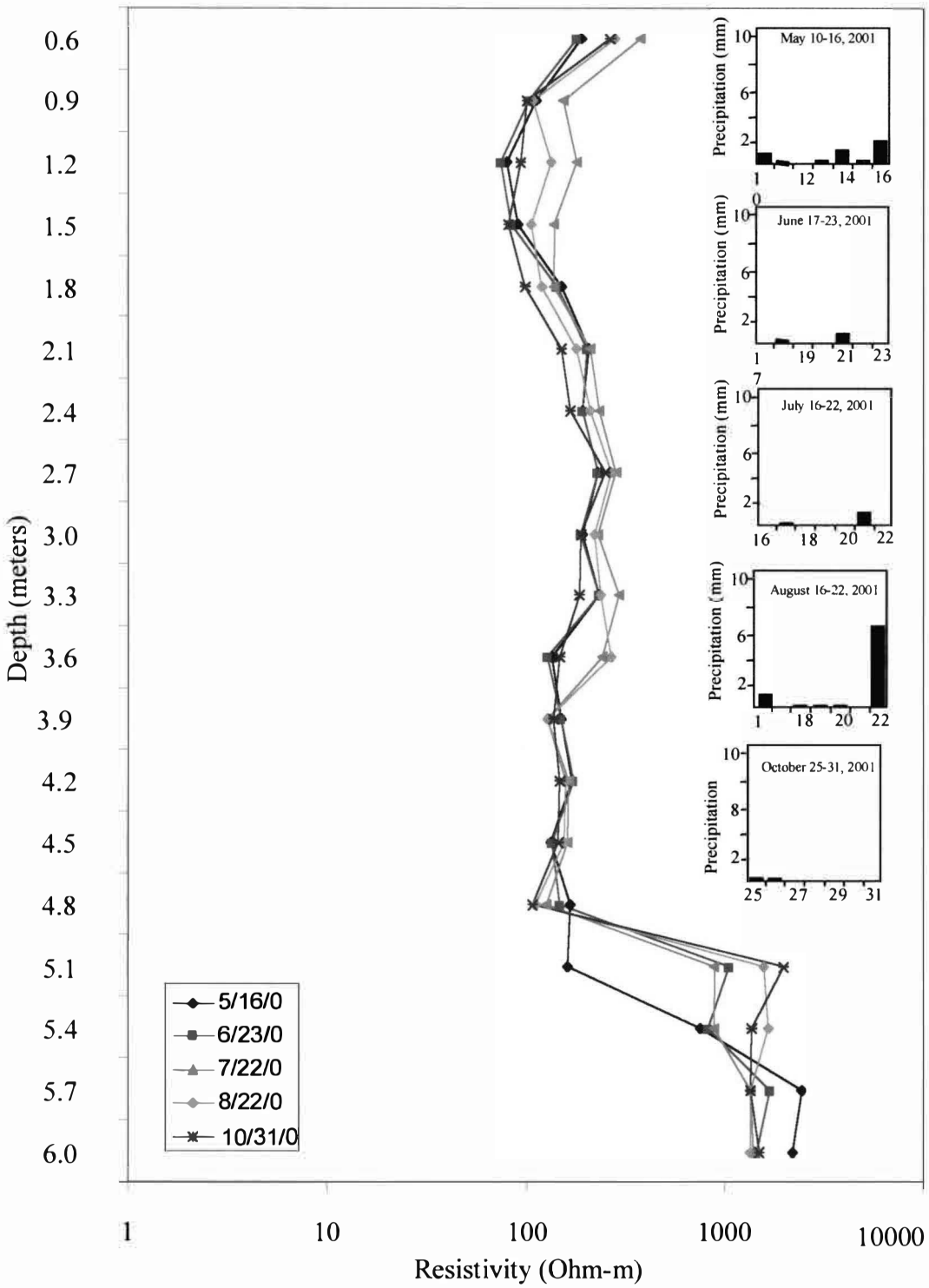

Figure 37. Resistivity Changes Over a Period of 5-months, Average Daily Precipitation Data for Each Week of Measurement Also Shown.

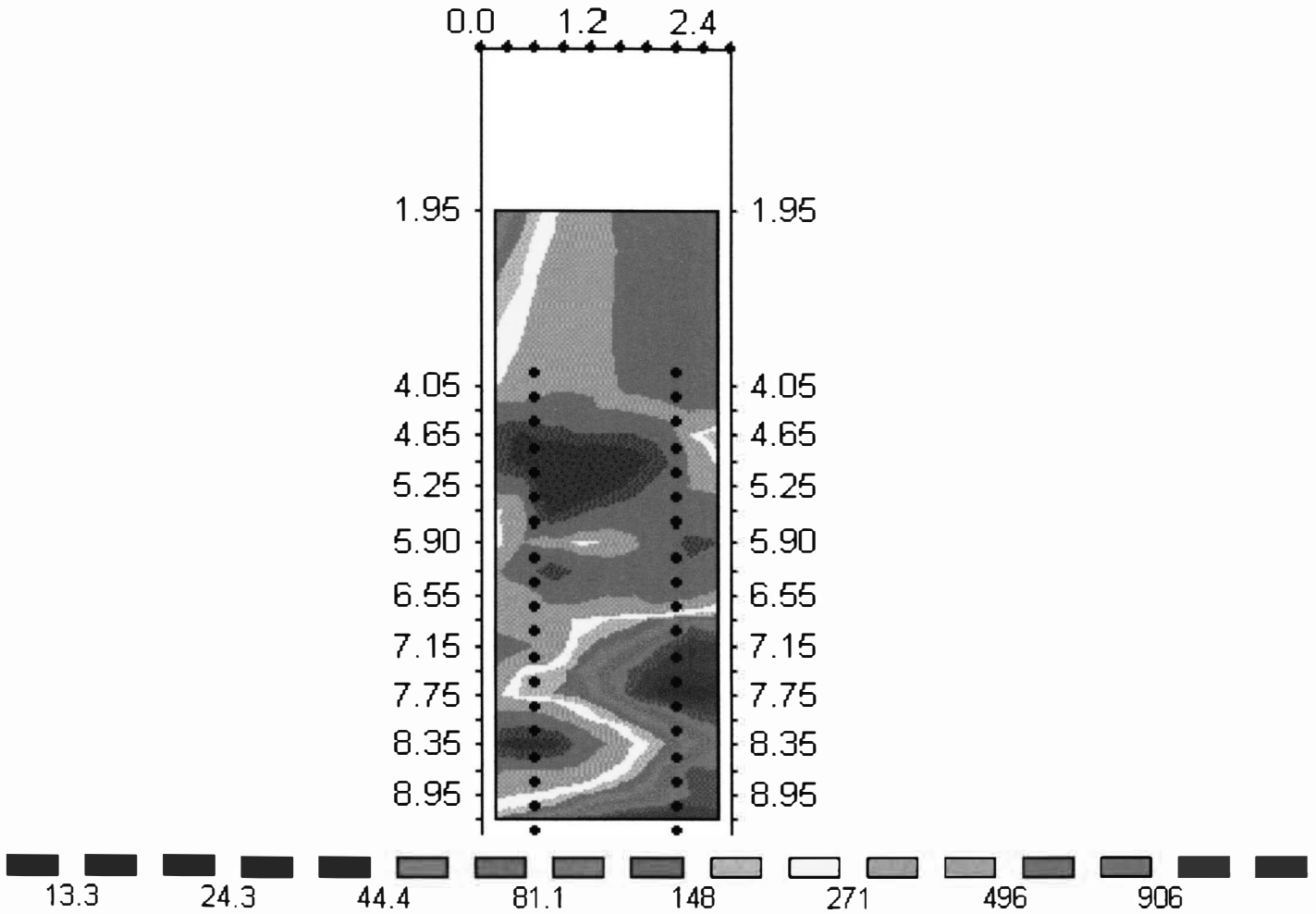

Figure 38. Resistivity Image in Ohm-m, Using Electrode Spacing 0.3m, Iteration 3 RMS error = 9%, Obtained from Cross-hole Dipole-Dipole Array. The Dots Represent Electrodes, Left (LVRP-2), Right (LVRP-3).

documented in nearby wells; therefore it is not certain if this conductive zone is stratigraphic in origin.

All the inversion results presented above are possible models of the earth resistivity distribution consistent with the measured data. The cross-hole pole-pole, cross-hole dipole-pole and cross-hole pole-dipole arrays gave very low potential readings and therefore the data measured could easily have been affected by background noise (Appendix D). They also have the disadvantage of employing remote electrodes, which may easily picked up random noise from telluric or other current sources. These noises add up during the inversion process and ultimately yield images that do not totally agree with the measured data.

The cross-hole dipole-dipole results gave higher voltage readings and therefore in terms of signal-to-noise can be judged to be the most accurate, figures 39 and 40 show the comparison and close agreement between the vertical and cross-hole profiles. The same cross-hole profile (cross-hole dipole-dipole) is used to compare the vertical (Wenner and pole-dipole) profiles from both probes. The cross-hole dipole-dipole overall is less noisy than both vertical profile results. The resistivity contrast and minor peaks and troughs are also more gradual than those recorded by the vertical measurements between depths of 1.4m to 3.1m. The cross-hole measurements also showed two successive resistivity peaks at 5.3m and 5.85m depth which may be lithologic in origin

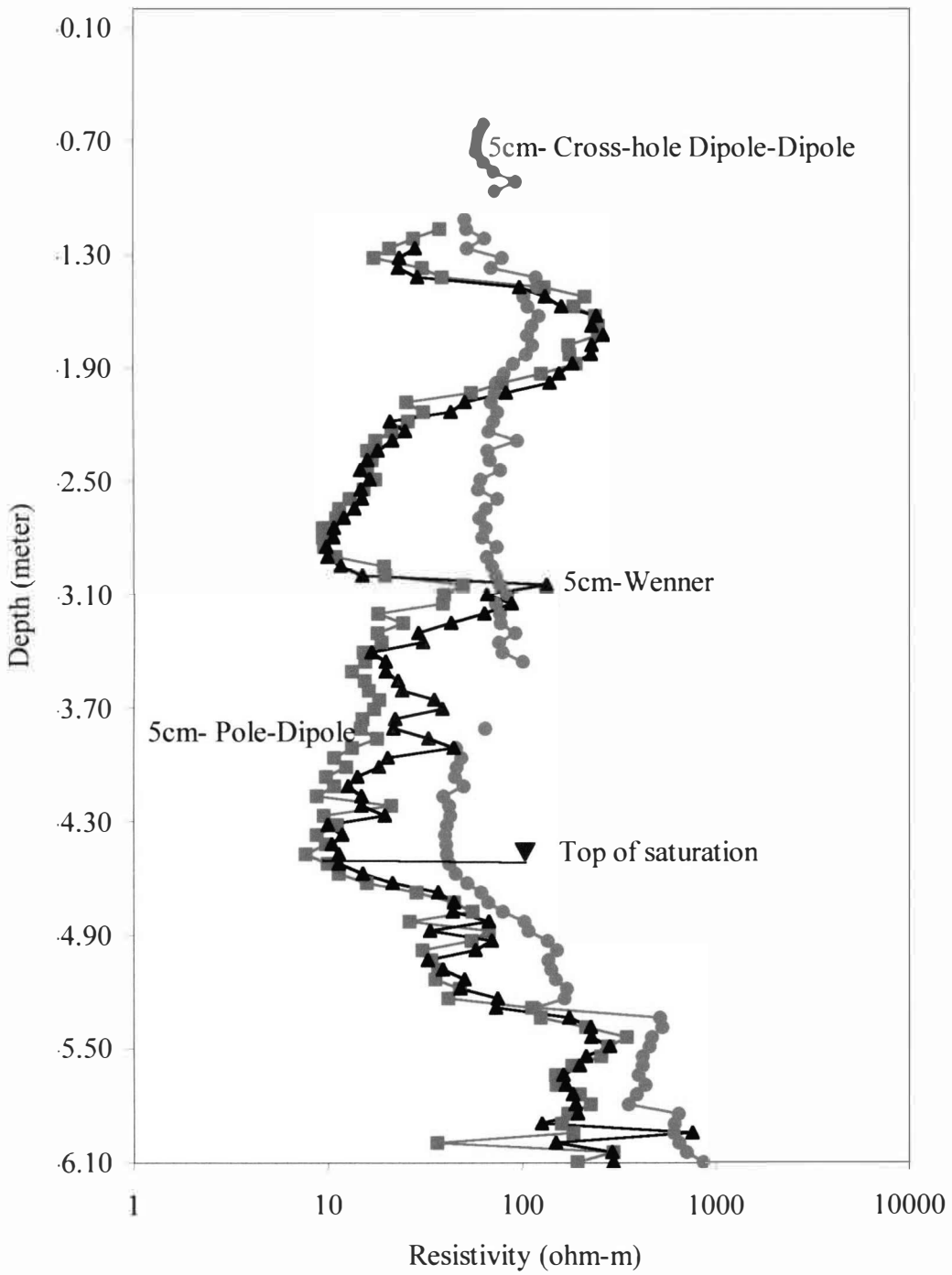

Figure 39. Resistivity Profile for Two Vertical Arrays and One Cross-hole Array Using 5 cm Spacing, LVRP-4.

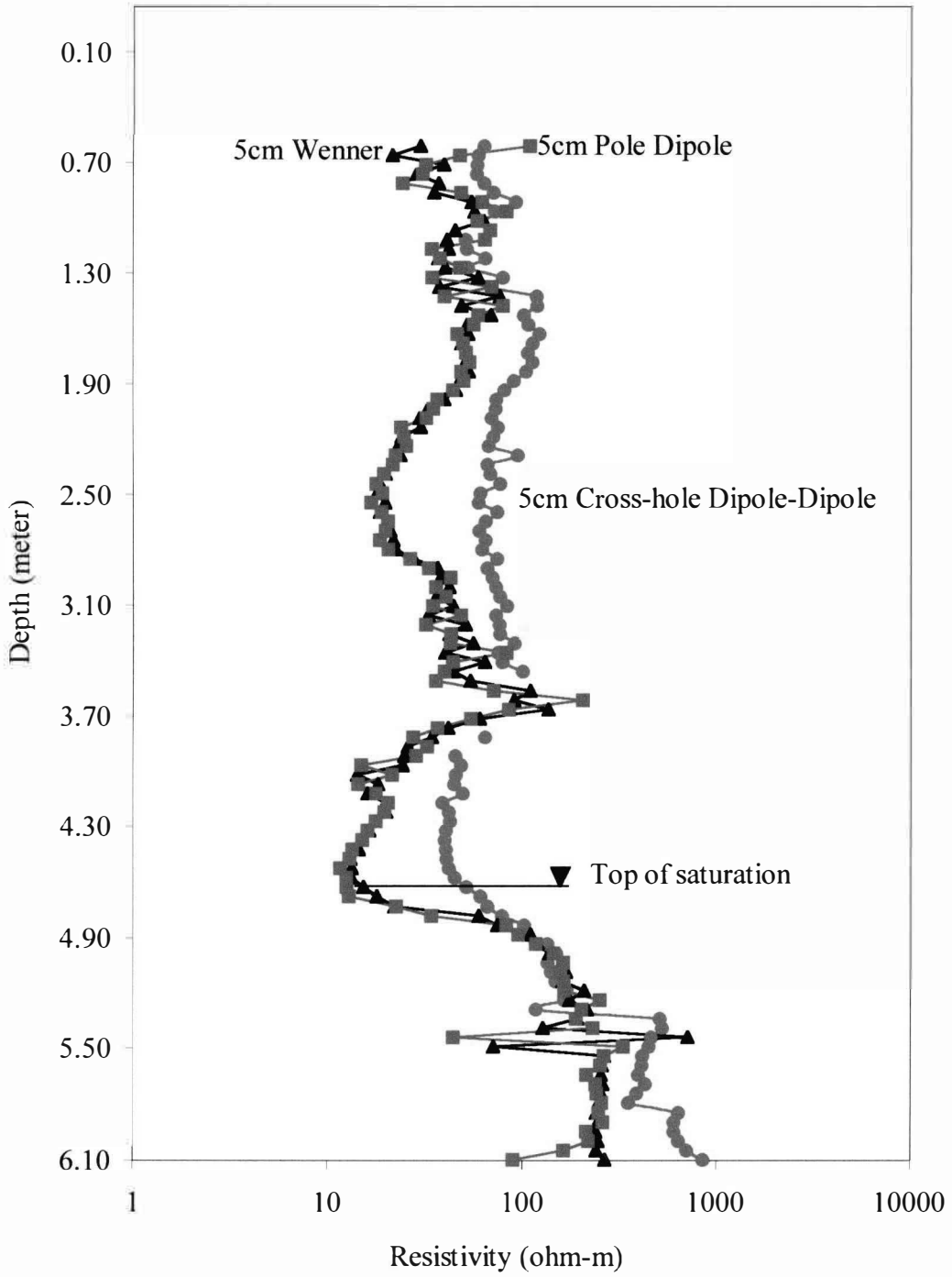

Figure 40. Resistivity Profile for Two Vertical Arrays and One Cross-hole Array Using 5 cm Spacing, LVRP-5.

CHAPTER VI

CONCLUSIONS AND RECOMMENDATIONS

Conclusions

The vertical resistivity profiles were used for preliminary measurements of the vertical distribution of resistivity with depth. The measurements were repeatable and assured proper working of the probes. This then allowed cross-hole measurements to be taken.

Two vertical measurement arrays (Wenner and pole-dipole) with "a" spacing of 5cm were employed in the vertical resistivity measurements. The profiles showed higher resistivities in the upper vadose zone which was interpreted as due to low moisture content resulting from evapo-transpiration. Below these, lower resistivities in the coarse sands and gravels were attributed to the high conductivity contribution from the bentonite slurry. Higher resistivities in the saturated zone was attributed to the natural collapse of that section of the hole and consequently minimal or no bentonite invasion.

An attempt was made to use and compare two inversion programs for the cross-hole measurements. (OC4 and Res2Dinv). The OC4 source code is for 2-D electrical resistance tomography acquired under licence from the Regents of the University of California. However, the code needed a UNIX operating system, was

programmed in Fortran-77 and required a separate visualization software (TOMO2D3D) or other commercial packages in order to see results. Due to all of the above and the costs involved, the simplier Windows-based Res2Dinv (Loke and Barker, 1996) which produced satisfactory results was used. It, however, has the limitatation of 64-electrodes per borehole. The probes installed in the study area had 120-electrodes per borehole. To accommodate this, measurements were acquired using electrode spacings of 0.3 meter

Of the four cross-hole measurement arrays, the cross-hole dipole-dipole array gave the highest voltage reading for the same input current when compared to the other arrays. Also, it does not suffer from the effect of remote potential electrodes, which may add telluric noise. Finally, the cross-hole dipole-dipole array reproduced images that were more consistent with the measured data (the inversion routine was able to converge to a small root-mean-square error between the observed and model data).

In terms of depth resolution, the cross-hole pole-pole and dipole-pole arrays produced better images when compared to the other arrays. The depth of the resistivity transition (top of saturation zone ?) produced from the inversion image compares favorably with ground water elevation measurements from the nearby monitoring well (MW-30). In addition, the inversion image from this array suggests that coarse sand and gravels were more prone to bentonite invasion. This is supported by low resistivity structures recovered from the image along the boreholes within the depth intervals of the coarse sands and gravels.

The IP measurements were unreliable and not repeatable. The IP measurements may have been negatively impacted by the problem of contact potentials generated when the stainless steel electrodes used in the probes came in contact with the bentonite slurry/ground water/hydrocarbon mixture.

Recommendations

Due to the heterogeneity of the geology as deduced from grainsize analysis, the use of bentonite slurry to backfill the annular space around the probes should be discouraged. The alternative in such cases was to use Geoprobe™ technology as suggested by Groncki, (1999). However, two of the local representatives familiar with the geology of the study area backed out from using their Geoprobe™ point citing potential damage and loss of point, hence extra cost for the client. The use of a hollow-stem auger to drill the holes exacerbated the invasion problem. The extent of invasion varies along the length of the probe making it difficult to quantify the relative changes in the distribution of resistivity with depth caused by this perturbation. Ideally, a well of slightly larger circumference than the probe should be drilled, minimizing the need for backfill of any material.

Due to the large number of data points required for cross-hole measurements, an automated data gathering resistivity instrument will greatly reduce the amount of time needed in acquiring the data.

As for IP measurements, unless there is a means of deploying non-polarizable electrodes in the subsurface, the use of stainless steel electrodes should be

discouraged because of the reasons stated earlier. However, more research with stainless steel electrodes with and without bentonite should be done. This can be done at the Asylum Lake geophysical test site where vertical resistivity probes have been installed with different techniques.

At the lakeside Refinery site, more probes should be installed in a row across the plume boudary to investigate the resistivity and chargeability change from non-impacted to impacted sediments.

Appendix A

Drilling Logs

Drilling Log for LVRP-4

Client	Adrian Ezeagu
Project	Vertical Resistivity Probe installation
Boring	LVRP-4
Location	Lakeside Refinery Complex, Kalamazoo, MI
Date	November, 2000
Driller	West Michigan Drilling
Drilling Method	8.26cm (3.25 inch) Hollow Stem Auger
Sampler	Split Spoon Sampler
Length of Boring	6.1 meters
Ground Surface Elevation	n/a
Water Level Measurement	4.85 meters
Backfill Method	Bentonite slurry and very fine sand

Sample Number	Depth (meters)		Split Spoon Blows				Sample Description (from ground surface/top of well)
	From	To	0-15cm	15-30cm	30-45cm	45-60cm	
1	0	0.6	3	2	3	4	Fine grained clay/silt, top 10.2 cm decayed matter
2	0.6	1.2	2	1	2	3	Clay/silt, brownish-red
3	1.2	1.8	2	3	3	4	Clay/silt, brownish
4	1.8	2.4	2	3	4	8	Medium grained sand + gravel (hit rock)
5	2.4	3.0	5	8	7	6	Medium grained sand + gravel
6	3.0	3.6	4	7	10	8	Clean (3.0 -3.3 m) and contaminated (3.3 -3.6 m) silt/sand + gravel
7	3.6	4.2	4	11	11	11	Dark brown contaminated silty sand + sand + gravel
8	4.2	4.8	7	10	10	10	Well sorted sand and gravel. Both samples gray in color and contaminated
9	4.8	5.4	7	11	10	4	Clean (4.8 -5.1 m) and contaminated (5.1-5.4 m) silt-sand + gravel
10	5.4	6.1	5	7	10	19	Sand, contaminated (5.1-5.4 m), clean (5.4-6.1 m)

Drilling Log for LVRP-5

Client	Adrian Ezeagu
Project	Vertical Resistivity Probe installation
Boring	LVRP-5
Location	Lakeside Refinery Complex, Kalamazoo, MI
Date	November, 2000
Driller	West Michigan Drilling
Drilling Method	8.26 cm (3.25 inch) Hollow Stem Auger
Sampler	Split Spoon Sampler
Length of Boring	6.1 m
Ground Surface Elevation	n/a
Water Level Measurement	4.6 m
Backfill Method	Bentonite slurry and very fine sand

Sample Number	Depth (meters)		Split Spoon Blows				Sample Description (from ground surface/top of well)
	From	To	0-15cm	15-30cm	30-45cm	45-60cm	
1	0	0.6	2	2	2	2	Fine grained clay/silt
2	0.6	1.2	2	2	4	3	Clay/silt, brownish
3	1.2	1.8	2	3	3	4	Clay/silt, brownish
4	1.8	2.4	2	2	2	4	Medium grained sand + gravel
5	2.4	3.0	3	7	7	10	Light brown sand + gravel, hydrocarbon contamination present (tip of contamination at 3.0 m)
6	3.0	3.6	6	9	10	7	Well sorted sand and gravel, medium grained, + contaminated
7	3.6	4.2	4	3	3	2	Sand, dark brown-gray, hydrocarbon present
8	4.2	4.8	3	3	2	2	Free product, black medium grained sand
9	4.8	5.4	3	8	8	9	Poor recovery, gray/black sand
10	5.4	6.1	5	12	12	17	Sand, contaminated (5.1-5.4 m) clean (5.4-6.1 m)

Appendix B

Grain Size Analysis

Sieve Opening (mm)	Weight Retained (g)	Cumulative Weight Retained (g)	Phi Units (ϕ)	Cumulative % Retained
8.00	8.85	8.85	-3	3.07
4.00	9.60	18.45	-2	6.39
2.00	18.06	36.51	-1	12.65
1.00	26.58	63.09	0	21.86
0.50	34.99	98.08	1	33.98
0.25	37.05	135.13	2	46.82
0.15	20.69	155.82	2.75	53.99
0.06	27.28	183.10	4	63.44
Bottom Pan	105.51	288.61	5	100.00

Original weight = 289.35g
Sample from 0.0-1.2 meters depth

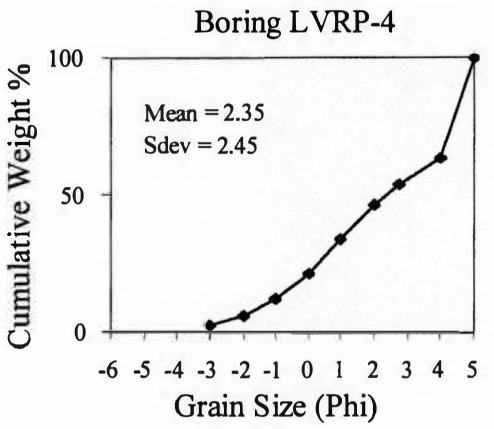

Sieve Opening (mm)	Weight Retained (g)	Cumulative Weight Retained (g)	Phi Units (ϕ)	Cumulative % Retained
2.00	1.99	1.99	-1	2.07
1.00	7.52	9.51	0	9.89
0.50	12.93	22.44	1	23.33
0.25	15.09	37.53	2	39.02
0.15	9.14	46.67	2.75	48.52
0.06	12.35	59.02	4	61.36
Bottom Pan	37.17	96.19	5	100.00

Original weight = 96.73g
Sample from 1.2-1.8 meters depth

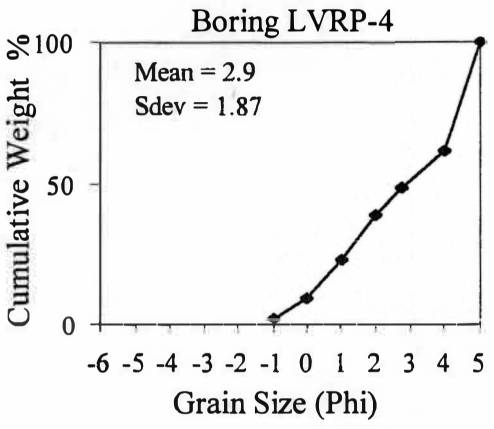

Sieve Opening (mm)	Weight Retained (g)	Cumulative Weight Retained (g)	Phi Units (ϕ)	Cumulative % Retained
16.00	5.54	5.54	-4	3.87
8.00	4.40	9.94	-3	6.95
4.00	11.60	21.54	-2	15.06
2.00	11.84	33.38	-1	23.34
1.00	11.21	44.59	0	31.18
0.50	19.56	64.15	1	44.86
0.25	32.07	96.22	2	67.29
0.15	17.89	114.11	2.75	79.80
0.06	14.79	128.90	4	90.14
Bottom Pan	14.10	143.00	5	100.00

Original weight = 143.57g
Sample from 1.8-2.4 meters depth

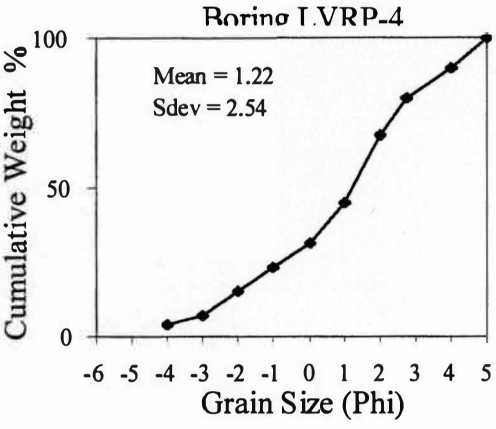

Sieve Opening (mm)	Weight Retained (g)	Cumulative Weight Retained (g)	Phi Units (ϕ)	Cumulative % Retained
16.00	0	0	-4	0.00
8.00	25.28	25.28	-3	6.66
4.00	36.54	61.82	-2	16.30
2.00	45.15	106.97	-1	28.20
1.00	41.75	148.72	0	39.20
0.50	47.23	195.95	1	51.65
0.25	63.29	259.24	2	68.33
0.15	40.70	299.94	2.75	79.06
0.06	33.90	333.84	4	88.00
Bottom Pan	45.54	379.38	5	100.00

Original weight = 380.94g
Sample from 2.4-3.6 meters depth

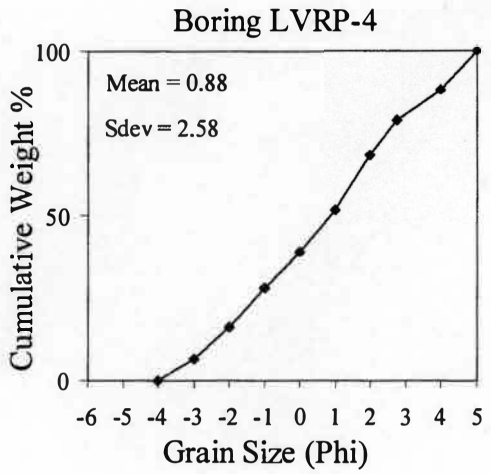

Sieve Opening (mm)	Weight Retained (g)	Cumulative Weight Retained (g)	Phi Units (ϕ)	Cumulative % Retained
16.00	8.35	8.35	-4	3.55
8.00	29.42	37.77	-3	16.08
4.00	20.40	58.17	-2	24.76
2.00	18.03	76.20	-1	32.43
1.00	11.97	88.17	0	37.53
0.50	14.22	102.39	1	43.58
0.25	32.00	134.39	2	57.20
0.15	25.10	159.49	2.75	67.88
0.06	28.53	188.02	4	80.03
Bottom Pan	46.93	234.95	5	100.00

Original weight = 236.14g
Sample from 3.6-4.2 meters depth

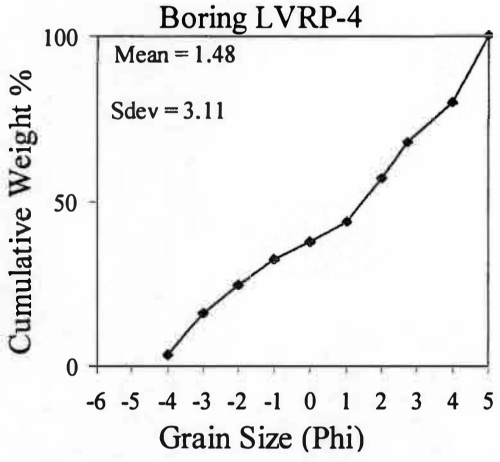

Sieve Opening (mm)	Weight Retained (g)	Cumulative Weight Retained (g)	Phi Units (ϕ)	Cumulative % Retained
64.00	0	0	-6	0
16.00	13.57	13.57	-4	5.62
8.00	43.24	56.81	-3	23.53
4.00	24.93	81.74	-2	33.86
2.00	19.78	101.52	-1	42.05
1.00	13.07	114.59	0	47.46
0.50	13.24	127.83	1	52.95
0.25	22.85	150.68	2	62.41
0.15	19.09	169.77	2.75	70.32
0.06	25.70	195.47	4	80.97
Bottom Pan	45.95	241.42	5	100.00

Original weight = 242.88g
Sample from 4.2-4.8 meters depth

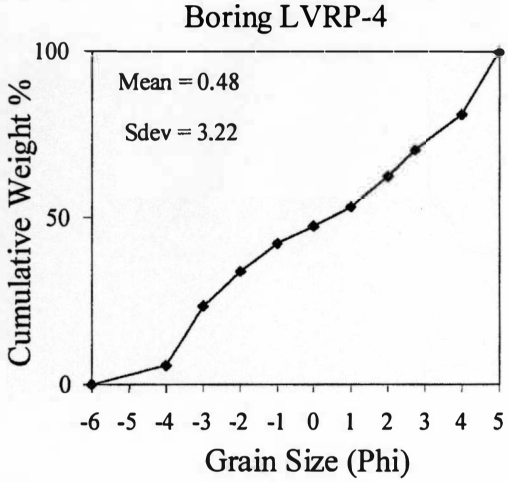

Sieve Opening (mm)	Weight Retained (g)	Cumulative Weight Retained (g)	Phi Units (ϕ)	Cumulative % Retained
64.00	0	0	-6	0.00
16.00	17.64	17.64	-4	7.23
8.00	23.00	40.64	-3	16.65
4.00	12.42	53.06	-2	21.73
2.00	13.27	66.33	-1	27.17
1.00	14.48	80.81	0	33.10
0.50	28.24	109.05	1	44.67
0.25	41.90	150.95	2	61.83
0.15	25.27	176.22	2.75	72.18
0.06	27.53	203.75	4	83.46
Bottom Pan	40.38	244.13	5	100.00

Original weight = 245.61g
Sample from 4.8-5.4 meters depth

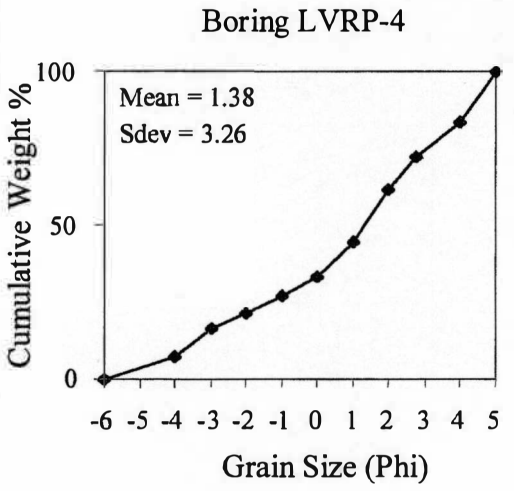

Sieve Opening (mm)	Weight Retained (g)	Cumulative Weight Retained (g)	Phi Units (ϕ)	Cumulative % Retained
16.00	11.76	0	-4	0
8.00	21.30	12.09	-3	8.65
4.00	15.56	24.47	-2	17.51
2.00	23.28	35.56	-1	25.44
1.00	19.74	44.63	0	31.93
0.50	31.44	57.39	1	41.06
0.25	55.04	81.02	2	57.96
0.15	23.07	97.81	2.75	69.97
0.06	18.51	114.69	4	82.05
Bottom Pan	16.76	139.78	5	100.00

Original weight = 237.83g
Sample from 5.4-6.1 meters depth

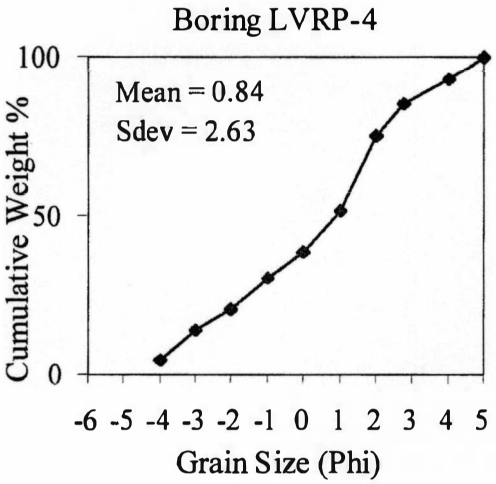

Sieve Opening (mm)	Weight Retained (g)	Cumulative Weight Retained (g)	Phi Units (ϕ)	Cumulative % Retained
8.00	5.37	5.37	-3	3.42
4.00	4.79	10.16	-2	6.47
2.00	6.70	16.86	-1	10.73
1.00	9.67	26.53	0	16.88
0.50	15.41	41.94	1	26.69
0.25	16.21	58.15	2	37.01
0.15	10.59	68.74	2.75	43.75
0.06	13.88	82.62	4	52.58
Bottom Pan	74.41	157.13	5	100.00

Original weight = 159.16g
Sample from 0-0.6 meters depth

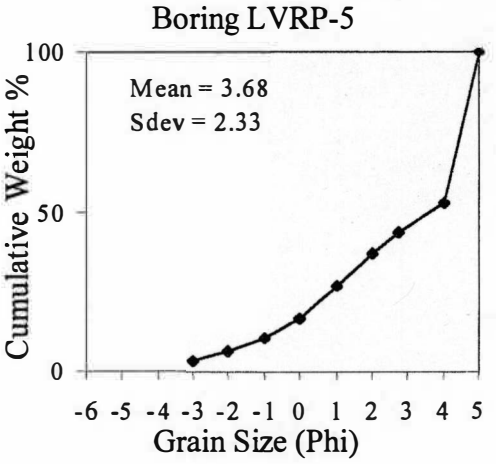

Sieve Opening (mm)	Weight Retained (g)	Cumulative Weight Retained (g)	Phi Units (ϕ)	Cumulative % Retained
8.00	3.47	3.47	-3	2.49
4.00	1.60	5.07	-2	3.64
2.00	4.75	9.82	-1	7.05
1.00	17.36	27.18	0	19.52
0.50	20.12	47.30	1	33.97
0.25	16.15	63.45	2	45.57
0.15	16.83	80.28	2.75	57.66
0.06	10.36	90.67	4	65.12
Bottom Pan	48.57	139.24	5	100.00

Original weight = 140.36g
Sample from 0.6-1.2 meters depth

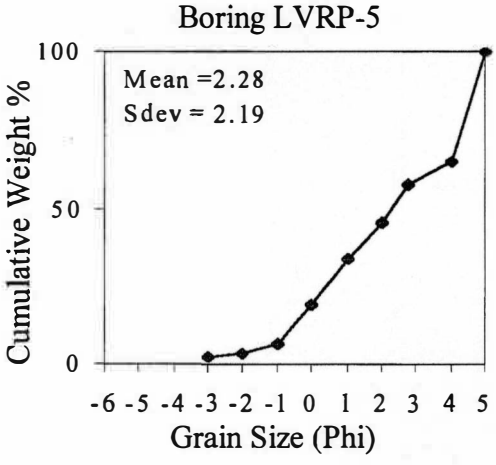

Sieve Opening (mm)	Weight Retained (g)	Cumulative Weight Retained (g)	Phi Units (ϕ)	Cumulative % Retained
2.00	3.90	3.90	-1	3.29
1.00	15.30	19.20	0	16.18
0.50	19.97	39.17	1	33.00
0.25	16.44	55.61	2	46.86
0.15	7.78	63.39	2.75	53.41
0.06	12.80	76.19	4	64.20
Bottom Pan	42.03	118.22	5	99.61

Original weight = 118.68g
Sample from 1.2-1.8 meters depth

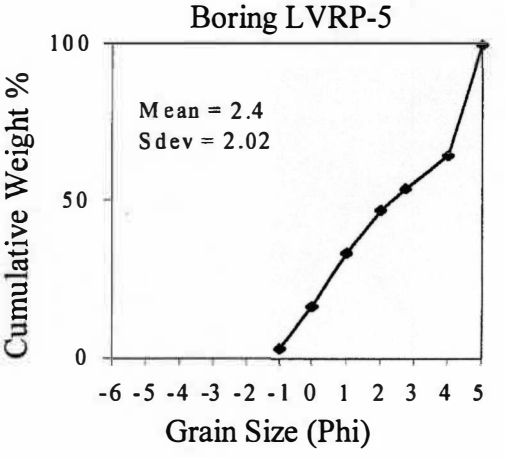

Sieve Opening (mm)	Weight Retained (g)	Cumulative Weight Retained (g)	Phi Units (ϕ)	Cumulative % Retained
16.00	0	0	-4	0
8.00	12.09	12.09	-3	8.65
4.00	12.38	24.47	-2	17.51
2.00	11.09	35.56	-1	25.44
1.00	9.07	44.63	0	31.93
0.50	12.76	57.39	1	41.06
0.25	23.63	81.02	2	57.96
0.15	16.79	97.81	2.75	69.97
0.06	16.88	114.69	4	82.05
Bottom Pan	25.09	139.78	5	100.00

Original weight = 140.3g
Sample from 1.8-2.4 meters depth

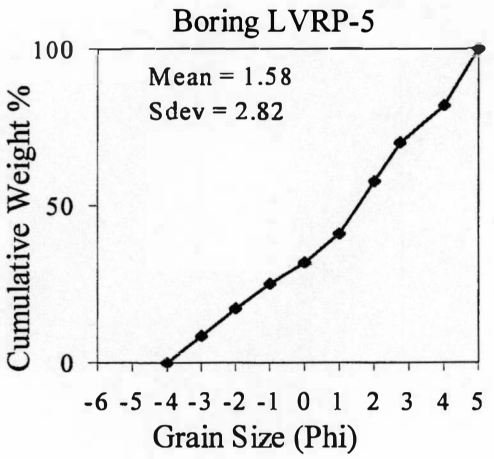

Sieve Opening (mm)	Weight Retained (g)	Cumulative Weight Retained (g)	Phi Units (ϕ)	Cumulative % Retained
16.00	0	0	-4	0
8.00	30.79	30.79	-3	15.49
4.00	15.00	45.79	-2	23.03
2.00	26.76	72.55	-1	36.50
1.00	24.09	96.64	0	48.61
0.50	25.08	121.72	1	61.23
0.25	26.08	147.80	2	74.35
0.15	15.56	163.36	2.75	82.18
0.06	14.80	178.16	4	89.62
Bottom Pan	20.63	198.79	5	100.00

Original weight = 199.58g
Sample from 2.4-3.0 meters depth

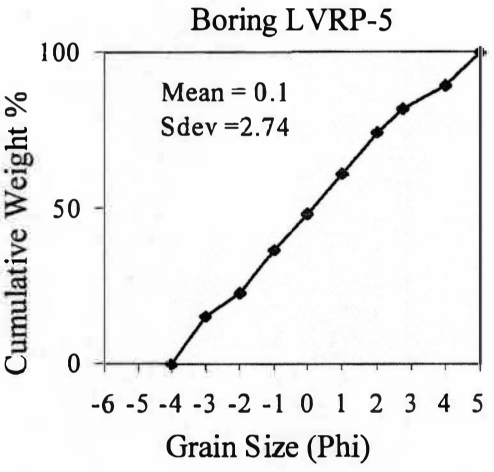

Sieve Opening (mm)	Weight Retained (g)	Cumulative Weight Retained (g)	Phi Units (ϕ)	Cumulative % Retained
64.00	0	0	-6	0.00
16.00	21.44	21.44	-4	10.96
8.00	15.50	36.94	-3	18.89
4.00	15.99	52.93	-2	27.07
2.00	16.51	69.44	-1	35.51
1.00	13.03	82.47	0	42.18
0.50	14.58	97.05	1	49.63
0.25	32.15	129.20	2	66.07
0.15	22.35	151.55	2.75	77.50
0.06	19.48	171.03	4	87.47
Bottom Pan	24.51	195.54	5	100.00

Original weight = 196.2g
Sample from 3.0-3.6 meters depth

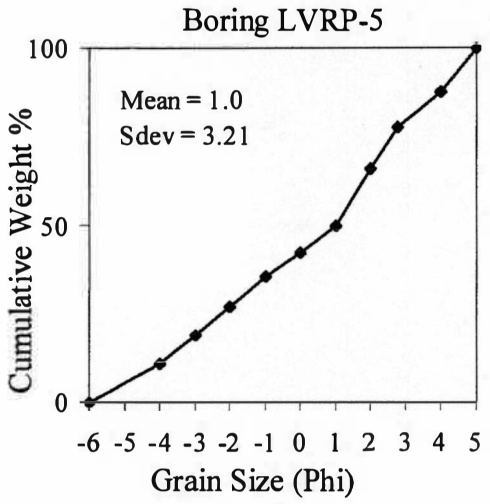

Sieve Opening (mm)	Weight Retained (g)	Cumulative Weight Retained (g)	Phi Units (ϕ)	Cumulative % Retained
16.00	0	0	-4	0.00
8.00	18.35	18.35	-3	8.96
4.00	15.72	34.07	-2	16.64
2.00	16.92	50.99	-1	24.90
1.00	13.19	64.18	0	31.34
0.50	16.04	80.22	1	39.18
0.25	31.66	111.88	2	54.64
0.15	23.88	135.76	2.75	66.30
0.06	23.64	159.40	4	77.84
Bottom Pan	45.37	204.77	5	100.00

Original weight = 205.31g
Sample from 3.6-4.2 meters depth

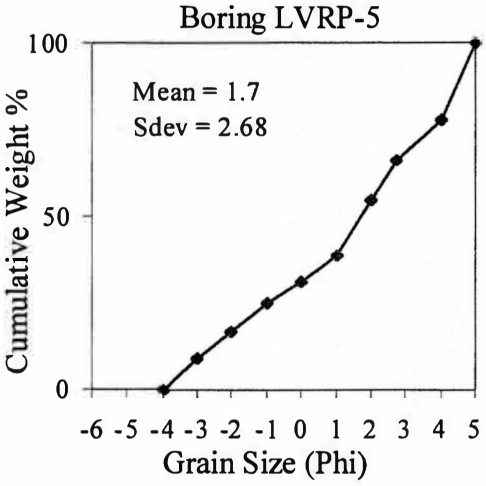

Sieve Opening (mm)	Weight Retained (g)	Cumulative Weight Retained (g)	Phi Units (ϕ)	Cumulative % Retained
16.00	7.77	7.77	-4	1.49
8.00	36.92	44.69	-3	8.55
4.00	55.60	100.29	-2	19.20
2.00	58.13	158.42	-1	30.32
1.00	52.53	210.95	0	40.38
0.50	53.62	264.57	1	50.64
0.25	69.94	334.51	2	64.03
0.15	49.87	384.38	2.75	73.58
0.06	45.95	430.33	4	82.37
Bottom Pan	92.10	522.43	5	100.00

Original weight = 524.9g
Sample from 4.2-4.8 meters depth

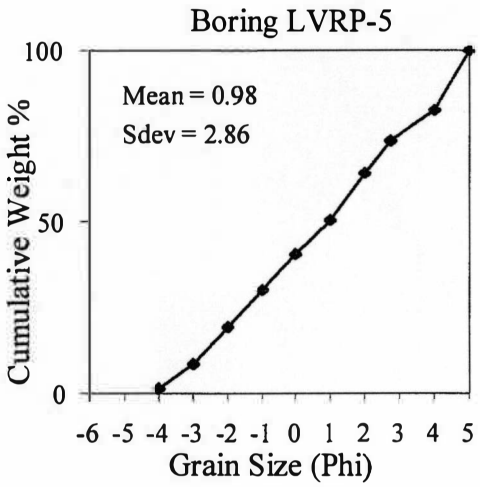

Sieve Opening (mm)	Weight Retained (g)	Cumulative Weight Retained (g)	Phi Units (ϕ)	Cumulative % Retained
64.00	0.00	0.00	-6	0.00
16.00	49.53	49.53	-4	15.39
8.00	13.80	63.33	-3	19.67
4.00	22.98	86.31	-2	26.81
2.00	25.44	111.75	-1	34.71
1.00	23.12	134.87	0	41.89
0.50	30.51	165.38	1	51.37
0.25	45.78	211.16	2	65.59
0.15	31.73	242.89	2.75	75.45
0.06	34.36	277.25	4	86.12
Bottom Pan	44.68	321.93	5	100.00

Original weight = 322.98g
Sample from 4.8-5.4 meters depth

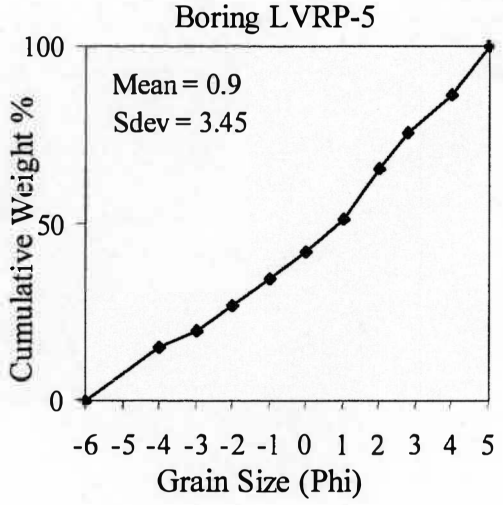

Sieve Opening (mm)	Weight Retained (g)	Cumulative Weight Retained (g)	Phi Units (ϕ)	Cumulative % Retained
16.00	0	0	-4	0
8.00	15.72	15.72	-3	8.65
4.00	9.71	25.43	-2	13.99
2.00	10.13	35.56	-1	19.56
1.00	10.62	46.18	0	25.40
0.50	41.75	87.93	1	48.37
0.25	62.18	150.11	2	82.57
0.15	16.84	166.95	2.75	91.84
0.06	7.41	174.36	4	95.91
Bottom Pan	7.43	181.79	5	100.00

Original weight = 182.04g
Sample from 5.4-6.1 meters depth

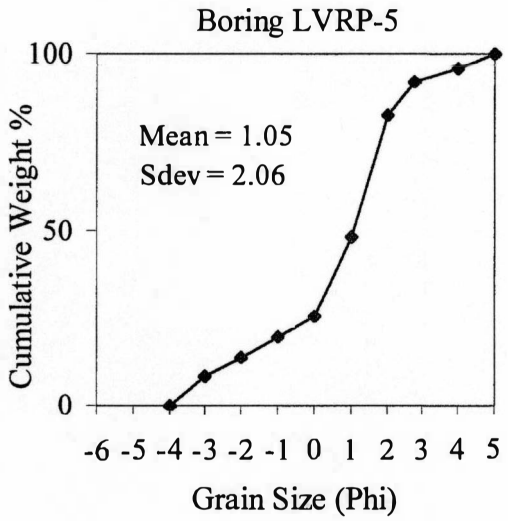

Appendix C

Vertical Resistivity Measurements

Pole-dipole array (a=5cm) Apparent Resistivity (ρa)=8πaV/I				Wenner array (a=5cm) Apparent Resistivity=4πaV/I				
LVRP-4		**LVRP-5**		**LVRP-4**		**LVRP-5**		
V	I	V	I	V	I	V	I	Depth (meter)
347.2	2.3	260.2	3.7	1222.4	2.7	1266.6	3.0	6.10
475.0	2.1	451.8	3.5	1178.8	2.6	1197.9	3.2	6.05
35.5	1.3	591.0	3.4	251.3	1.1	1247.6	3.2	5.99
194.8	1.4	548.2	3.3	1183.3	1.0	1260.5	3.4	5.94
160.1	1.3	673.6	3.3	194.9	1.0	1252.9	3.3	5.89
185.1	1.4	627.9	3.2	184.5	0.6	1234.6	3.3	5.84
179.3	1.0	657.1	3.3	193.7	0.7	1336.2	3.5	5.79
170.1	1.1	644.8	3.4	181.6	0.6	1286.0	3.2	5.74
120.3	1.0	624.6	3.3	138.8	0.5	1367.4	3.4	5.69
119.9	1.0	576.1	3.4	137.1	0.5	1335.3	3.4	5.64
136.4	1.0	675.2	3.4	157.4	0.5	1287.0	3.2	5.59
182.8	0.9	648.3	3.2	156.9	0.5	1129.5	2.7	5.54
175.2	0.8	642.7	2.5	203.7	0.5	115.0	1.0	5.49
218.6	0.8	42.2	1.2	170.2	0.5	1166.0	1.0	5.44
159.4	1.0	234.4	1.3	215.1	0.6	201.4	1.0	5.38
198.5	2.0	217.7	1.5	184.7	0.7	202.9	0.7	5.33
259.6	3.0	219.8	1.4	91.0	0.8	200.0	0.6	5.28
112.7	3.5	196.3	1.0	144.2	1.2	198.9	0.7	5.23
77.9	2.1	172.7	1.3	126.4	1.7	236.1	0.7	5.18
57.3	2.1	179.3	1.4	249.5	3.2	124.6	0.5	5.13
109.4	3.8	114.4	0.9	107.4	1.8	98.3	0.4	5.08
101.0	3.8	66.4	0.5	52.3	1.0	179.9	0.7	5.03
35.2	1.5	154.3	1.4	303.4	3.4	119.0	0.6	4.98
157.6	3.7	128.4	1.4	197.1	1.8	71.7	0.4	4.93
113.7	2.2	108.1	1.4	48.4	0.9	145.2	0.8	4.88
34.2	1.7	123.3	1.9	150.6	1.4	125.8	1.1	4.83
70.0	1.6	89.4	3.3	75.6	1.1	116.8	1.3	4.78
54.5	1.6	86.1	4.9	95.4	1.4	61.2	1.8	4.72
66.6	3.0	50.0	5.0	86.5	1.5	82.4	2.9	4.67
52.2	4.2	49.2	5.0	50.7	1.5	103.1	4.3	4.62
41.0	4.6	48.9	5.0	69.1	2.9	87.1	4.2	4.57
35.1	4.5	44.1	4.8	89.0	5.0	88.9	4.3	4.52
26.4	4.4	48.9	4.8	101.8	5.8	83.7	4.1	4.47
34.6	4.6	49.0	4.7	84.3	5.2	99.1	4.4	4.42
31.7	4.7	60.5	5.1	89.0	4.8	97.1	4.2	4.37
35.6	4.1	62.8	5.0	53.4	3.4	100.8	3.9	4.32

LVRP-4		LVRP-5		LVRP-4		LVRP-5		
V	I	V	I	V	I	V	I	Depth (meter)
25.2	3.4	66.9	4.8	112.3	3.7	117.3	4.3	4.27
71.6	4.3	72.4	4.7	100.7	4.3	136.5	4.4	4.22
29.6	4.4	80.1	5.0	75.3	3.2	128.6	4.1	4.17
36.5	4.3	68.2	4.9	75.6	3.8	87.4	3.5	4.11
35.4	4.7	47.5	4.2	93.2	4.2	115.8	4.1	4.06
41.7	4.3	77.9	4.6	6.6	0.2	53.4	2.4	4.01
30.7	3.7	30.3	2.6	138.4	4.4	75.5	2.0	3.96
44.7	4.3	56.6	2.5	108.8	1.6	89.6	2.3	3.91
62.9	4.5	70.1	2.8	5.1	0.1	56.3	1.4	3.86
39.0	3.4	53.7	2.5	62.2	1.8	39.0	0.7	3.81
44.4	3.8	29.7	1.0	51.2	1.5	29.9	0.5	3.76
56.6	4.2	23.7	0.6	12.1	0.2	20.8	0.2	3.71
55.4	3.9	16.4	0.2	82.0	1.5	43.9	0.2	3.66
36.8	2.9	49.7	0.3	119.2	3.2	53.2	0.4	3.61
51.3	4.2	81.7	1.5	89.3	2.5	29.6	0.2	3.56
34.4	3.3	24.4	0.9	46.8	1.5	20.5	0.2	3.51
39.3	3.2	40.1	1.3	88.4	2.9	58.3	0.8	3.45
40.1	3.4	67.1	1.9	44.4	1.7	76.9	0.8	3.40
42.9	2.9	262.2	4.0	78.9	1.6	65.1	1.0	3.35
51.7	3.7	128.4	3.8	61.2	1.3	128.8	1.5	3.30
58.6	3.1	125.4	3.7	78.6	1.2	206.9	3.1	3.25
50.0	3.5	104.7	4.2	82.7	0.8	244.8	3.1	3.20
70.1	2.3	163.3	4.3	153.1	1.1	157.4	3.0	3.15
99.5	3.2	120.3	4.4	120.2	1.2	232.4	3.3	3.10
108.4	2.8	140.3	4.4	16.8	0.1	200.2	3.5	3.05
2.5	0.0	123.7	4.4	86.8	3.7	238.0	3.6	3.00
74.9	4.9	150.6	4.5	99.5	5.4	232.6	3.9	2.95
41.8	4.8	125.5	4.8	80.6	5.2	228.6	4.0	2.90
39.8	5.3	105.0	5.0	70.7	4.6	169.7	3.9	2.84
39.4	5.3	79.3	4.9	95.7	5.7	147.2	4.2	2.79
34.2	4.6	69.4	4.8	91.1	5.4	153.9	4.5	2.74
46.3	5.4	76.5	4.9	83.3	4.4	141.0	4.3	2.69
46.3	5.1	76.9	4.8	111.6	5.2	138.4	4.4	2.64
49.2	4.8	74.9	5.0	111.9	4.7	165.8	5.7	2.59
60.9	5.1	75.7	5.8	110.5	4.7	136.2	4.4	2.54
68.2	5.0	78.0	5.2	123.9	4.8	136.5	4.9	2.49
65.6	5.2	72.4	5.2	97.6	4.2	166.8	5.7	2.44
67.0	5.1	75.8	5.0	109.0	4.4	154.2	5.0	2.39

LVRP-4		LVRP-5		LVRP-4		LVRP-5		
V	I	V	I	V	I	V	I	Depth (meter)
57.9	4.6	87.4	5.2	131.3	4.7	160.4	4.9	2.34
61.8	4.5	89.9	5.1	139.5	4.1	170.5	4.6	2.29
80.8	4.9	101.1	5.1	117.1	3.0	162.9	4.5	2.24
98.5	4.9	93.0	4.8	89.7	2.7	129.5	3.4	2.18
83.3	3.4	68.6	3.7	175.0	2.6	190.6	4.0	2.13
60.4	3.0	106.8	4.2	38.7	0.5	175.5	3.8	2.08
117.0	2.7	113.3	4.2	47.8	0.4	111.9	2.2	2.03
30.2	0.5	83.9	2.9	87.9	0.4	143.7	2.3	1.98
40.9	0.4	94.2	2.7	54.2	0.2	139.4	1.9	1.93
65.8	0.4	95.0	2.4	50.6	0.2	126.8	1.7	1.88
56.3	0.4	98.4	2.6	69.2	0.2	154.6	1.9	1.83
44.1	0.3	129.4	3.1	64.1	0.2	121.9	1.5	1.78
71.2	0.4	101.4	2.5	60.8	0.2	151.8	1.9	1.73
65.7	0.3	128.5	3.3	60.1	0.2	171.7	2.3	1.68
54.7	0.3	133.5	3.7	65.1	0.2	147.6	1.8	1.63
48.5	0.3	141.6	3.2	37.0	0.2	153.4	1.9	1.57
65.2	0.4	117.9	2.5	59.3	0.3	190.1	1.8	1.52
32.8	0.3	138.5	2.2	53.0	0.4	133.1	1.8	1.47
67.4	2.2	77.8	2.5	13.1	0.3	219.2	1.8	1.42
77.9	3.2	182.5	3.3	59.0	1.6	75.6	1.3	1.37
42.9	3.2	62.4	2.3	69.0	1.9	149.8	1.6	1.32
52.7	3.2	103.5	2.8	55.6	1.3	128.8	2.1	1.27
58.3	2.7	87.6	3.0			97.3	1.7	1.22
49.0	1.7	64.2	2.4			128.1	2.0	1.17
		166.9	3.3			82.4	1.3	1.12
		84.4	1.6			95.7	1.4	1.07
		69.6	1.5			161.0	1.6	1.02
		128.8	2.0			133.3	1.5	0.97
		213.8	4.4			133.6	1.6	0.91
		183.6	4.8			100.0	1.8	0.86
		83.2	4.4			200.4	3.5	0.81
		98.3	4.1			122.2	2.7	0.76
		76.6	3.1			157.3	2.6	0.71
		111.4	3.0			114.3	3.4	0.66
						119.4	2.6	0.61

Appendix D

Cross-hole Resistivity Measurements

Syscal Array (cross-hole dipole-dipole)			A, B (current Electrodes): z = M,N (Potential electrodes) depth(m) Electrodes X-locations (0.6 =LVRP-4, 2.1 =LVRP-5)							
Voltage	Current	Resistance	A(x)	(z)	B(x)	(z)	M(x)	(z)	N(x)	(z)
1037.38	2.11	490.80	0.60	5.10	2.10	5.70	0.60	4.80	2.10	6.00
895.29	1.91	469.70	0.60	5.10	2.10	6.00	0.60	4.80	2.10	5.70
1023.56	2.09	489.50	0.60	5.10	2.10	5.70	0.60	4.80	2.10	5.40
1081.98	2.12	510.50	0.60	5.10	2.10	5.40	0.60	4.80	2.10	5.10
1307.93	2.12	617.50	0.60	5.10	2.10	5.10	0.60	4.80	2.10	4.80
523.84	2.26	231.40	0.60	5.10	2.10	4.80	0.60	4.80	2.10	4.50
505.48	2.06	244.80	0.60	5.10	2.10	4.50	0.60	4.80	2.10	4.20
588.95	2.41	244.80	0.60	5.10	2.10	4.20	0.60	4.80	2.10	3.90
581.90	2.44	238.90	0.60	5.10	2.10	3.90	0.60	4.80	2.10	3.60
375.24	1.34	281.00	0.60	5.10	2.10	3.60	0.60	4.80	2.10	3.30
160.73	0.54	298.80	0.60	5.10	2.10	3.30	0.60	4.80	2.10	3.00
563.76	2.06	274.00	0.60	5.10	2.10	3.00	0.60	4.80	2.10	2.70
449.84	1.73	259.70	0.60	5.10	2.10	2.70	0.60	4.80	2.10	2.40
541.07	2.07	261.60	0.60	5.10	2.10	2.40	0.60	4.80	2.10	2.10
564.33	2.16	261.70	0.60	5.10	2.10	2.10	0.60	4.80	2.10	1.80
327.39	1.24	263.40	0.60	5.10	2.10	1.80	0.60	4.80	2.10	1.50
342.50	1.29	266.30	0.60	5.10	2.10	1.50	0.60	4.80	2.10	1.20
361.45	0.91	395.30	0.60	4.80	2.10	5.70	0.60	4.50	2.10	6.00
335.19	0.85	393.10	0.60	4.80	2.10	6.00	0.60	4.50	2.10	5.70
282.33	0.89	316.60	0.60	4.80	2.10	5.70	0.60	4.50	2.10	5.40
332.32	0.89	373.70	0.60	4.80	2.10	5.40	0.60	4.50	2.10	5.10
503.24	0.88	573.60	0.60	4.80	2.10	5.10	0.60	4.50	2.10	4.80
40.52	0.82	49.70	0.60	4.80	2.10	4.80	0.60	4.50	2.10	4.50
51.38	0.79	64.80	0.60	4.80	2.10	4.50	0.60	4.50	2.10	4.20
52.04	0.86	60.70	0.60	4.80	2.10	4.20	0.60	4.50	2.10	3.90
46.07	0.84	55.00	0.60	4.80	2.10	3.90	0.60	4.50	2.10	3.60
49.38	0.63	77.90	0.60	4.80	2.10	3.60	0.60	4.50	2.10	3.30
32.61	0.40	82.40	0.60	4.80	2.10	3.30	0.60	4.50	2.10	3.00
70.96	0.83	85.90	0.60	4.80	2.10	3.00	0.60	4.50	2.10	2.70
55.50	0.75	74.00	0.60	4.80	2.10	2.70	0.60	4.50	2.10	2.40
55.23	0.81	68.30	0.60	4.80	2.10	2.40	0.60	4.50	2.10	2.10
56.07	0.84	66.40	0.60	4.80	2.10	2.10	0.60	4.50	2.10	1.80
36.95	0.66	56.40	0.60	4.80	2.10	1.80	0.60	4.50	2.10	1.50
36.93	0.68	54.10	0.60	4.80	2.10	1.50	0.60	4.50	2.10	1.20
528.18	1.27	416.00	0.60	4.50	2.10	5.70	0.60	4.20	2.10	6.00

			A, B (current Electrodes): M,N (Potential electrodes)					
Array (cross-hole dipole-pole)			Electrodes X-locations (0.6 =LVRP-4, 2.1 =LVRP-5)					
Voltage	Current	Resistance	A(x)	(z)	B(x)	(z)	M(x)	(z)
103.36	2.46	42.00	0.60	4.20	2.10	0.60	0.60	3.90
36.55	0.87	42.10	0.60	4.20	2.10	0.90	0.60	3.90
24.07	0.57	42.20	0.60	4.20	2.10	1.20	0.60	3.90
80.68	1.93	41.80	0.60	4.20	2.10	1.50	0.60	3.90
65.28	1.57	41.60	0.60	4.20	2.10	1.80	0.60	3.90
107.35	2.60	41.30	0.60	4.20	2.10	2.10	0.60	3.90
108.54	2.67	40.70	0.60	4.20	2.10	2.40	0.60	3.90
109.74	2.74	40.10	0.60	4.20	2.10	2.70	0.60	3.90
96.84	2.45	39.60	0.60	4.20	2.10	3.00	0.60	3.90
24.52	0.63	39.10	0.60	4.20	2.10	3.30	0.60	3.90
71.82	1.86	38.50	0.60	4.20	2.10	3.60	0.60	3.90
30.32	0.79	38.50	0.60	4.20	2.10	3.90	0.60	3.90
108.41	2.87	37.80	0.60	4.20	2.10	4.20	0.60	3.90
100.44	2.59	38.80	0.60	4.20	2.10	4.50	0.60	3.90
34.45	0.88	39.20	0.60	4.20	2.10	4.80	0.60	3.90
36.31	0.90	40.20	0.60	4.20	2.10	5.10	0.60	3.90
86.87	2.14	40.60	0.60	4.20	2.10	5.40	0.60	3.90
77.73	1.98	39.30	0.60	4.20	2.10	5.70	0.60	3.90
69.17	1.68	41.10	0.60	4.20	2.10	6.00	0.60	3.90
50.47	1.25	40.30	0.60	4.50	2.10	0.60	0.60	4.20
26.32	0.65	40.50	0.60	4.50	2.10	0.90	0.60	4.20
18.34	0.45	40.60	0.60	4.50	2.10	1.20	0.60	4.20
44.39	1.10	40.20	0.60	4.50	2.10	1.50	0.60	4.20
40.47	1.01	40.00	0.60	4.50	2.10	1.80	0.60	4.20
49.33	1.25	39.50	0.60	4.50	2.10	2.10	0.60	4.20
48.02	1.23	39.20	0.60	4.50	2.10	2.40	0.60	4.20
51.07	1.32	38.70	0.60	4.50	2.10	2.70	0.60	4.20
46.52	1.22	38.20	0.60	4.50	2.10	3.00	0.60	4.20
17.88	0.48	37.60	0.60	4.50	2.10	3.30	0.60	4.20
54.25	1.47	36.80	0.60	4.50	2.10	3.60	0.60	4.20
21.51	0.58	36.80	0.60	4.50	2.10	3.90	0.60	4.20
50.38	1.37	36.80	0.60	4.50	2.10	4.20	0.60	4.20
47.43	1.28	36.90	0.60	4.50	2.10	4.50	0.60	4.20
24.56	0.66	37.50	0.60	4.50	2.10	4.80	0.60	4.20
25.82	0.68	38.10	0.60	4.50	2.10	5.10	0.60	4.20
51.50	1.33	38.60	0.60	4.50	2.10	5.40	0.60	4.20
50.98	1.31	38.90	0.60	4.50	2.10	5.70	0.60	4.20
46.29	1.19	39.00	0.60	4.50	2.10	6.00	0.60	4.20

			A, B (current Electrodes): M,N (Potential electrodes)					
Array (cross-hole pole-dipole)			Electrodes X-locations (0.6 =LVRP-4, 2.1 =LVRP-5)					
Voltage	Current	Resistance	A(x)	(z)	M(x)	(z)	N(x)	(z)
166.97	4.07	41.10	0.60	4.50	0.60	4.20	2.10	6.00
161.63	3.94	41.00	0.60	4.50	0.60	4.20	2.10	5.70
154.96	3.81	40.60	0.60	4.50	0.60	4.20	2.10	5.40
150.63	3.77	39.90	0.60	4.50	0.60	4.20	2.10	5.10
148.09	3.74	39.60	0.60	4.50	0.60	4.20	2.10	4.80
145.86	3.69	39.50	0.60	4.50	0.60	4.20	2.10	4.50
143.63	3.64	39.50	0.60	4.50	0.60	4.20	2.10	4.20
142.44	3.60	39.60	0.60	4.50	0.60	4.20	2.10	3.90
141.48	3.56	39.70	0.60	4.50	0.60	4.20	2.10	3.60
141.63	3.53	40.20	0.60	4.50	0.60	4.20	2.10	3.30
141.80	3.48	40.70	0.60	4.50	0.60	4.20	2.10	3.00
141.72	3.44	41.20	0.60	4.50	0.60	4.20	2.10	2.70
141.92	3.40	41.80	0.60	4.50	0.60	4.20	2.10	2.40
144.27	3.43	42.10	0.60	4.50	0.60	4.20	2.10	2.10
143.77	3.38	42.50	0.60	4.50	0.60	4.20	2.10	1.80
142.63	3.35	42.60	0.60	4.50	0.60	4.20	2.10	1.50
140.18	3.30	42.50	0.60	4.50	0.60	4.20	2.10	1.20
139.76	3.27	42.80	0.60	4.50	0.60	4.20	2.10	0.90
137.95	3.22	42.90	0.60	4.50	0.60	4.20	2.10	0.60
152.51	4.25	35.90	0.60	4.20	0.60	3.90	2.10	6.00
149.70	4.20	35.70	0.60	4.20	0.60	3.90	2.10	5.70
147.23	4.17	35.30	0.60	4.20	0.60	3.90	2.10	5.40
143.56	4.15	34.60	0.60	4.20	0.60	3.90	2.10	5.10
140.76	4.11	34.20	0.60	4.20	0.60	3.90	2.10	4.80
139.32	4.11	33.90	0.60	4.20	0.60	3.90	2.10	4.50
138.43	4.09	33.80	0.60	4.20	0.60	3.90	2.10	4.20
137.82	4.07	33.80	0.60	4.20	0.60	3.90	2.10	3.90
137.52	4.05	33.90	0.60	4.20	0.60	3.90	2.10	3.60
138.79	4.03	34.40	0.60	4.20	0.60	3.90	2.10	3.30
140.21	4.02	34.90	0.60	4.20	0.60	3.90	2.10	3.00
141.61	4.00	35.40	0.60	4.20	0.60	3.90	2.10	2.70
143.49	3.99	36.00	0.60	4.20	0.60	3.90	2.10	2.40
144.80	3.97	36.50	0.60	4.20	0.60	3.90	2.10	2.10
145.64	3.96	36.80	0.60	4.20	0.60	3.90	2.10	1.80
145.29	3.94	36.80	0.60	4.20	0.60	3.90	2.10	1.50

Array (cross-hole pole-pole)			A, B (current Electrodes): M,N (Potential electrodes) Electrodes X-locations (0.6 =LVRP-4, 2.1 =LVRP-5)			
Voltage	current	No.of electrodes	A (x-location)	z-depth (m)	M (x-location)	z-depth (m)
4.55	2.59	2.00	0.60	4.20	0.60	1.20
4.67	2.56	2.00	0.60	4.20	0.60	1.50
5.48	2.55	2.00	0.60	4.20	0.60	1.80
8.09	2.53	2.00	0.60	4.20	0.60	2.10
10.35	2.52	2.00	0.60	4.20	0.60	2.40
14.78	2.51	2.00	0.60	4.20	0.60	2.70
19.20	2.50	2.00	0.60	4.20	0.60	3.00
30.08	2.50	2.00	0.60	4.20	0.60	3.30
44.58	2.50	2.00	0.60	4.20	0.60	3.60
89.35	2.50	2.00	0.60	4.20	0.60	3.90
104.24	2.49	2.00	0.60	4.20	0.60	4.50
55.62	2.49	2.00	0.60	4.20	0.60	4.80
30.12	2.48	2.00	0.60	4.20	0.60	5.10
14.69	2.48	2.00	0.60	4.20	0.60	5.40
10.76	2.47	2.00	0.60	4.20	0.60	5.70
10.24	2.47	2.00	0.60	4.20	0.60	6.00
3.61	2.47	2.00	0.60	4.20	2.10	1.20
3.84	2.46	2.00	0.60	4.20	2.10	1.50
4.27	2.46	2.00	0.60	4.20	2.10	1.80
4.85	2.45	2.00	0.60	4.20	2.10	2.10
6.11	2.45	2.00	0.60	4.20	2.10	2.40
7.45	2.44	2.00	0.60	4.20	2.10	2.70
8.76	2.45	2.00	0.60	4.20	2.10	3.00
10.43	2.44	2.00	0.60	4.20	2.10	3.30
11.40	2.45	2.00	0.60	4.20	2.10	3.60
12.22	2.44	2.00	0.60	4.20	2.10	3.90
12.05	2.44	2.00	0.60	4.20	2.10	4.20
11.84	2.44	2.00	0.60	4.20	2.10	4.50
10.98	2.43	2.00	0.60	4.20	2.10	4.80
9.08	2.44	2.00	0.60	4.20	2.10	5.10
7.54	2.43	2.00	0.60	4.20	2.10	5.40
6.90	2.42	2.00	0.60	4.20	2.10	5.70

BIBLIOGRAPHY

Archie, G.E., 1942, The electrical resistivity log as an aid in determining some reseroir characteristics. Trans. A.I.M.E. Vol. 146. P54-64.

Atekwana, E.A., Sauck, W.A., Werkema Jr., D.D., 2000, Investigations of geoelectrical signatures at a hydrocarbon contaminated site: Journal of Applied Geophysics, 44, pp. 167-180.

Bing, Z., and Greenhalgh, S.A., 2000, Cross-hole Resistivity Tomography using Different Electrode Configurations: Geophysical Prospecting 48, pp. 887-912.

Boggs, S., 1995, Principles of Sedimentology and Stratigraphy, Prentice Hall, 774 p.

Brass, G., Flathe, H., and Schulz, R., 1981, Resistivity Profiling with Different Electrode Arrays over a Graphite Deposit: Geophysical Prospecting 29, pp. 589-600.

Ciarlet, P.G., 1991, The Finite Element Method for Elliptic Problems, in Ciarlet, P.G. and Lions, J.L., eds., Handbook of Numerical Analysis: North-Holland Publishing Company, 2, pp. 17-35.

Daily, W., and Ramirez, A., 1992, Electrical Resistivity Tomography of Vadose Water Movement: Water Resources Research, 28, pp. 1429-1422.

Daily, W., Ramirez, A., LaBrecque, D., and Barber, W., 1995, Electrical Resistance Tomography Experiment at the Oregon Graduate Institute: Journal of Applied Geophysics, 33, pp. 227-237.

Deutsch, M., Vanlier, K.E., and Giroux, P.R., 1960, Groundwater Hydrology and Glacial Geology of the Kalamazoo Area, Michigan Geological Survey Progress Report 23, 122p.

Folk, R.L., and Ward, W.C., 1957, Brazos River Bar: A Study in the Significance of Grain Size Parameters: Journal of Sedimentary Petrology, 27, pp. 3-26.

Groncki, J.M., 1999, Calibration, Installation Techniques, and Initial Measurements for Vertical Resistivity Probes used in Hydrogeological Investigations: unpublished Masters thesis, Western Michigan University, Kalamazoo, MI.

Hallenburg, J.K., 1998, Standard Methods of Geophysical Formation Evaluation: Lewis Publishers, pp. 1-35

Henderson, R., and Webster, J., 1978, An Impedance Camera for Spatially Specific Measurements of the Thorax: IEEE Trans. Biomedical Engineering, BME-15, 250.

Hodges, R.E., and Teasdale, W.E., 1991, Considerations Related to Drilling Methods in Planning and Performing Borehole Geophysical Logging for Groundwater Studies: U.S. Geol. Survey Water Resources Investigation Report 91-4090.

Keller, G.V., 1966, Electrical Properties of Rocks and minerals. In: S.P. Clark Jr. (editor), Handbook of Physical Constants. Geol. Soc. Am. Mem., 97 : 533-557 (revised ed.)

Keys, W.S., 1997, A Practical Guide to Borehole Geophysics in Environmental Investigations: Lewis Publishers, 176p.

Krumbein, W.C., 1934, Size Frequency Distribution of Sediments: Journal of Sedimentary Petrology, 4, pp. 65-77.

Kumar, R., 1973, Resistivity Type Curves over Outcropping Vertical Dyke-1: Geophysical Prospecting, 21, pp. 560-578.

LaBrecque, D., and Ward, S., 1988, Two Dimensional Inversion of Cross-borehole Resistivity Data using Multiple Boundaries: presented at the 58th annual inter. meeting Society of Exploration Geophysics, extended abstracts, pp. 194-197.

Loke, M.H., and Barker, R.D., 1996, Rapid Least-squares Inversion of Apparent Resistivity Pseudosections by a Quasi-Newton Method: Geophysical Prospecting, 44, pp. 131-152.

Maillol, J.M., Seguin, M.K., Gupta, O.P., Akhauri, H.M., and Sen, N., 1999, Electrical Resistivity Tomography Survey for Delineating Uncharted Mine Galleries in West Bengal, India: Geophysical Prospecting, 47, pp.103-116.

Olhoeft, G. R., 1992, Geophysical Detection of Hydrocarbon and Organic chemical contamination: Proceedings of the Symposium on the Application of Geophysics to Environmental and Engineering Problems, 587-594.

Park, S.K., and Van, G.P., 1991, Inversion of Pole-Pole Data for 3-D Resistivity Structure beneath Arrays of Electrodes: Geophysics, 56, pp. 951-960.

Ramirez, A., Daily, W., LaBrecque, D., Owen, E., and Chestnut, D., 1993, Monitoring an Underground Steam Injection Process using Electrical Resistance Tomography: Water Resources Research, 29, pp. 73-87.

Sasaki, Y., 1994, 3-D Resistivity Inversion using Finite Element Method: Geophysics, 59, pp. 1839-1848.

Sauck, W.A., 2000, A Model for the Resistivity Structure of LNAPL Plumes and their Environs in Sandy Sediments: Journal of Applied Geophysics, 44, pp. 151-165.

Schlumberger, C., 1920, Etude de la Prospection Electrique du Sous-sol: Gauthiers-Villars

Schneider, G.W., and Greenhouse, J.P., 1992, Geophysical Detection of Perchloroethylene in a Sandy Aquifer using Resistivity and Nuclear Logging Techniques: Proceedings of the Symposium on the Application of Geophysics to Environmental and Engineering Problems, Oakbrook, Illinois, pp. 619-628.

Sheriff, R.E., 1991, Encyclopedic Dictionary of Exploration Geophysics, 3rd ed.: Society of Exploration Geophysics, Tulsa, Oklahoma.

Shima, H., 1992, Two Dimensional Automatic Resistivity Inversion Technique using Alpha Centers: Geophysics, 55, pp. 682-694.

Telford, W.M., Geldart, L.P., and Sheriff, R.E., 1990, Applied Geophysics, second edition, Cambridge University Press, Cambridge, U.K.

Thomée, V., 1989, Finite Difference Methods for Linear Parabolic Equations in Ciarlet, P.G. and Lions, J.L., eds., Handbook of Numerical Analysis: North-Holland Publishing Company, 1, 5-196.

Vanhala, H., Soininen, H., Kukkoneni., 1992, Detecting Organic-Chemical Contaminants by Spectral-Induced Polarization Method in Glacial Till Environment: Geophysics, 57 (8), pp. 1014-1017.

Ward, S.H., Sternberg B.K., LaBrecque D.J., and Poulton M.M., 1995, Recommendations for IP research: the leading Edge, 14, 243-247.

Wendland, W.L., 1987, Strongly Elliptic Boundary Integral Equations, in Iserles, A. and Powell, M.J.D., eds., The State of the Art in Numerical Analysis: Clarendon Press, pp. 511-562.

Weston, Roy, Inc., 1997, Final Report for USEPA: Assessment of Subsurface Contamination: Lakeside Refinery Site, Kalamazoo, Michigan.